ACCSCIENCE PUBLISHING

# Advances in

# Radiotherapy & Nuclear Medicine



ISSN: 3060-8554 (Print)
ISSN: 2972-4392 (Online)
Volume 2 · Issue 1
March 2024

ACCSCIENCE PUBLISHING

# Advances in Radiotherapy & Nuclear Medicine

**Print ISSN: 3060-8554**
**Online ISSN: 2972-4392**

***Advances in Radiotherapy & Nuclear Medicine*** is a peer-reviewed and open-access journal that aims to publish and disseminate novel research in the breadth of radiation oncology, physics, and biology.

The journal aims to advance our understanding in the radiotherapy and provide a platform to oncologists and physicians to showcase their findings in original fundamental and clinical research as well as to present new ideas that highlight the changes in the radiation oncological clinical practice.

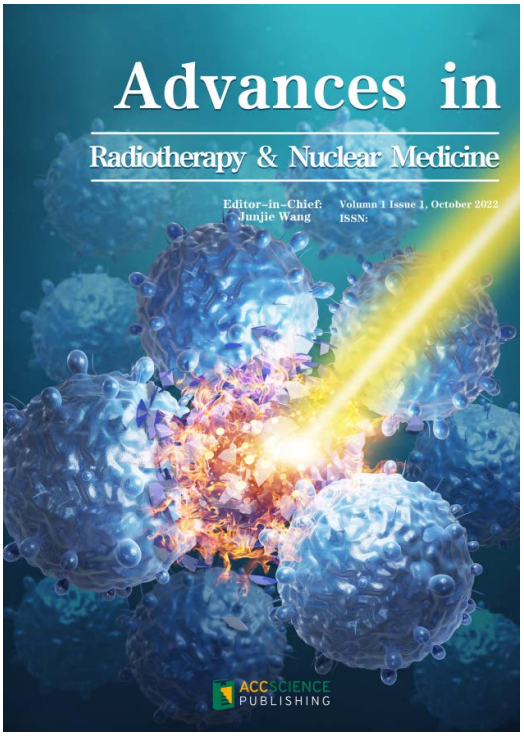


## About the Publisher

AccScience Publishing is a publishing company based in Singapore. We publish a range of high-quality, open-access, peer-reviewed journals and books from a broad spectrum of disciplines.

Contact Us

**Managing Editor**
arnm.office@accscience.sg

**AccScience Publishing**
8 Burn Road, #15-03 Trivex, Singapore 369977.

Volume 2 • Issue 1 • March 2024
ISSN 3060-8554 (print) ISSN 2972-4392 (online)

# Advances in Radiotherapy & Nuclear Medicine



ACCSCIENCE PUBLISHING

Access Science Without Barriers

*ADVANCES IN RADIOTHERAPY & NUCLEAR MEDICINE*

ISSN: 3060-8554 (print)
ISSN: 2972-4392 (online)

**Editorial and Production Credits**

Publisher: AccScience Publishing
Managing Editor: Freda Wang
Production Editor: Ian Wong
Article Layout and Typeset: Sinjore Technologies (India)



**Supplementary file**

Supplementary files of articles can be obtained at https://accscience.com/journal/ARNM/2/1.

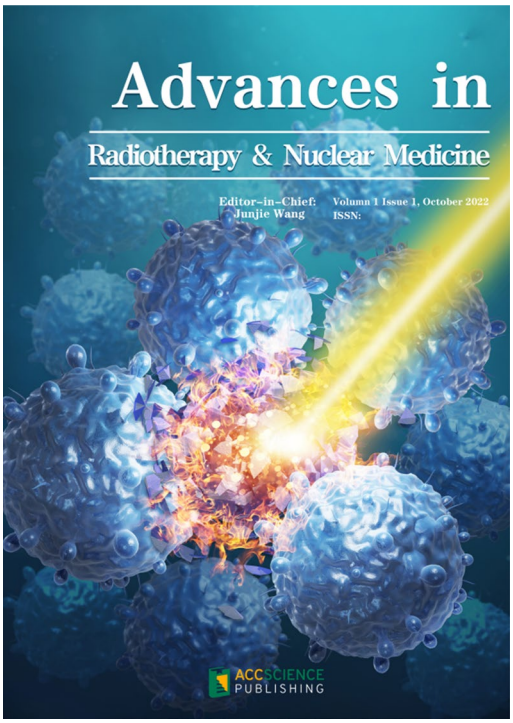


**Disclaimer**

AccScience Publishing is not liable to the statements, perspectives, and opinions contained in the publications. The appearance of advertisements in the journal shall not be construed as a warranty, endorsement, or approval of the products or services advertised and/or the safety thereof. AccScience Publishing disclaims responsibility for any injury to persons or property resulting from any ideas or products referred to in the publications or advertisements. AccScience Publishing remains neutral with regard to jurisdictional claims in published maps and institutional affiliations.

# Advances in Radiotherapy & Nuclear Medicine

Editorial Board

ACCSCIENCE PUBLISHING

Volume 2 | Issue 1 | March 2024 |

**Advances in Radiotherapy & Nuclear Medicine**

https://accscience.com/journal/ARNM

# CONTENTS

ACCSCIENCE PUBLISHING

Advances in Radiotherapy & Nuclear Medicine

ORIGINAL RESEARCH ARTICLE

# Comprehensive analysis of myelosuppression of pediatric patients receiving radiotherapy

**Yijie Sun[1], Hongjia Liu[2], Chenguang Li[2], Yubin Li[3], Huamu Xie[4], and Yibao Zhang[2]***

[1]Department of Education, Peking University People's Hospital, Beijing, China

[2]Key Laboratory of Carcinogenesis and Translational Research (Ministry of Education/Beijing), Department of Radiation Oncology, Peking University Cancer Hospital & Institute, Peking University Health Science Center Institute of Medical Technology, Beijing, China

[3]Department of Education, Peking University Health Science Centre, Beijing, China

[4]State Key Laboratory of Nuclear Physics and Technology, School of Physics, Institute of Heavy Ion Physics, Peking University, Beijing, China

## Abstract

Pediatric oncology management necessitates distinct strategies for radiotherapy due to the heightened sensitivity of pediatric bone marrow to radiation exposure compared to adults. Therefore, this study aimed to compare the risk of radiation-induced myelosuppression between pediatric and adult patients by analyzing the correlations between gender, age, active marrow distribution, and radiation-induced myelosuppression. The medical records of 49 pediatric patients aged <15 years were retrospectively analyzed. Subgroup analyses based on sex and age were conducted to compare this pediatric patient data with data from adult patients reported in the literature. The observed rate of radiation-induced myelosuppression in the pediatric group was 59.18%, which was approximately twice the rate for the adult group (34%) reported in literature. Notably, the rates of leukopenia and granulocytopenia were observed in 53% and 45% of patients suffering from radiation-induced myelosuppression, respectively, compared to rates of thrombocytopenia and hemoglobinopenia observed in only 10% of patients, indicating that white blood cells and granulocytes are more sensitive indicators of radiation-induced myelosuppression. Our findings revealed that pediatric patients receiving radiotherapy in the head-and-neck regions face a higher risk of radiation-induced myelosuppression than adult patients due to the changes in active bone marrow during childhood development. Therefore, careful consideration of radiation-induced myelosuppression is essential during protocol optimization for pediatric patients receiving radiotherapy outside the pelvic region.

***Keywords:*** Target delineation; Pediatric oncology patients; Myelosuppression; Radiation-induced injury; Radiotherapy

***Corresponding author:**
Yibao Zhang
(zhangyibao@pku.edu.cn)

**Citation:** Sun Y, Liu H, Li C, Li Y, Xie H, Zhang Y. Comprehensive analysis of myelosuppression of pediatric patients receiving radiotherapy. *Adv Radiother Nucl Med*. 2024;2(1):2519. https://doi.org/10.36922/arnm.2519

**Received:** December 23, 2023

**Accepted:** February 26, 2024

**Published Online:** March 26, 2024



## 1. Introduction

Pediatric tumors are the sixth-largest contributor to the global tumor burden.[1] Despite their substantial impact, there exists a significant scarcity of data on the management

of pediatric oncology patients compared to adult patients. Literature suggests that strategies for protecting critical organs in children should be differentiated from those employed for adults.[2-4]

Red bone marrow is one of the most sensitive tissues to radiation exposure. A study involving over 1 million European children revealed that even a low distribution of radiation dose (≥10 mGy) to active bone marrow could elevate relative risks for all hematological malignancies.[5] Throughout childhood, the distribution of red bone marrow undergoes significant changes across growth stages.[4] Radiation-induced damage to the red bone marrow results in functional inhibition, which manifests as a decrease in the number of blood cells,[6] leading to anemia and other symptoms.[7] In children, red bone marrow is distributed throughout the body and varies with age.[8] However, the existing guidelines in radiotherapy do not explicitly consider the distribution of red bone marrow in children of different ages during protocol optimization.

## 2. Materials and methods

### 2.1. Materials

Ethical approval for this retrospective study was obtained from the Institutional Review Board of Peking University Cancer Hospital and Institute (IRB#2019YJZ76). Forty-nine pediatric patients (33 males and 16 females) with a mean age of 11 (range: 5 – 15) years who underwent radiotherapy at our hospital from January 2009 to December 2019 were retrospectively selected. We utilized the basic architecture of the information aggregation tool reported by Liu *et al.*[9] to automatically extract and cluster medical record data, such as basic patient information, weekly routine blood examinations during treatment, and other relevant data for subsequent analysis. We subgrouped patients based on gender and age to analyze myelosuppression results and compared them with adult data reported in the literature.[10] The radiotherapy lesion sites in the patients enrolled in this study include head and neck (39), chest and abdomen (6), foot (1), femur (1), tibia and fibula (1), and upper limb (1); 37 out of 49 patients received chemotherapy before or during radiotherapy. The prescribed dose to the gross tumor volume (GTV) ranged from 20 – 70 Gy delivered in 10 – 33 fractions. The prescribed dose to the clinical tumor volume (CTV) ranged from 18 – 60 Gy delivered in 10 – 33 fractions. As suggested in the literature, the percentage of red bone marrow content in the skull of children aged 0 – 10 years decreases from 25.3% to 11.6%, whereas the red bone marrow content in the skull of children aged 10 – 15 years decreases by only 4.3%.[8] Therefore, the pediatric patients were subdivided into a toddler group (≤10 years old) and a young adult group (>10 years old) with a boundary of 10 years old for further analysis.

### 2.2. Evaluation of myelosuppression

The World Health Organization classifies post-radiotherapy adverse events into a grading system using four indicators: hemoglobin, leukocytes, granulocytes, and platelets (Table 1). In our study, Table 1 was used to grade myelosuppression in pediatric patients, with myelosuppression events defined as grade II or higher occurrences.[6]

### 2.3. Statistical methods

To reduce the bias in retrospective clinical studies caused by differences in baseline covariates among subgroups of patients, the present study used the nearest neighbor matching algorithm of the MatchIt software package to perform propensity score matching.[11] The data obtained using the above methods were statistically analyzed using R 3.6.1 software. Categorical data were analyzed using Fisher's exact test, while continuous data were tested using the *t*-test for a normal distribution and Wilcoxon's rank-sum test for a non-normal distribution. The significance was set at $P < 0.05$.

## 3. Results

### 3.1. Comparison of myelosuppression in children and adults

Myelosuppression was observed in 29 (59.18 %) out of 49 pediatric patients included in this study. A total of 53% of patients had leukopenia, 45% had granulocytopenia, and the incidence of thrombocytopenia and hemoglobinopenia was only 10%. Regarding patients with myelosuppression, 66% had leukopenia and granulocytopenia; thrombocytopenia and hemoglobinopenia were observed in 17.2% of patients. In contrast, the incidence of myelosuppression in adult patients reported in the literature was significantly lower, with only 34% of leukopenia of grade II or higher.[10,12]

### 3.2. Subgroup analysis of pediatric patients

#### *3.2.1. Subgrouping according to gender*

The patients were divided according to their gender. As shown in Table 2, no significant association was observed

**Table 1. Parameters of myelosuppression grade**

| Indicators of toxicity | Grades | | | | |
|---|---|---|---|---|---|
| | 0 | I | II | III | IV |
| Hemoglobin (g/L) | ≥110 | 109 – 95 | 94 – 80 | 79 – 65 | <65 |
| Leucocyte ($10^9$/L) | ≥4.0 | 3.9 – 3.0 | 2.9 – 2.0 | 1.9 – 1.0 | <1.0 |
| Granulocyte ($10^9$/L) | ≥2.0 | 1.9 – 1.5 | 1.4 – 1.0 | 0.9 – 0.5 | <0.5 |
| Platelet ($10^9$/L) | ≥100 | 99 – 75 | 74 – 50 | 49 – 25 | <25 |


https://doi.org/10.36922/arnm.2519

between gender- and radiation-induced myelosuppression (odds ratio [OR] = 1.75; 95% confidence interval [CI]: 0.52 – 5.87; $P > 0.05$).

#### 3.2.2. Subgrouping according to age

The patients were divided according to age, using a cutoff of 10. No differences were observed between the two age subgroups in terms of the location of radiotherapy in the study, as depicted in Table 3. As shown in Table 4, no significant association was observed between age- and radiation-induced myelosuppression (OR = 1.40, 95% CI: 0.42 – 4.26, $P > 0.05$).

#### 3.2.3. Subgrouping analysis

To determine the radiation dose, the patients were divided into two groups using propensity score matching.

First, the two groups were divided according to their gender. After propensity score matching, ten male and ten female patients were included, and the differences in age, prescribed dose, treatment fraction, and treatment duration between the two groups were not statistically significant ($P > 0.05$). Detailed information is presented in Table 5. The relationship between gender and myelosuppression after propensity score matching is presented in Table 6. The results revealed that gender was not associated with post-radiotherapy myelosuppression (OR = 1.47, 95% CI: 0.19 – 12.40, $P > 0.05$).

Next, patients were stratified based on an age cutoff of 10 years, and the differences in gender, prescribed dose, treatment fraction, and treatment duration between the two groups were depicted using median and quartile ranges due to the different sample sizes. After propensity score matching, 14 patients aged ≤10 years and 14 patients aged >10 years were included in the study. The differences in gender, prescribed dose, treatment fraction, and treatment duration between the two groups were not statistically significant ($P > 0.05$). Detailed information is provided in Table 7. A case–control study of the relationship between age and myelosuppression after radiotherapy is presented in Table 8, revealing no association between age and post-radiotherapy myelosuppression after grouping by age (OR = 0.76, 95% CI: 0.13 – 4.20, $P > 0.05$).

**Table 2. Relationship between sex and bone marrow suppression after radiotherapy**

| | Myelosuppression after radiotherapy | |
|---|---|---|
| | Yes | No |
| Male | 21 | 12 |
| Female | 8 | 8 |

**Table 3. Location of radiotherapy in two age subgroups**

| Radiotherapy regions | Age≤10 | Age>10 |
|---|---|---|
| Head and neck | 18 | 21 |
| Chest and abdomen | 1 | 5 |
| Foot | 0 | 1 |
| Femur | 0 | 1 |
| Tibia | 0 | 1 |
| Fibula | 0 | 1 |
| Upper limbs | 0 | 1 |

**Table 4. Relationship between age and bone marrow suppression after radiotherapy**

| Age | Myelosuppression after radiotherapy | |
|---|---|---|
| | Yes | No |
| ≤10 years | 11 | 9 |
| >10 years | 18 | 11 |

## 4. Discussion

Radiation-induced injury to normal tissues and organs is a key challenge in radiotherapy. Due to growth and development, the consequences and long-term risks of radiological injury are more severe in children than in adults.[13] As a result, there is a consensus among scholars to make special considerations for pediatric patients during treatment plan optimization that is different from those for adults. However, the specific implementation strategies for different organs require further study.

The work by Pearce *et al.*[14] demonstrated that exposure to ionizing agents during computed tomography (CT) scanning significantly increased the risk of leukemia in pediatric patients by affecting the red bone marrow. As the radiotherapy dose is much higher than the imaging dose, exposure to radiotherapy in the red bone marrow of pediatric patients increases the risk of uncertain effects, such as secondary carcinogenicity. Radiotherapy also directly increases the risk of side effects such as myelosuppression, which is clinically manifested by significant changes in routine blood parameters and is one of the major risks during radiotherapy in pediatric patients. The present study revealed that, compared to the reported incidence of radiation-induced myelosuppression of more than grade II in approximately 32% of adult patients in the head and neck regions, the incidence in pediatric patients was 59.18%, approximately double that of adults. Another study on radiation-induced myelosuppression of more than grade III in adults and children observed a similar phenomenon: the percentage of leukopenia of more than grade III was 32%, which was higher than that of 3% in the

**Table 5. Description of baseline data before and after propensity matching according to gender**

| Variant | Before matching | | After matching | | *P*-value |
|---|---|---|---|---|---|
| | Male patient (*n*=33) | Female patient (*n*=16) | Male patient (*n*=10) | Female patient (*n*=10) | |
| Age (years) | 12 (9, 14) | 10 (9, 14) | 11 (9, 14) | 10 (9, 13) | 0.71 |
| Prescribed dose (Gy) | 30 (22, 56) | 40 (23.25, 50) | 30 (24, 49) | 38 (22.5, 47.5) | 0.94 |
| Treatment fraction | 15 (11, 28) | 20 (12, 25) | 15 (12, 24) | 19 (11, 24) | 0.88 |
| Duration of treatment (days) | 17 (14, 35) | 27 (14, 31) | 19 (15, 32) | 28 (15, 32) | 0.74 |

Note: The values are presented as median (quartile ranges).

**Table 6. Relationship between sex after propensity matching and bone marrow suppression after radiotherapy**

| Myelosuppression after radiotherapy | Male patient | Female patient |
|---|---|---|
| Yes | 4 | 5 |
| No | 6 | 5 |

adult group, while the percentage of thrombocytopenia of more than grade III was 8%, which was also higher than that of 4.7% in the adult group.[13] The higher incidence of radiation-induced myelosuppression in pediatric patients may be related to the following factors: (i) higher radiosensitivity in pediatric patients[15] and (ii) current protocol optimization only considers red bone marrow protection when designing radiotherapy plans for the pelvic region, lacking targeted protection for the red bone marrow distributed in the whole body in children, which varied with age.

To further investigate the correlation between radiation-induced myelosuppression and pediatric patients' gender and age and to provide more precise evidence for optimizing protocols, we analyzed the data in subgroups according to gender and further subdivided patients with a cutoff of 10 years of age but did not observe a significant correlation. However, another study of 79 children concluded that children younger than 6 years old were significantly more likely to develop thrombocytopenia (29% vs. 8.7%) and were twice as likely to develop neutropenia as children older than 6 years old (41% vs. 21%).[16] This may be related to the small sample size of our study. In addition, the red bone marrow content in the head-and-neck region declined rapidly in children aged 0 to 10 years, and the ratio of red bone marrow in the head-and-neck region to whole-body red bone content gradually decreased after the age of 10.

Our study revealed that leukopenia and granulocytopenia were the most sensitive indicators of myelosuppression in pediatric patients (53% and 45%, respectively) and that 66% of patients with myelosuppression experienced both leukopenia and granulocytopenia. In contrast, platelets and hemoglobin were less sensitive, consistent with previous reports on adult patients.[17] In a study involving 52 pediatric patients, the incidence of leukopenia exceeding grade II surpassed that of grade II thrombocytopenia (69% *vs.* 5.7%).[17] These data suggest the potential variation in the effects of radiotherapy on different hematopoietic cell types.

Myelosuppression is an important factor in the interruption and discontinuation of radiotherapy, often resolving after treatment cessation; however, in severe cases, patients require prompt clinical intervention, such as recombinant human granulocyte stimulating factor injection. A report on radiation-induced myelosuppression in pediatric patients observed that 69% of the patients developed higher than grade II leukopenia, and the number of leukocytes began to recover on the 5$^{th}$ day after the occurrence of the lowest value; 5.7% of the patients developed grade II thrombocytopenia; and the number of platelets began to recover on the 4$^{th}$ day after the occurrence of the lowest value.[17] However, the study did not elaborate on the treatment of pediatric patients after the occurrence of myelosuppression. The rate of recovery of routine blood markers with different treatments after myelosuppression depends on future large-scale prospective randomized controlled trials.

Due to the retrospective study design, we were unable to investigate the volume and dose of red bone marrow. The bone marrow was not segmented during the treatment planning stage, and the dose to the bone marrow was not optimized. One challenge in segmenting the bone marrow from the cancellous bone was the relatively large spatial resolution of the planning CT images, making this process time-consuming and clinically concerning. Therefore, according to literature, the dose to the bone marrow is usually approximated using the dose to the bone[18] or estimated from the total dose.[14] Moreover, the medical records of some patients could not be fully retrieved to study the impact of chemotherapy, as they were treated at other hospitals before undergoing radiotherapy at our institution. These limitations require further investigations in the future based on a more reliable prospective and randomized study design with a larger patient volume.

**Table 7. Description of baseline data before and after propensity matching according to age**

| Variants | Before matching | | After matching | | *P*-value |
|---|---|---|---|---|---|
| | Age≤10 years (*n*=20) | Age>10 years (*n*=29) | Age≤10 years (*n*=14) | Age>10 years (*n*=14) | |
| Gender | | | | | |
| Male | 11 | 22 | 11 | 10 | 1 |
| Female | 9 | 7 | 3 | 4 | |
| Prescribed dose (Gy) | 23.25 (21.225, 33) | 50 (30, 60) | 24 (21, 47.5) | 26.65 (22, 50) | 0.30 |
| Treatment fraction | 12 (11, 17) | 20 (15, 30) | 12 (11, 24) | 13 (11, 24) | 0.59 |
| Duration of treatment (days) | 16 (14, 28) | 28 (14, 37) | 17 (15, 29) | 16 (15, 34) | 0.85 |

Note: The values are presented as median (quartile ranges) for prescribed dose, treatment fraction, and duration of treatment.

**Table 8. Relationship between age after propensity matching and bone marrow suppression after radiotherapy**

| Myelosuppression after radiotherapy | Age≤10 years | Age>10 years |
|---|---|---|
| Yes | 7 | 8 |
| No | 7 | 6 |

In summary, based on data from 49 radiotherapy patients under 15 years old, our study revealed that the incidence of myelosuppression of grade II or higher was approximately twice as high as that in adults, suggesting that the dynamic changes in the distribution of red bone marrow with age should be taken into account in protocol optimization for pediatric patients. In addition, beyond traditional focus areas such as the pelvic region and red bone marrow in the head-and-neck region should be considered in pediatric patients. In addition, other factors affecting radiotherapy should also be taken into consideration.[19,20] Additional age-group-based segmentation strategies for pediatric patients require support from prospective large-sample studies.

## 5. Conclusion

This study revealed that there was higher incidence of myelosuppression of grade II or higher in pediatric patients than in adults. However, no significant association was observed between age or gender and radiation-induced myelosuppression. These results underscore the importance of carefully considering radiation-induced myelosuppression during the protocol optimization of radiotherapy.

## Acknowledgments

None.

## Funding

This study was supported by the National Nature Science Foundation of China (award number: 12275012) and the Natural Science Foundation of Beijing Municipality (award number: Z210008).

## Conflict of interest

The authors declare that they have no competing interests.

## Author contributions

*Conceptualization:* Yibao Zhang
*Formal analysis:* Yijie Sun, Chenguang Li
*Investigation:* Hongjia Liu, Chenguang Li, Huamu Xie
*Methodology:* Yijie Sun, Hongjia Liu
*Writing – original draft:* Yijie Sun
*Writing – review & editing:* Yibao Zhang

## Ethics approval and consent to participate

Ethical approval was obtained for this retrospective study (IRB#2019YJZ76) from the Peking University Cancer Hospital and Institute, China.

## Consent for publication

Waiver of informed consent applies to this retrospective study.

## Availability of data

Data used in this work are available from the corresponding author on reasonable request.

## References

1. Force LM, Abdollahpour I, Advani SM, *et al*. The global burden of childhood and adolescent cancer in 2017: An analysis of the Global Burden of Disease Study 2017. *Lancet Oncol*. 2019;20(9):1211-1225.

   doi: 10.1016/s1470-2045(19)30339-0

2. Steinmeier T, Schleithoff SS, Timmermann B. Evolving radiotherapy techniques in paediatric oncology. *Clin Oncol* (*R Coll Radiol*). 2019;31(3):142-150.

   doi: 10.1016/j.clon.2018.12.005

3. Hindorf C, Glatting G, Chiesa C, Lindén O, Flux G. EANM Dosimetry committee guidelines for bone marrow and whole-body dosimetry. *Eur J Nucl Med Mol Imaging*.

2010;37(6):1238-1250.

doi: 10.1007/s00259-010-1422-4

4. Hua CH, Mascia AE, Seravalli E, Lomax AJ, Seiersen K, Ulin K. Advances in radiotherapy technology for pediatric cancer patients and roles of medical physicists: COG and SIOP Europe perspectives. *Pediatr Blood Cancer*. 2021;68(Suppl 2):e28344.

doi: 10.1002/pbc.28344

5. Bosch de Basea Gomez M, Thierry-Chef I, Harbron R, *et al*. Risk of hematological malignancies from CT radiation exposure in children, adolescents and young adults. *Nat Med*. 2023;29:3111-3119.

doi: 10.1038/s41591-023-02620-0

6. Sylvester R. WHO handbook for reporting results of cancer treatment: WHO offset publication #48 World Health Organization, Geneva, 1979, 45 pages, 6 Swiss Francs. *Control Clin Trials*. 1980;1(3):276-277.

doi: 10.1016/0197-2456(80)90009-4

7. Gilreath JA, Stenehjem DD, Rodgers GM. Diagnosis and treatment of cancer-related anemia. *Am J Hematol*. 2014;89(2):203-212.

doi: 10.1002/ajh.23628

8. Cristy M. Active bone marrow distribution as a function of age in humans. *Phys Med Biol*. 1981;26(3):389-400.

doi: 10.1088/0031-9155/26/3/003

9. Liu H, Wang J, Huang Y, *et al*. Development and validation of a Web-crawler-based medical records information aggregation tool. *Chin J Med Phys*. 2021;11(5):1444-1448.

doi: 10.3969/j.issn.1005-202X.2021.11.022

10. Harari PM, Harris J, Kies MS, *et al*. Postoperative chemoradiotherapy and cetuximab for high-risk squamous cell carcinoma of the head and neck: Radiation Therapy Oncology Group RTOG-0234. *J Clin Oncol*. 2014;32(23):2486-2495.

doi: 10.1200/jco.2013.53.9163

11. Ho D, Imai K, King G, Stuart EA. MatchIt: Nonparametric preprocessing for parametric causal inference. *J Stat Softw*. 2011;42(8):1-28.

doi: 10.18637/jss.v042.i08

12. Zamboglou N, Achterrath W, Schnabel T, Lenaz L, Kolotas C, Schmitt G. Simultaneous radiotherapy and chemotherapy with carboplatin in inoperable squamous cell carcinoma of the head and neck: A phase II study. *Cancer Invest*. 1992;10(5):349-355.

doi: 10.3109/07357909209024794

13. Jefferies S, Rajan B, Ashley S, Traish D, Brada M. Haematological toxicity of cranio-spinal irradiation. *Radiother Oncol*. 1998;48(1):23-27.

doi: 10.1016/s0167-8140(98)00024-3

14. Pearce MS, Salotti JA, Little MP, *et al*. Radiation exposure from CT scans in childhood and subsequent risk of leukaemia and brain tumours: A retrospective cohort study. *Lancet*. 2012;380(9840):499-505.

doi: 10.1016/s0140-6736(12)60815-0

15. Constine LS, Ronckers CM, Hua CH, *et al*. Pediatric normal tissue effects in the clinic (PENTEC): An International Collaboration to analyse normal tissue radiation dose-volume response relationships for paediatric cancer patients. *Clin Oncol* (*R Coll Radiol*). 2019;31(3):199-207.

doi: 10.1016/j.clon.2019.01.002

16. Chang EL, Allen P, Wu C, Ater J, Kuttesch J, Maor MH. Acute toxicity and treatment interruption related to electron and photon craniospinal irradiation in pediatric patients treated at the University of Texas M. D. Anderson Cancer Center. *Int J Radiat Oncol Biol Phys*. 2002;52(4):1008-1016.

doi: 10.1016/s0360-3016(01)02717-1

17. Kumar N, Miriyala R, Thakur P, *et al*. Impact of acute hematological toxicity on treatment interruptions during cranio-spinal irradiation in medulloblastoma: A tertiary care institute experience. *J Neurooncol*. 2017;134(2):309-315.

doi: 10.1007/s11060-017-2524-7

18. Zhang Y, Yan Y, Nath R, Bao S, Deng J. Personalized estimation of dose to red bone marrow and the associated leukaemia risk attributable to pelvic kilo-voltage cone beam computed tomography scans in image-guided radiotherapy. *Phys Med Biol*. 2012;57(14):4599-4612.

doi: 10.1088/0031-9155/57/14/4599

19. Wang Y, Wang H, Zheng A, *et al*. Study on setup errors for different body carcinoma radiotherapy with image guidance in TOMO-HD. *Chin J Radiol Health*. 2021;30(3):331-338.

doi: 10.13491/j.issn.1004-714x.2021.03.015

20. Hui H, Wang Q, Cui L, *et al*. Application of multimedia information technology on precision radiotherapy for patients with head and neck malignant tumors. *Chin J Radiol Health*. 2022;31(2):239-244.

doi: 10.13491/j.issn.1004-714X.2022.02.020

ACCSCIENCE PUBLISHING

Advances in Radiotherapy & Nuclear Medicine

ORIGINAL RESEARCH ARTICLE

# Blood glucose level affects iodine-123 labeled MIBG uptake in the lung

**Andreas Lim[1,2], Minseok Suh[1], and Gi Jeong Cheon[1]***

[1]Department of Nuclear Medicine, Seoul National University Hospital, Seoul, Republic of Korea

[2]Department of Nuclear Medicine and Molecular Theragnostic, Indriati General Hospital, Sukoharjo, Indonesia

## Abstract

The aim of this study was to evaluate the correlation of blood glucose and the metaiodobenzylguanidine (MIBG) uptake in lung and compare the difference between the lung uptake of MIBG in diabetic and non-diabetic patients. Patients who underwent iodine-123 MIBG whole-body scan (WBS) in the Department of Nuclear Medicine Seoul National University Hospital between January 2014 and July 2022 were recruited and analyzed. Semi-quantitative analysis of the mean value of lung-to-mediastinum ratio (LMR) was performed. Correlation was analyzed with Pearson correlation test and mean difference was analyzed with independent *t*-test. There were 36 patients in diabetic group and 57 patients in non-diabetic group with mean age of 56 ± 14.1 and 52 ± 14.6 years, respectively. The mean 24-h LMRs in diabetic and non-diabetic groups were 1.38 ± 0.20 and 1.17 ± 0.14, respectively. Fasting glucose showed a mean value of 136 ± 37.7 and 96 ± 8.2 mg/dL, respectively. There was a significant positive correlation in diabetic ($r = 0.397$; $P = 0.016$) and non-diabetic groups ($r = 0.579$; $P < 0.001$) with significant mean difference (0.21; $P < 0.001$). In conclusion, lung uptake of MIBG is positively correlated with blood sugar level, with diabetic patients displaying higher lung uptake of MIBG compared with non-diabetic patients. In addition, higher lung uptake of MIBG is evident in patients with higher fasting glucose level and even in non-diabetic patients. Thus, in the situations where MIBG therapy is required, the radiation dose to the lungs must be carefully adjusted for patients with high blood sugar level.

***Keywords:*** Blood glucose level; Lung uptake; MIBG

***Corresponding author:**
Gi Jeong Cheon
(larrycheon@gmail.com)

**Citation:** Lim A, Suh M, Cheon GJ. Blood glucose level affects iodine-123 labeled MIBG uptake in the lung. *Adv Radiother Nucl Med*. 2024;2(1):2506. https://doi.org/10.36922/arnm.2506

**Received:** December 21, 2023

**Accepted:** January 8, 2024

**Published Online:** March 27, 2024



## 1. Introduction

Metaiodobenzylguanidine (MIBG) is an analog of the adrenergic neuron-blocking agent guanethidine, and it bears a high-degree resemblance in the aspects of uptake, storage, release mechanisms, and structure with neurotransmitter norepinephrine (NE), which is predominantly released from the sympathetic nerve endings.[1-3] MIBG can be labeled with several radioiodine nuclides, such as I-131, and I-123, and has been used to image and treat neuroendocrine tumours.[3]

I-131 emits two types of radiation: Beta minus (β-) used for therapy purposes, and gamma (γ) for diagnostic purposes.[4] In rare case, I-131 could cause pulmonary fibrosis if there is diffuse uptake in the lung and the risk is increasing with higher cumulative amount given over an extended period.[5,6]

Diabetes has been linked to the increased uptake and retention of MIBG in the lung due to the dysfunction of sympathetic nerve.[7-10] It is also believed that the enhanced permeability of the pulmonary endothelial cells could also increase the uptake of MIBG in the lung.[11] A study conducted by Hempel *et al.* found that high glucose concentration could increase the permeability of the endothelial cell.[12] To the best of our knowledge, lung uptake of MIBG in non-diabetic patients has never been reported in the literature.

The aim of this study was to evaluate the correlation between blood glucose and lung uptake of MIBG and to compare the difference in lung uptake of MIBG between diabetic and non-diabetic patients.

## 2. Materials and methods

### 2.1. Materials

All patients who underwent I-123 MIBG whole-body scan (WBS) in the Department of Nuclear Medicine, Seoul National University Hospital (SNUH), between January 2014 and July 2022 were recruited and analyzed (Figure 1). Adult patients aged older than 19 years[13] were included in this study. Patients with metastasis in chest area and patients who did not have fasting glucose were excluded from this study.

### 2.2. Methods

#### *2.2.1. Study protocol*

Single-photon emission computerized tomography/computed tomography from General Electric Healthcare with low-energy, high-resolution collimator, with an energy window of 159 keV ± 7.5, was used in this study.

I-123 MIBG with a dosage of 110 – 370 MBq was injected slowly through intravenous mode. Whole-body planar image, from head to thigh, was acquired at 24-h post-injection with bed speed of 6 cm/min.

#### *2.2.2. Image analysis*

Image analysis was performed semi-quantitatively (Figure 2). A region of interest (ROI), measuring $2 \times 3$ cm$^2$, was drawn manually and placed on the right-middle lung and on the mediastinum to calculate the lung-to-mediastinum ratio (LMR).

#### *2.2.3. Statistical analysis*

Data are expressed as mean ± standard deviation (SD). Pearson's correlation test was used to evaluate the statistical significance between the uptake of I-123 MIBG in the lung and the fasting glucose level. The Pearson's coefficient (r) values were stratified into three groups, based on the strength of the association: small, medium, and large association (Table 1).[14]

Independent *t*-test was used to evaluate statistical significance of the difference between the different groups. $P < 0.05$ was statistically significant. IBM SPSS® Statistic v. 27 software was used in statistical analyses.

#### *2.2.4. Ethical clearance*

This retrospective study has been approved by SNUH Institutional Review Board.

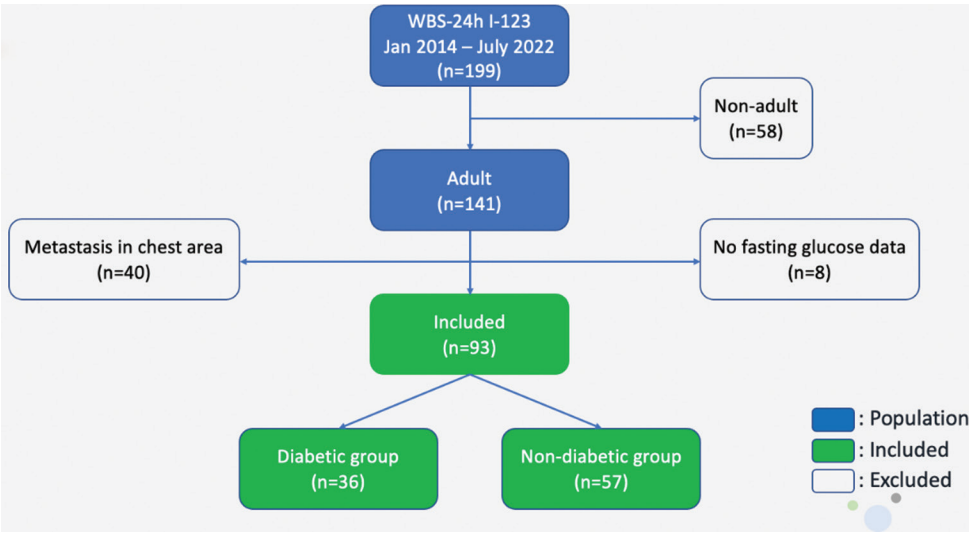


**Figure 1.** Subjects selection workflow. A total of 199 patients were recruited and analyzed. Based on the exclusion criteria, 106 patients were excluded from this study. The patients recruited in this study ($n$ = 93) were divided into two groups based on their diabetic status.

## 3. Results

### 3.1. Patients' characteristics

A total of 199 patients had undergone I-123 MIBG whole body scan from January 2014 to July 2022. A total 106 patients were excluded from this study, with 58 of them being non-adult patients, 40 having metastasis in chest area, and eight having no fasting glucose data. Ninety-three patients were included in this study and were divided into two groups based on their diabetic status. Diabetic group consisted of 36 patients (21 males and 15 females), while non-diabetic group consisted of 57 patients (28 males and 29 females), with mean age of 56 ± 14.1 years and 52 ± 14.6 years, respectively. Patients' characteristics of both diabetic and non-diabetic groups are summarized in Table 2.

Fasting glucose showed a mean value of 136 ± 37.7 mg/dL in diabetic group and 96 ± 8.2 mg/dL in non-diabetic group. The time interval between the I-123 MIBG WBS and the fasting glucose determination was 17 ± 39.9 days and 21 ± 32.6 days, respectively, for diabetic and non-diabetic groups.

### 3.2. Iodine-123 MIBG lung-to-mediastinum ratio

In this study, the 24-h LMRs for patients in diabetic group and those in non-diabetic group were 1.38 ± 0.20 and 1.17 ± 0.14, respectively (Figure 3).

### 3.3. Correlation between fasting glucose and I-123 MIBG LMR

Pearson's correlation analysis revealed a significant positive, large association between fasting glucose and 24-h LMR, regardless of diabetic status, with Pearson's $r = 0.596$ ($P < 0.001$; Figure 4).

The correlations between fasting glucose level and mean 24-h LMR of diabetic group and non-diabetic group were also separately analyzed in this study. These two factors were correlated with a medium strength of association in the diabetic group (Pearson's $r = 0.397$; $P = 0.016$) (Figure 5). A strong correlation between fasting glucose level and mean 24-h LMR was detected in the non-diabetic group, with Pearson's $r = 0.579$ ($P < 0.001$) (Figure 5).

## 4. Discussion

A neuroendocrine tumor (NET) is a rare tumor that can develop in many different organs of the body. It is formed from cells that release hormones into the blood in response to a signal from the nervous system. Some examples of NET are carcinoid tumors, islet cell tumors, medullary thyroid cancer, pheochromocytomas, Merkel cell cancer, and small-cell lung cancer.[15,16]

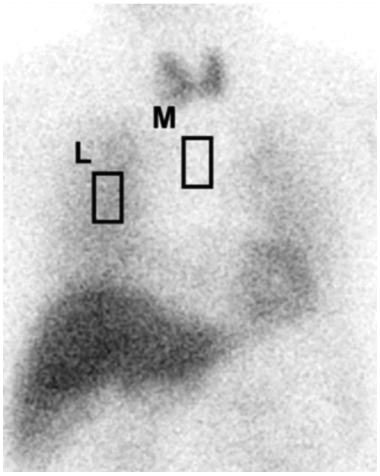


**Figure 2.** Semi-quantitative analysis. A 2 × 3 $cm^2$ region of interest was drawn manually and placed on the right-middle lung and on the mediastinum to calculate the lung-to-mediastinum ratio.

**Table 1. Pearson's coefficient (*r*) between lung uptake of I-123 MIBG and fasting glucose level**

| Strength of association | Coefficient (*r*) | |
|---|---|---|
| | Positive | Negative |
| Small | 0.1 – 0.3 | −0.1 – −0.3 |
| Medium | 0.3 – 0.5 | −0.3 – −0.5 |
| Large | 0.5 – 1.0 | −0.5 – −1.0 |

Abbreviation: MIBG: Metaiodobenzylguanidine.

**Table 2. Patients' characteristics**

| | Diabetic group (*n*=36) | Non-diabetic group (*n*=57) | *P* |
|---|---|---|---|
| Mean age (years) | 56±14.1 | 52±14.6 | 0.21 |
| Gender | | | 0.343 |
| Male | 21 (58%) | 28 (49%) | |
| Female | 15 (42%) | 29 (51%) | |
| Fasting glucose (mg/dL) | 136±37.7 | 96±8.2 | <0.001 |
| Time interval between MIBG imaging and fasting glucose determination (day) | 17±39.9 | 21±32,6 | 0.184 |

Note: Data of quantitative variables are expressed as mean±SD, where data of categorical variables are expressed as count (percentage).
Abbreviation: MIBG: Metaiodobenzylguanidine.

MIBG has been shown to be able to locate and treat NET.[17,18] It can be labeled with radioactive iodine nuclides, such as I-131 and I-123. Figures 6-8 show I-123 MIBG WBSs of three representative cases recruited in this study. All NETs share a set of similarities, in terms of the neuroendocrine secretory granules stored by the tumors, amine precursor uptake mechanism, and biogenic amine

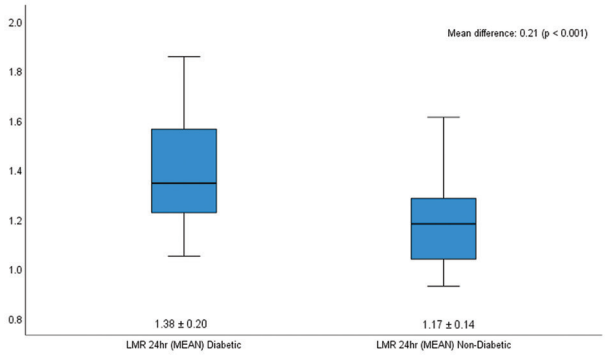


**Figure 3.** Mean 24-h lung-to-mediastinum ratio (LMR) in diabetic and non-diabetic groups. Diabetic group showed a mean 24-h LMR value of 1.38 ± 0.20 and non-diabetic group 1.17 ± 0.14. There was a significant mean difference between these groups (0.21; $P < 0.001$).

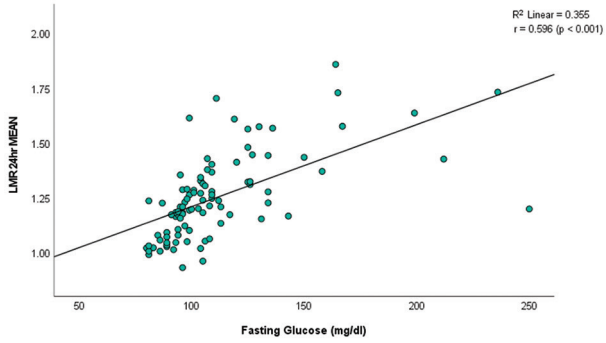


**Figure 4.** Correlation between fasting glucose level and mean 24-h lung-to-mediastinum ratio (LMR). There was a significant positive correlation between fasting glucose level and mean 24-h LMR, irrespective of diabetic status, with Pearson's $r = 0.596$ ($P < 0.001$).

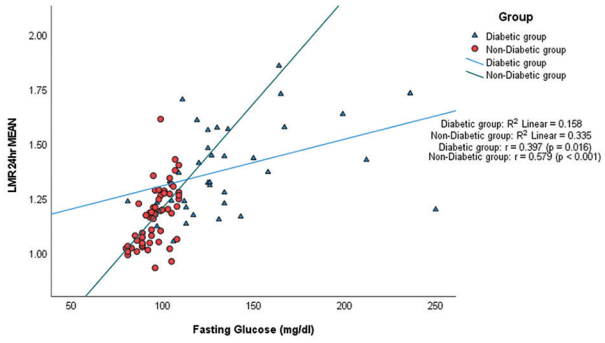


**Figure 5.** Correlation between fasting glucose and mean 24-h lung-to-mediastinum ratio in diabetic and non-diabetic groups. Pearson's correlation analysis revealed significant positive correlations, separately, in diabetic ($r = 0.397$; $P = 0.016$) and non-diabetic groups ($r = 0.579$; $P < 0.001$).

synthesis, storage, and reuptake, but in some tissues, peptide hormone or neuromodulator is the main secretory element.[1-3,19] MIBG enters the adrenal medullae by a specific, energy-dependent uptake mechanism (uptake 1)

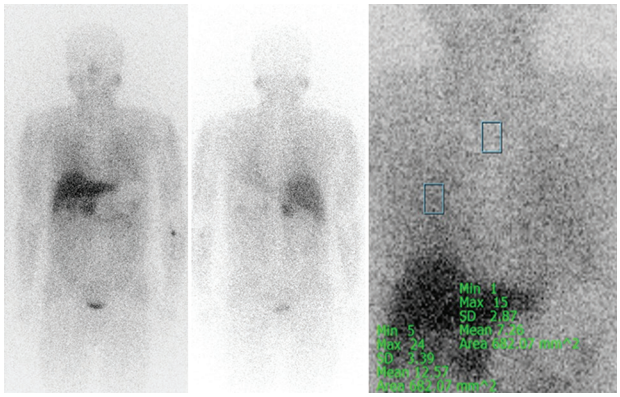

**Figure 6.** A 67-year-old diabetic man diagnosed with paraganglioma underwent I-123 MIBG whole-body scan. His fasting glucose level was 236 mg/dL, and his 24-h lung-to-mediastinum ratio was 1.73.

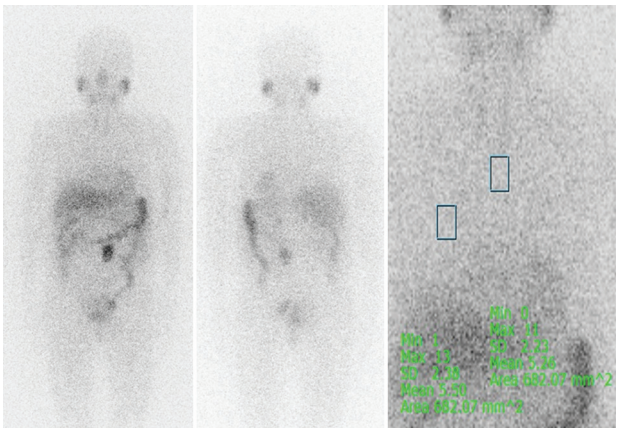

**Figure 7.** A 63-year-old non-diabetic woman diagnosed with paraganglioma underwent I-123 MIBG whole-body scan. Her fasting glucose level was 93 mg/dL, and her 24-h lung-to-mediastinum ratio (LMR) was 1.05, which was lower than the LMR of a representative diabetic patient (Figure 6).

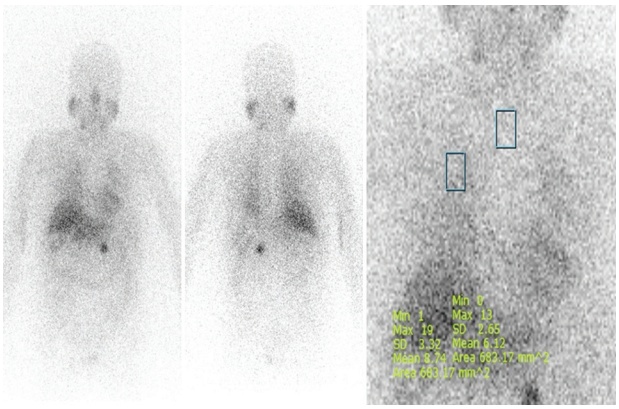

**Figure 8.** An 83-year-old non-diabetic woman diagnosed with pheochromocytoma underwent I-123 MIBG whole-body scan. Her fasting glucose level was 107 mg/dL with a 24-h lung-to-mediastinum ratio of 1.43. The scan indicates that MIBG uptake could also increase in non-diabetic patients.

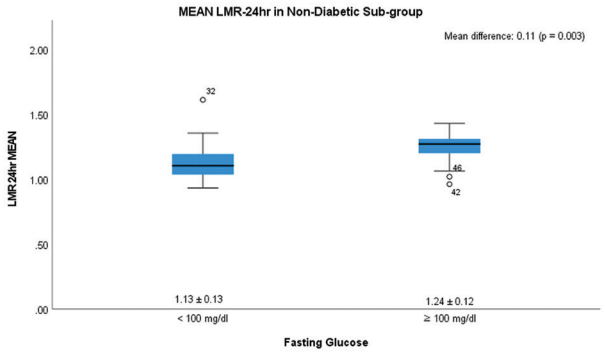


**Figure 9.** Mean 24-h lung-to-mediastinum ratio (LMR) in subgroups of non-diabetic patients. The mean 24-h LMR values for <100 mg/dL group and ≥100 mg/dL group were 1.13 ± 0.13 and 1.24 ± 0.12, respectively. These mean 24-h LMR values showed a significant difference of 0.11 ($P = 0.003$).

in which it competes with NE, although the kinetics are not those of competitive inhibition.[20,21]

I-131 is one of radioactive iodine nuclides. It emits beta particles (606 keV) and gamma radiation (364 keV); thus, it could be used for therapy and diagnostic purposes.[4,22] I-123 is a pure gamma emitter (159 keV) and is an excellent nuclide for diagnostic purposes.[23]

Several studies have reported the incidents of pulmonary fibrosis accompanied by the increased uptake and retention of I-131 in the lung.[5,6] A study conducted by Murashima *et al.* found that MIBG uptake in the lung was increased in diabetic patients, while Unlü and Inanir found that the lung uptake of MIBG in diabetic patients not only increased but also manifested prolonged retention.[9,10] In this study, diabetic patients experienced increased MIBG uptake in lung, with a mean LMR value of 1.38 ± 0.20. This could be caused by the dysfunction of sympathetic nervous system or the enhanced permeability of the pulmonary endothelial cells that could happen in diabetic patients as previously described.[7-11] We also observed the increase of MIBG uptake in the lung as well in the non-diabetic patients with a mean LMR value of 1.17 ± 0.14. For further analysis, we divided the non-diabetic patients into two groups based on fasting glucose levels: <100 mg/dL group and ≥100 mg/dL group. Analysis of the further stratified non-diabetic patients revealed that the mean LMR value was higher in ≥100 mg/dL group with a mean difference of 0.11 ($P = 0.003$; Figure 9).

Several studies have found that prediabetic status may increase the prevalence of cardiac autonomic neuropathy (CAN).[24,25] Impaired fasting glucose and impaired glucose tolerance are two forms of glucose dysmetabolism that fit the general definition of prediabetes. The fasting glucose level in prediabetic individuals falls within the range of 100 – 125 mg/dL.[26] We believed that being in the prediabetic status and having suffered early CAN would contribute to the increased lung uptake of MIBG observed in non-diabetic patients.

This study failed to analyze the correlation of the increased MIBG uptake in the lung with the effect of pulmonary cells irradiation. However, this study unveiled a significant positive correlation with large association strength between glucose level and lung uptake of MIBG, regardless of the diabetic status ($r = 0.596$; $P < 0.001$). Thus, a prospective study is warranted to further investigate this correlation.

Several limitations in this study should be acknowledged. First, the patients recruited in this study were retrospectively examined; second, the time intervals between fasting glucose determination and MIBG imaging were inconsistent across patients. Further prospective study involving large sample size should be conducted to confirm the result of this study.

## 5. Conclusion

Lung uptake of MIBG is positively correlated with blood sugar level, with higher MIBG uptake in diabetic patients than in non-diabetic patients. Furthermore, higher lung uptake of MIBG is also manifested by patients with higher fasting glucose level and even non-diabetic patients. Therefore, it is of clinical importance to exercise caution when administering radiation dose to patients with high blood sugar level if MIBG therapy is deemed necessary.

## Acknowledgments

None.

## Funding

This study is supported by the National Research Foundation of Korea (NRF-2020R1A2C2011428).

## Conflict of interest

The authors declare that they have no conflicts of interest.

## Author contributions

*Conceptualization:* All authors
*Investigation:* Andreas Lim
*Methodology:* Andreas Lim
*Formal analysis:* Andreas Lim, Minseok Suh
*Writing – original draft:* Andreas Lim
*Writing – review & editing:* Minseok Suh, Gi Jeong Cheon

## Ethics approval and consent to participate

This retrospective study was approved by SNUH Institutional Review Board (IRB No. H-2211-109-1380)

and performed in accordance with the ethical standards laid down in the 1964 Declaration of Helsinki and its later amendments.

## Consent for publication

Not applicable.

## Availability of data

Data used in this work are available from the corresponding author on reasonable request.

## References

1. Wieland DM, Wu J, Brown LE, Mangner TJ, Swanson DP, Beierwaltes WH. Radiolabeled adrenergic neuron-blocking agents: Adrenomedullary imaging with [131I] iodobenzylguanidine. *J Nucl Med*. 1980;21:349-353.
2. Sisson JC, Wieland DM, Sherman P, Mangner TJ, Tobes MC, Jacques S Jr. Metaiodobenzylguanidine as an index of the adrenergic nervous system integrity and function. *J Nucl Med*. 1987;28:1620-1624.
3. Kayano D, Kinuya S. Current consensus on I-131 MIBG therapy. *Nucl Med Mol Imaging*. 2018;52:254-265.

   doi: 10.1007/s13139-018-0523-z
4. Dendy PP, Goldstone KE, Parkin A, Barber RW. Radiation protection. In: Sharp PF, Gemmell HG, Murray AD, editors. *Practical Nuclear Medicine*. London: Springer-Verlag; 2005. p. 91-111.

   doi: 10.1007/b136183
5. Haugen BR, Alexander EK, Bible KC, *et al*. 2015 American Thyroid Association management guidelines for adult patients with thyroid nodules and differentiated thyroid cancer: The American Thyroid Association guidelines task force on thyroid nodules and differentiated thyroid cancer. *Thyroid*. 2016;26:1-133.

   doi: 10.1089/thy.2015.0020
6. Liu B, Zeng Y, Wang J, Zhao Z, Mu D, Kuang A. Lungs absorbed dose in radioiodine therapy of differentiated thyroid carcinoma with diffuse pulmonary metastases. *Sheng Wu Yi Xue Gong Cheng Xue Za Zhi*. 2010;27:851-854.
7. Murata K, Sumida Y, Murashima S, *et al*. A novel method for the assessment of autonomic neuropathy in type 2 diabetic patients: A comparative evaluation of 123I-MIBG myocardial scintigraphy and power spectral analysis of heart rate variability. *Diabet Med*. 1996;13:266-272.

   doi: 10.1002/(SICI)1096-9136(199603)13:3<266:AID-DIA72>3.0.CO;2-4
8. Mäntysaari M, Kuikka J, Mustonen J, *et al*. Noninvasive detection of cardiac sympathetic nervous dysfunction in diabetic patients using [123I] metaiodobenzylguanidine. *Diabetes*. 1992;41:1069-1075.

   doi: 10.2337/diab.41.9.1069
9. Murashima S, Takeda K, Matsumura K, *et al*. Increased lung uptake of iodine-123-MIBG in diabetics with sympathetic nervous dysfunction. J Nucl Med. 1998;39:334-338.
10. Unlü M, Inanir S. Prolonged lung retention of iodine-123-MIBG in diabetic patients. *J Nucl Med*. 1998;39:116-118.
11. Mu X, Hasegawa S, Yoshioka J, *et al*. Clinical value of lung uptake of iodine-123 metaiodobenzylguanidine (MIBG), a myocardial sympathetic nerve imaging agent, in patients with chronic heart failure. *Ann Nucl Med*. 2001;15:411-416.
12. Hempel A, Maasch C, Heintze U, *et al*. High glucose concentrations increase endothelial cell permeability via activation of protein kinase CA. *Circ Res*. 1997;81:363-371.

    doi: 10.1161/01.res.81.3.363
13. Canêo LF, Neirotti R. The importance of the proper definition of adulthood: What is and what is not included in a scientific publication. *Braz J Cardiovasc Surg*. 2017;32(1):60.

    doi: 10.21470/1678-9741-2016-0049
14. Schober P, Boer C, Schwarte LA. Correlation coefficients: appropriate use and interpretation. *Anesth Analg*. 2018;126(5):1763-1768.

    doi: 10.1213/ANE.0000000000002864
15. *Neuroendocrine Tumours*; 2017. Available from: https://www.nhs.uk/conditions/neuroendocrine-tumours [Last accessed on 2023 Dec 20].
16. Hong CM, Jeong YJ, Kim HW, et al. KSNM60 in Nuclear Endocrinology: from the Beginning to the Future. Nucl Med Mol Imaging. 2022;56(1):17-28.

    doi: 10.1007/s13139-021-00728-0
17. Moll L, Mcewan A, Shapiro B, *et al*. Iodine-131 MIBG scintigraphy of neuroendocrine tumors other than pheochromocytoma and neuroblastoma. *J Nucl Med*. 1987;28(6):979-988.
18. Binderup T, Knigge U, Loft A, *et al*. Functional imaging of neuroendocrine tumors: A head-to-head comparison of somatostatin receptor scintigraphy, 123I-MIBG scintigraphy, and 18F-FDG PET. *J Nucl Med*. 2010;51:704-712.

    doi: 10.2967/jnumed.109.069765
19. Gould VE, Memoli V, Chejfec G, *et al*. The AUPD cell system and its neoplasms: Observations on the significance and limitations of the concept. *Surg Clin N Am*. 1979;59:93-107.

    doi: 10.1016/s0039-6109(16)41736-6
20. Jaques S Jr., Tobes MC, Sisson JC, Baker JA, Wieland DM. Comparison of the sodium dependency of uptake of meta-Iodobenzylguanidine and norepinephrine into cultured bovine adrenomedullary cells. *Mol Pharmacol*. 1984;26(3):539-546.

21. Tobes MC, Jaques S, Wieland DM, Sisson JC. Effect of uptake-one inhibitors on the uptake of norepinephrine and metaiodobenzylguanidine. *J Nucl Med*. 1985;26(8):897-907.

22. Mody VV, Singh AN, Deshmukh R, Shah S. Chapter 40 - Thyroid hormones, iodine and iodides, and antithyroid drugs. In: Ray SD, editor. *A Worldwide Yearly Survey of New Data in Adverse Drug Reactions*. Vol. 37. Netherlands: Elsevier; 2015. p. 513-519. Available from: https://www.sciencedirect.com/science/article/pii/S0378608015000446?via%3Dihub [Last accessed on 2022 Nov 09].

23. Mandel SJ, Shankar LK, Benard F, Yamamoto A, Alavi A. Superiority of iodine-123 compared with iodine-131 scanning for thyroid remnants in patients with differentiated thyroid cancer. *Clin Nucl Med*. 2001;26:6-9.

24. Eleftheriadou A, Williams S, Nevitt S, *et al*. The prevalence of cardiac autonomic neuropathy in prediabetes: A systematic review. *Diabetologia*. 2021;64:288-303.

doi: 10.1007/s00125-020-05316-z

25. Zilliox LA, Russell JW. Is there cardiac autonomic neuropathy in prediabetes? *Auton Neurosci*. 2020;229:102722.

doi: 10.1016/j.autneu.2020.102722

26. Nathan DM, Davidson MB, DeFronzo RA, *et al*. Impaired fasting glucose and impaired glucose tolerance: Implications for care. *Diabetes Care*. 2007;30:753-759.

doi: 10.2337/dc07-9920

ACCSCIENCE PUBLISHING

Advances in Radiotherapy & Nuclear Medicine

ORIGINAL RESEARCH ARTICLE

# Assessing the adequacy of a 5-mm planning target volume margin for 4D-CT scan-based image-guided radiotherapy for locally advanced carcinoma of the lung

**Animesh Saha[1]*, Aditi Mishra[1], Shreya Manna[1], Ajay Banik[1], Suchanda Goswami[1], Jibak Bhattacharya[1], Tanmoy Mukhopadhay[1], Prosenjit Soren[2], Sayantan Mondal[2], Saptaswa Chattopadhyay[2], Biplab Sarkar[2], Suvra Biswal[2], Kiruba George[2], Mousin Gazi[2], and Sandipan Roy Chowdhury[2]**

[1]Department of Radiation Oncology, Apollo Multispeciality Hospitals, Kolkata, West Bengal, India

[2]Department of Medical Physics, Apollo Multispeciality Hospitals, Kolkata, West Bengal, India

## Abstract

In developed nations, 4D-computed tomography (4D-CT)-based image-guided radiotherapy (IGRT) has become the standard for treating lung carcinoma patients, with the primary goal of achieving disease cure. However, its usage in India remains limited. Here, we compared target volume delineation for radical radiation planning in patients with locally advanced lung carcinoma using helical free-breathing CT (FBCT) and 4D-CT. In addition, we assessed the adequacy of a 5-mm planning target volume (PTV) margin with 4D-CT planning. Fifty patients with locally advanced lung cancer were enrolled in the study. Each patient underwent contouring based on 4D-CT to generate an internal target volume, and a 5-mm PTV margin (PTV_4D) was added for radical radiation. Subsequently, each patient underwent two intensity-modulated radiation therapy (IMRT) plans with comparable planning and optimization parameters. One plan was based on the FBCT-based volume (PTV_3D), while the other was based on the 4D-CT-based volume (PTV_4D). PTV, organ at risk (OAR) dose, and PTV coverage by 95% of the prescribed dose (PTVD 95_3D *vs.* PTVD 95_4D) were compared between the two schemes. Results revealed that 4D-CT-based planning reduced PTV (mean PTV volume: 539 cc *vs.* 782 cc) and lowered OAR doses (mean lung dose: 13 Gy *vs.* 15 Gy; mean esophagus dose: 18.5 Gy *vs.* 21.15 Gy; mean spinal cord max dose: 35.59 Gy *vs.* 37.39 Gy). At 3 months after treatment imaging, 40% of the patients showed a complete response, 48% showed a partial response, 4% showed stable disease, and 8% showed progressive disease. In conclusion, 4D-CT-based radiation planning for locally advanced lung carcinoma with a reduced PTV margin of 5 mm can dramatically decrease the PTV and OAR doses without sacrificing PTV coverage compared to FBCT-based planning. However, daily online image guidance or at least a well-defined offline image guidance protocol is recommended when employing such a small PTV margin.

***Keywords:*** Lung cancer; 4D-CT; Image-guided radiotherapy; Planning target volume

***Corresponding author:**
Animesh Saha
(720292@apollohospitals.com)

**Citation:** Saha A, Mishra A, Manna S, *et al.* Assessing the adequacy of a 5-mm planning target volume margin for 4D-CT scan-based image-guided radiotherapy for locally advanced carcinoma of the lung. *Adv Radiother Nucl Med*. 2024;2(1):2784. https://doi.org/10.36922/arnm.2784

**Received:** January 19, 2024

**Accepted:** March 12, 2024

**Published Online:** March 27, 2024

## 1. Introduction

Lung cancer ranks as the second most common cancer with an incidence of 11.6% and carries the highest mortality rate at 18.4%.[1] Radiotherapy is a common component of the multimodal management of lung cancer. The most common course of treatment for locally advanced or stage III non-small cell lung cancers (NSCLCs) is concurrent chemoradiotherapy or radical radiotherapy alone.[2,3] Similarly, patients with limited-stage small-cell lung cancer and certain stage IV NSCLC patients with oligometastatic disease are also treated with radical radiotherapy. For patients with early-stage NSCLC (stages I and II) who are not suitable candidates for surgery or stereotactic adjuvant radiotherapy (SABR), radiotherapy alone or combined with other multimodality management strategies can be employed.[4-6] However, a significant percentage of lung cancer patients experience locoregional recurrence after treatment with radiotherapy or chemo-radiotherapy.[1,7] Although the reason for such recurrence is multifactorial, geographical misses and suboptimal doses of gross disease secondary to tumor motion play a pivotal role. Conventionally, helical free-breathing CT scans (FBCT) have been the standard for lung radiotherapy treatment planning for many years.

In general, a population-based safety margin is used around both gross disease (gross tumor volume [GTV]) and microscopic disease (clinical target volume [CTV]) to determine the final radiotherapy planning target volume (PTV).[8] However, lung tumors can move erratically during respiration in an unpredictable manner. The inability to encompass the range of tumor motion might lead to inadequate tumor coverage, and using larger generalized population-based margins can cause unnecessary toxicity to nearby organs at risk (OARs).[9-11] 4D-Computed tomography (4D-CT) has shown promising results in mitigating motion management issues associated with radiotherapy in lung cancer.[12] 4D-CT scans have become the standard to derive detailed information regarding the pattern and range of respiratory motion.[13] Since tumor motion is inherently considered when using 4D-CT scans, a smaller safety margin for set-up error (PTV) can be used during lung radiotherapy planning.[14] In 76% of the treatment fractions, Steiner *et al*. demonstrated that a 5-mm PTV margin was sufficient to capture the 4D-CT-based motion data, with brief intervals of excess motion (varying from 1% to 20% of the treatment period).[15] However, there is a risk of geographical miss with a very small PTV margin when setting up 4D-CT-based image-guided radiotherapy (IGRT) for lung cancer. In this study, we aimed to compare the dosimetric and volumetric differences in target volume delineation for radical radiotherapy planning in patients with locally advanced lung cancer between helical FBCT and 4D-CT. In addition, we assessed the feasibility of achieving a lower PTV margin with 4D-CT planning.

## 2. Methods

### 2.1. Participants

This prospective, non-randomized cohort study was conducted at a tertiary cancer care center in Eastern India between January 2021 and March 2023. Ethical approval for this study was obtained from the Institutional Ethics Committee of Apollo Multi-Speciality Hospital, Kolkata (approval no.: IEC/2021/DNB/04/17). The inclusion criteria were as follows (i) Age: 18 – 70 years old; (ii) biopsy-proven lung cancer (NSCLC or SCLC); (iii) locally advanced NSCLC (stage III); (iv) early-stage NSCLC (stages I and II) who are not suitable for surgery or SABR; (v) limited stage small cell lung cancer; and (vi) patients receiving a radiotherapy dose of 60 – 66 Gy in 30 – 33 fractions over 6 – 6.6 weeks, possessing adequate lung function to undergo definitive radiotherapy, and willingness to provide consent for participation in the study. The exclusion criteria were as follows (i) patients not willing to provide consent; (ii) patients unable to cooperate during 4D-CT scanning; and (iii) patients receiving palliative radiotherapy.

### 2.2. Helical FBCT and 4D-CT procedure

Helical FBCT and 4D-CT planning scans were derived during the same session with the patient in the same treatment position. The standard institutional protocol was adhered to for FBCT imaging. The patient's breathing cycle was monitored for 4D-CT image capture using either the real-time position management system (Varian Medical Systems Inc., USA) or the Philips bellows device (Philips Healthcare, USA), employing infrared reflector markers and infrared cameras.[10,16] The GTV_3D was contoured on an FBCT scan using fluorodeoxyglucose positron emission tomography (PET) image fusion to identify primary and/or nodal illness. The number of nodes and mediastinal disease were contoured on the mediastinal window, whereas parenchymal tumors were contoured at the lung window level. The CTV_3D was created by expanding the GTV_3D by 5 mm in all directions and then modifying it to remove natural barriers, such as air and bone. To account for internal margin and setup faults, the PTV_3D was calculated as CTV_3D + 1 cm axial and 1.3 cm superior/inferior expansions. Organs at risk were contoured according to the standard Radiation Therapy Oncology Group (RTOG) contouring guidelines.[17]

A fusion of PET-CT was used for 4D-CT-based contouring whenever available, although it was not

mandatory. The maximum intensity projection picture was used to contour the GTV_4D for primary and/or nodal illnesses. Phases spanning 0 – 90% of the respiratory cycle were separately examined to ensure adequate contouring of IGTV_4D or composite GTV_4D. Subsequently, CTV_4D or internal target volume_4D (ITV_4D) was defined by expanding IGTV_4D by 5 mm and modifying it to remove natural barriers, such as bones and air. To account for setup errors only, PTV_4D was defined as CTV_4D plus a 0.5-cm isotropic expansion (Figure 1).

Intensity-modulated radiation therapy plans were created in accordance with departmental policy whereby 95% PTV should cover at least 95% of the prescribed dose in the Eclipse (V15.6.03) planning system.[18,19] All plans were optimized using the photon optimizer algorithm, and the dose calculation was performed using the anisotropic analytic algorithm (AAA-dose calculation algorithm). The main aim was to minimize the OAR dose as much as possible without disturbing PTV coverage. Each plan was evaluated using the dose-volume histogram generated by the planning system. Each patient received two radiation plans: one based on a volume estimated from FBCT data and the other utilizing a volume estimated from FBCT data together with comparable geometry, gantry angles or arcs, and additional optimization and planning factors. All research participants underwent IMRT with plans created using volumes based on 4D-CT. Next, the plans based on FBCT were replicated on the volume dataset for 4D-CT. A cone-beam CT scan (CBCT) image guidance was provided daily to the study participants.

Next, the two plans were compared as follows:

(i) IGTV_4D versus GTV_3D: two datasets with one volume representing gross pulmonary and nodal tumors.
(ii) IGTVP_4D versus GTVP_3D: only two datasets showed gross pulmonary disease contours.
(iii) IGTVN_4D versus GTVN_3D: only two datasets with gross nodal disease contours.
(iv) PTV_4D and PTV_3D. PTV for two sets of data: PTVD 95_4D and PTVD 95_3D. In both plans, 95% of the recommended dosage for PTV_3D and PTV_4D was covered by the volume. The extrapolated plan (of the FBCT-based target volume) for PTV_4D was evaluated for this comparison.

(i) Histogram of dose-volume dosage that the OAR (heart, lungs, spinal cord, and esophagus) received in both schemes.
(ii) Dice similarity coefficient (DIC): the dice similarity coefficient was computed to investigate the overlap between PTV_3D and PTV_4D. In DIC, the region of overlap between two measures in a single patient is denoted by "a," the area identified in the first measure but not in the second is denoted by "b," and the area identified in the second measure but not in the first is denoted by "c." DIC was calculated using the following formula[12] (Equation I),

$$DIC=2a/(2a + b + c) \quad (I)$$

Before initiating treatment, every patient underwent daily scans with the scan length configured using scan parameters to cover the entire PTV length (ascertained from the contours displayed in this window). With matching axes set to translations, the scan length was first automatically matched using the "bone and soft tissue" preset. Every automated match was examined manually, with a particular focus on the region containing the gross tumor volume or high-dose volumes. The changes in the mediolateral (x), craniocaudal (y), and anteroposterior (z) translational axes were tabulated, and the error vector ($\sqrt{x^2} + \sqrt{y^2} + \sqrt{z^2}$) was generated using summary data from pre-treatment kilo-voltage computed tomography (KVCT)

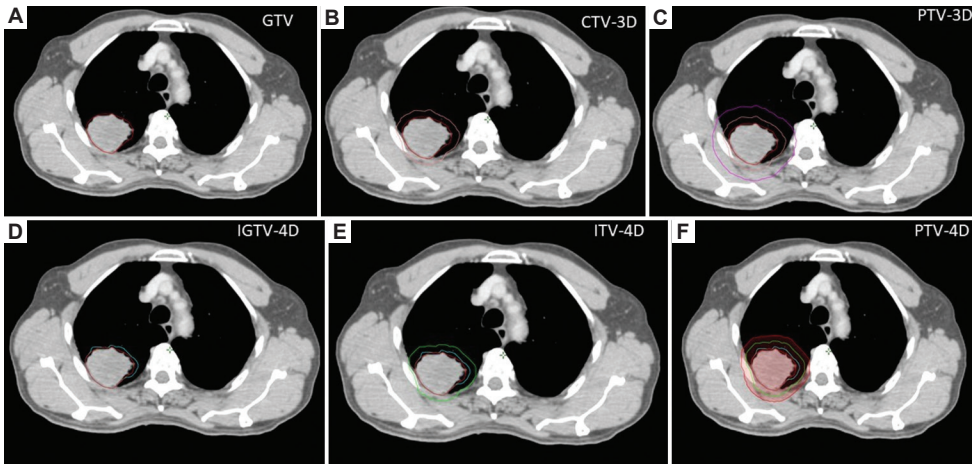


**Figure 1.** Contouring approach for helical free-breathing computed tomography (A, B, and C) and 4D-computed tomography-based (D, E, and F) planning scans.

before each treatment fraction. We computed the error vector, systematic error (δ), and random error (Σ) for each of the three axes independently using this dataset. The "Marcel van Herk" formula (Equation II) was used to determine the PTV margins:

$$PTV = 2.5 \Sigma + 0.7 \delta \quad (II)$$

In addition, a retrospective analysis of setup data for 1010 fractions of 50 patients was conducted to assess PTV coverage. For each patient, individual CBCT scan images were examined for primary PTV coverage using both the lung and mediastinal windows, with images of the primary tumor located outside the PTV recorded.

### 2.3. Statistical analysis

The means, medians, ranges of values, and frequencies for non-continuous values were computed for each examined dose and volume metric. The paired *t*-test was used to compare the relevant parameters. All statistical analyses were performed twice at the 5% significance level. Statistical analyses were performed using SPSS version 21.

## 3. Results

Patient characteristics are summarized in Table 1. A total of 50 patients were recruited in this study, with the majority (88%) being male. The median age of the patients was 66 years (range = 47 – 77 years, with a standard deviation of 8.00). All patients underwent whole-body PET-CT and brain MRI for staging as well as pulmonary function tests, including measurement of the diffusing capacity of the lungs for carbon monoxide (DLCO). The median forced expiratory volume in the 1st s was 1.4 L (range = 0.95 – 2.62 L, with a standard deviation of 0.412). The median DLCO was 60% (range = 44 – 89%, with a standard deviation of 12.14). Most patients had NSCLC (88%), and 12% had limited SCLC. Among the NSCLC cases, 44% were squamous, 36% were adenocarcinomas, and 8% were adenosquamous. The majority of patients (52%) had an Eastern Cooperative Oncology Group (ECOG) Performance Status (PS) of 1, 40% had an ECOG PS of 2, and 8% had an ECOG PS of 0. Most patients were classified according to the American Joint Committee on Cancer (AJCC) 8th edition staging as stage III (60%), while 20% had stage II disease and 20% had stage IV oligometastatic disease treated with radical intent. The majority of patients (96%) were treated with 60 Gy in 30 fractions over 6 weeks, with only two patients receiving 66 Gy in 33 fractions over 6.6 weeks.

The PTV was significantly low with 4D-CT-based planning compared to FBCT-based planning (mean PTV volume 539cc *vs.* 782cc) (Table 2). In addition, OAR doses (Table 3) were significantly lower in the 4D-CT-based planning. The mean heart dose was 11.6 Gy *vs.* 14.6 Gy, the mean heart V60 was 2.02% *vs.* 4.04%, and mean heart V45 was 7.4% *vs.* 12.3%. Lung dose was recorded as the combined volume of both lungs minus the GTV (lungs-GTV). The mean lung doses were 13 Gy *vs.* 15 Gy, lung V20 was 23.7% *vs.* 27%, lung V10 was 33.9% *vs.* 38.8%, and lung V5 was 47.7% *vs.* 53%. The mean esophagus dose was 18.5 Gy *vs.* 21.15 Gy, and the mean esophagus was V60 4.22% and 5.15%, respectively. The maximum spinal cord doses were 35.59 Gy *vs.* 37.39 Gy.

The histogram in Figure 2 illustrates the DIC, showing that the mean DIC for PTV_3D and PTV_4D was 0.81

**Table 1. Patients' characteristics**

| Parameters | Category | Number (*N*=50) | Percentage |
|---|---|---|---|
| Sex | Male | 44 | 88 |
| | Female | 6 | 12 |
| Histopathology | Adenocarcinoma | 18 | 36 |
| | Squamous cell carcinoma | 22 | 44 |
| | Adeno-squamous carcinoma | 4 | 8 |
| | Small cell carcinoma | 6 | 12 |
| ECOG performance status | ECOG PS 0 | 4 | 8 |
| | ECOG PS 1 | 26 | 52 |
| | ECOG PS 2 | 20 | 40 |
| T stage | T1 | 4 | 8 |
| | T2 | 10 | 20 |
| | T3 | 12 | 24 |
| | T4 | 24 | 48 |
| N stage | N0 | 8 | 16 |
| | N1 | 12 | 24 |
| | N2 | 14 | 28 |
| | N3 | 16 | 32 |
| M stage | M0 | 44 | 88 |
| | M1 | 6 | 12 |
| AJCC stage | Stage IIB | 10 | 20 |
| | Stage IIIA | 6 | 12 |
| | Stage IIIB | 18 | 36 |
| | Stage IIIC | 10 | 20 |
| | Stage IV | 6 | 12 |
| Radiotherapy dose-fractionation | 60 Gy/30 fractions over 6 weeks | 48 | 96 |
| | 66 Gy/33 fractions over 6 weeks | 2 | 4 |

Abbreviations: AJCC: American Joint Committee on Cancer; ECOG: Eastern Cooperative Oncology Group.

(81%). This result implies that in 19% of the patients, the volumes were not at the same anatomical position. Such deviations indicate the likelihood of PTV displacement due to tumor or nodal movements during the respiratory cycle. DIC has a median value of 0.8 (range: 0.75 – 0.87).

**Table 2. Comparison of treatment volumes between two planning datasets**

| Parameter | No. of patients | Mean volume (cc) | Standard deviation | *P*-value |
|---|---|---|---|---|
| GTV_3D | 50 | 171.55 | 134.42 | <0.0001 |
| IGTV_4D | 50 | 187.22 | 134.42 | |
| GTVP_3D | 50 | 156.52 | 139.81 | <0.0001 |
| IGTVP_4D | 50 | 168.69 | 141.15 | |
| GTVN_3D | 50 | 15.16 | 26.78 | <0.0001 |
| IGTVN_4D | 50 | 18.89 | 31.93 | |
| PTV_3D | 50 | 781.67 | 336.58 | <0.0001 |
| PTV_4D | 50 | 539.39 | 243.07 | |

Abbreviations: GTV: Gross tumor volume; PTV: Planning target volume.

For the purpose of our study, we created two radiotherapy plans based on FBCT-based volume and another based on 4D-CT-based volume using similar geometry, gantry angles or arcs, and other radiotherapy planning and optimization parameters. All study patients received IMRT with plans generated using 4D-CT-based volumes. For study purposes, FBCT-based plans were copied onto the 4D-CT volume dataset and vice versa. The mean 95% coverage of the FBCT-based PTV (PTVD 95_4D) by the 4DCT-based plan was 76.47% (median = 76.8%, range = 65.4 – 87.1%). The mean 95% coverage of the 4D-CT-based PTV (PTVD 95_3D) by the FBCT-based plan was 97.77% (median = 99.5%, range = 81 – 100%). This suggests that the plan generated based on the FBCT-based volume was sufficiently large to ensure 95% coverage of the 4D-CT-based volume. However, this leads

**Table 3. Comparison of organ at risk doses between two planning datasets**

| Parameter | Planning dataset | No. of patients | Mean | Standard deviation | Percentage decline with 4D-CT | *P*-value |
|---|---|---|---|---|---|---|
| Lung-V20 (%) | 3D | 50 | 27.05 | 6.7 | 9 | <0.0001 |
| | 4D | 50 | 23.73 | 5.9 | | |
| Lung-V10 (%) | 3D | 50 | 38.85 | 12.48 | 12.6 | <0.0001 |
| | 4D | 50 | 33.97 | 10.03 | | |
| Lung-V5 (%) | 3D | 50 | 53.07 | 16.6 | 10.2 | <0.0001 |
| | 4D | 50 | 47.64 | 14.4 | | |
| Mean lung dose (Gy) | 3D | 50 | 15.08 | 4.45 | 13.2 | <0.0001 |
| | 4D | 50 | 13.09 | 3.85 | | |
| Heart-V60 (%) | 3D | 50 | 4.04 | 4.25 | 50 | <0.0001 |
| | 4D | 50 | 2.02 | 2.21 | | |
| Heart-V45 (%) | 3D | 50 | 12.33 | 9.56 | 39.9 | <0.0001 |
| | 4D | 50 | 7.41 | 5.49 | | |
| Heart-V40 (%) | 3D | 50 | 14.33 | 10.64 | 35.4 | <0.0001 |
| | 4D | 50 | 9.26 | 6.62 | | |
| Mean heart dose (Gy) | 3D | 50 | 14.62 | 8.66 | 20.4 | <0.0001 |
| | 4D | 50 | 11.64 | 7.04 | | |
| Oesophagus-V60 (%) | 3D | 50 | 5.15 | 6.53 | 18.05 | 0.154 |
| | 4D | 50 | 4.22 | 5.08 | | |
| Oesophagus- mean dose (Gy) | 3D | 50 | 21.15 | 11.64 | 12.5 | <0.0001 |
| | 4D | 50 | 18.50 | 10.35 | | |
| Spinal cord-max dose (Gy) | 3D | 50 | 37.39 | 8.93 | 4.8 | <0.0001 |
| | 4D | 50 | 35.59 | 8.05 | | |
| Spinal cord PRV (dose to 1 cc) (Gy) | 3D | 50 | 37.90 | 9.17 | 6.6 | <0.0001 |
| | 4D | 50 | 35.37 | 8.15 | | |

Abbreviations: PRV: Planning risk volume; 4D-CT: 4D-computed tomography.

to unnecessary irradiation of at-risk organs. In contrast, the plans generated based on the 4D-CT-based volume are smaller and cannot adequately cover the FBCT-based volume. This does not necessarily mean inferior PTV coverage, as we have seen in our study that none of the patients experienced locoregional recurrence.

Response assessment scans were performed 4 weeks to 3 months after the completion of concurrent chemoradiotherapy. Those planned for adjuvant durvalumab had a response assessment CT scan at 4 – 6 weeks; otherwise, patients underwent a response assessment scan 3 months after the completion of treatment. Forty percent of patients developed a complete response. Forty-eight percent of the patients developed a partial response. Two patients had a stable disease (Table 4). Locoregional progression was not observed. Four patients who developed progressive disease recurred distally (two patients progressed in the brain, one in the abdominal nodes, and the other in the liver). These four patients already had M1 disease but were treated radically in view of oligometastatic disease.

We retrospectively analyzed the setup data (CBCT) of 1,010 fractions of 50 patients for PTV coverage and shifts. Offline imaging verification of uncorrected setup errors revealed that 95% (960 fractions) of the time, the primary tumor was within the PTV. After image matching and correction, we got a systematic and random error of $\Sigma_{x,y,z}$ of 0.15,0.33, and 0.21 cm and $\delta_{x,y,z}$ of 0.14,0.46, and 0.23 cm with a required PTV margin of 0.69 cm, 1.16 cm, and 0.47 cm in the X, Y, and Z axes. The corrected translational vector resulted in a systematic and random error of 0.11 and 0.3 cm, with a required PTV margin of 0.48 cm. Shifts of more than 5 mm in the X, Y, and Z axes were noted in 1%, 32.67%, and 7.9% of cases, respectively.

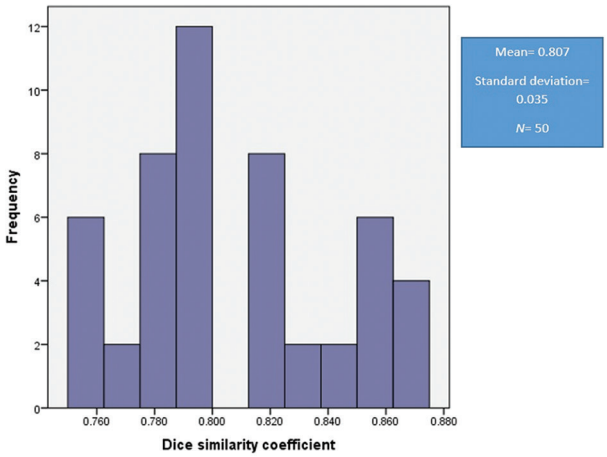


**Figure 2.** Histogram showing Dice similarity coefficient.

**Table 4. Radiological response to treatment**

| RECIST criteria response | Number (*N*=50) | Percentage |
|---|---|---|
| Complete response | 20 | 40 |
| Partial response | 24 | 48 |
| Stable disease | 2 | 4 |
| Progressive disease | 4 | 8 |

## 4. Discussion

Our study revealed that 4D-CT-based radiotherapy planning for locally advanced lung cancer with a reduced PTV margin of 5 mm can significantly reduce PTV and OAR doses without compromising PTV coverage compared to FBCT-based planning with a population-based PTV margin. This study will also help other centers set up 4D-CT image-based guided radiotherapy for locally advanced lung cancer with a reduced PTV margin, provided they meet standard licensing requirements and have trained staff and facilities for real-time position management systems, infrared cameras, and infrared reflective markers.

Previously, most radiotherapy centers used helical FBCT for lung radiotherapy contouring and planning. This FBCT is associated with several inherent problems: (i) it does not account for breathing movement; (ii) it often produces distorted images owing to motion artifacts during the CT scan; (iii) it may result in blurred gross tumors due to respiratory and tumor motion and may create uncertainties in target delineation, which will eventually lead to suboptimal target coverage and unnecessary dose to OARs.[20] Considering the respiratory motion, the 4D-CT scan reconstructs the 3D volume as a function of time. Multiple 3D imaging datasets reflecting the entire trajectory of the lung tumor and OARs were produced by the 4D-CT scan. The ITV, consisting of the total GTV, is determined by considering all imaging datasets. Therefore, when planning 4D-CT-based lung radiation, a narrower PTV margin can be employed, but only to account for daily setup uncertainties.[21]

Numerous researchers have assessed 4D-CT's usefulness in radical lung radiation treatment. In their study, Rietze *et al.* demonstrated that the GTV contoured on a helical CT scan was less than the GTV calculated as a summation of all phases of the respiratory cycle from 4D datasets (39.9 vs. 24.4 $cm^3$). They also highlighted how the geometry of the GTV obtained from a helical scan was modified by image artifacts[14]. Alasti *et al.* compared 4D-CT-based planning and helical CT-based planning in 24 NSCLC patients, revealing that the GTV determined by helical CT was approximately 25% smaller than that determined by 4D-CT. In addition, they demonstrated that in comparison to traditional helical CT-based planning,

lung V20 (volume of lung minus GTV receiving 20 Gy) and mean lung dose can be decreased with 4D-CT-based planning.[22] These results (Table 2) are consistent with our results; the combined GTV based on 4D-CT (IGTV-4D) exceeded the GTV based on FBCT 187.2 cc vs. 171.5 cc, as expected.

Ahmed *et al.* compared conventional three-dimensional (3D) conformal radiotherapy (3DCRT) plans made with regular helical FBCT with plans developed using 4D-CT contoured volumes to ascertain whether target volume coverage is adequate. They discovered that the combined GTV produced on 4D-CT (IGTV_4D) for both main and nodal disease, together or separately, was considerably greater than the GTV generated on a helical FBCT (GTV_3D) scan. Although not statistically significant, the average PTV produced on helical FBCT (PTV_3D) was greater than the average PTV generated on 4D-CT (PTV_4D). They extrapolated the radiotherapy plan based on 3D-CT on the target volume generated on 4D-CT and revealed that PTV_4D coverage with a 95% isodose line was inferior by approximately 10%. The spinal cord and esophagus doses were significantly lower with 4D-CT-based planning.[12] In this study, Ju *et al.* examined the dosimetric benefits of 4D-CT-based PTV generation over the traditional PTV definition with a population-based margin for lung cancer radiation. They concluded that radiation planning and PTV definition based on 4D-CT can reduce the dosage to OARs (lung, heart, etc.), enhance target coverage, and decrease the PTV in patients with minor respiratory motion. This technique can prevent geographic target misses in patients with considerable respiratory motion, particularly in those whose motion exceeds 1.5–2 cm, without appreciably increasing the dose of OARs.[23]

In a comparative study, Cole *et al.* examined the possible dosimetric and clinical advantages of employing 4D-CT rather than 3D-CT when planning radical radiotherapy for non-small cell lung cancer. They demonstrated that plans based on 4DCT had reduced PTV volumes, doses to organs at risk, and expected rates of normal tissue complication probability.[24] Therefore, 4D-CT has the potential to increase the therapeutic ratio and pave the way for dose escalation in radiotherapy for lung cancer. Hence, most current dose escalation study protocols emphasize the incorporation of motion management techniques, including 4D-CT, in radical radiotherapy treatment planning for locally advanced lung cancer.[1,25,26]

Marcel Van Herk developed the PTV margin recipe (PTV margin = $2.5\Sigma + 0.7\delta$) based on the analysis of the systemic and random geometric uncertainties, aiming to determine the minimal margin required to reach 90% of the population with a full coverage of 95% of the recommended dosage.[27] PTV margins is also a combination of internal and setup margins.[28] Hence, if the internal margin or internal motion is taken care of by motion management techniques such as 4D-CT, only the setup margin needs to be added to the PTV margin. In principle, this should reduce the PTV margin compared with the general population margin without the use of motion management techniques. However, the extent to which the reduced margin is safe remains questionable. The PTV margin calculation for head and neck cancer and lung cancer using the Van Herk formula was slightly different. In head and neck cancer, the internal margin is almost zero, and the entire PTV margin is set up by error only. However, the internal margin is significant in lung cancer. There are certain other inherent problems with using Van Herk's formula in lung radiotherapy; for example, the construction of this dose model does not consider the target size, tissue density, or plan conformity and assumes that the dosimetric effects of motion can be modeled with a convolution.[29] Ample evidence suggests that a PTV margin of ≤5 mm is adequate for treating early-stage lung cancer or small lung metastases with stereotactic ablative radiotherapy using motion management techniques, including 4D-CT.[30-33] Hence, it should not be different in locally advanced lung cancers with larger tumors and/or nodes. In our study, PTV margins calculated from set-up errors using Van Herk's formula were >5 mm in the X and Y axes, but these might not be true representations of the PTV margin, as we have already added the ITV margin based on 4D-CT assessment. However, the margin of the translational vector is within 5 mm. Offline imaging verification confirmed that for uncorrected setup errors, the primary tumor was within the PTV margin of 5 mm in 95% of cases, and with imaging correction, the primary tumor was within the PTV in 100% of cases.

However, this study had limitations. First, set-up errors are the main, but not the only, contributor to interfraction uncertainties. Physiological and anatomical changes can make a difference in some patients, and this analysis does not address this issue. Second, the analysis of the setup error data was a retrospective assessment of errors based on daily imaging. Third, the lack of 4D-cone beam CT (CBCT) in our center might have added more precision in ascertaining the safe PTV margin. Finally, 4D-CT itself has limitations, including motion artifacts, irregular breathing patterns, and rigorous quality assurance.[34-36]

## 5. Conclusion

4D-CT-based IGRT planning for locally advanced lung cancer with a reduced PTV margin of 5 mm can significantly reduce PTV and OAR doses without compromising PTV coverage compared to FBCT-based planning with a

population-based PTV margin. However, daily online image guidance or at least a well-defined offline image guidance protocol with such small PTV margins is recommended.

## Acknowledgments

The authors acknowledge the support and hard work of all colleagues.

## Funding

None.

## Conflict of interest

The authors declare that they have no competing interests.

## Author contributions

*Conceptualization:* Animesh Saha, Aditi Mishra, Biplab Sarkar
*Formal analysis:* Animesh Saha, Suchanda Goswami, Mousin Gazi
*Investigation:* Animesh Saha, Aditi Mishra, Shreya Manna, Ajay Banik, Jibak Bhattacharya, Prosenjit Soren, Sayantan Mondal, Suvra Biswal
*Methodology:* Animesh Saha, Aditi Mishra, Shreya Manna, Ajay Banik, Suchada Goswami,
Tanmoy Mukhopadhay, Saptaswa Chattopadhyay, Kiruba George
*Writing – original draft:* Animesh Saha, Aditi Mishra
*Writing – review & editing:* Animesh Saha, Sandipan Roy Chowdhury.

## Ethics approval and consent to participate

Ethical committee approval was obtained for this study. The reference number is IEC Ref: IEC/2021/DNB/04/17, and the approval date was 03.04.2021. The approval letter from the ethics committee is attached separately. Informed consent was obtained from all participants. Informed consent forms were attached separately.

## Consent for publication

Consent for study publication has been obtained from the study participants, and their identities have not been disclosed anywhere in this article.

## Availability of data

The data are presented in Excel format with the authors (Dr. Animesh Saha and Dr. Aditi Mishra) which can be shared if required.

## References

1. Bradley JD, Paulus R, Komaki R, *et al*. Standard-dose versus high-dose conformal radiotherapy with concurrent and consolidation carboplatin plus paclitaxel with or without cetuximab for patients with stage IIIA or IIIB non-small-cell lung cancer (RTOG 0617): A randomised, two-by-two factorial phase 3 study. *Lancet Oncol*. 2015;16(2):187-199.

   doi: 10.1016/S1470-2045(14)71207-0

2. Curran WJ Jr., Paulus R, Langer CJ, *et al*. Sequential vs. Concurrent chemoradiation for stage III non-small cell lung cancer: Randomized phase III trial RTOG 9410. *J Natl Cancer Inst*. 2011;103(19):1452-1460.

   doi: 10.1093/jnci/djr325

3. Fournel P, Robinet G, Thomas P, *et al*. Randomized phase III trial of sequential chemoradiotherapy compared with concurrent chemoradiotherapy in locally advanced non-small-cell lung cancer: Groupe Lyon-Saint-Etienne d'Oncologie Thoracique-Groupe Français de Pneumo-Cancérologie NPC 95-01 study. *J Clin Oncol*. 2005;23(25):5910-5917.

   doi: 10.1200/JCO.2005.03.070

4. Ashworth A, Rodrigues G, Boldt G, Palma D. Is there an oligometastatic state in non-small cell lung cancer? A systematic review of the literature. *Lung Cancer*. 2013;82(2):197-203.

   doi: 10.1016/j.lungcan.2013.07.026

5. Din OS, Harden SV, Hudson E, *et al*. Accelerated hypo-fractionated radiotherapy for non small cell lung cancer: Results from 4 UK centres. *Radiother Oncol*. 2013;109(1):8-12.

   doi: 10.1016/j.radonc.2013.07.014

6. Faivre-Finn C, Snee M, Ashcroft L, *et al*. Concurrent once-daily versus twice-daily chemoradiotherapy in patients with limited-stage small-cell lung cancer (CONVERT): An open-label, phase 3, randomised, superiority trial. *Lancet Oncol*. 2017;18(8):1116-1125.

   doi: 10.1016/S1470-2045(17)30318-2

7. Le Chevalier T, Arriagada R, Tarayre M, *et al*. Significant effect of adjuvant chemotherapy on survival in locally advanced non-small-cell lung carcinoma. *J Natl Cancer Inst*. 1992;84(1):58.

   doi: 10.1093/jnci/84.1.58

8. ICRU. *ICRU Report 62: Prescribing, Recording and Reporting Photon Beam Therapy* (Supplement to ICRU 50). Available from: https://www.icru.org/report/prescribing-recording-and-reporting-photon-beam-therapy-report-62

9. Chen QS, Weinhous MS, Deibel FC, Ciezki JP, Macklis RM. Fluoroscopic study of tumor motion due to breathing: Facilitating precise radiation therapy for lung cancer patients. *Med Phys*. 2001;28(9):1850-1856.

   doi: 10.1118/1.1398037

10. Keall PJ, Mageras GS, Balter JM, *et al*. The management of

respiratory motion in radiation oncology report of AAPM task group 76. *Med Phys*. 2006;33(10):3874-3900.

doi: 10.1118/1.2349696

11. Plathow C, Ley S, Fink C, *et al*. Analysis of intrathoracic tumor mobility during whole breathing cycle by dynamic MRI. *Int J Radiat Oncol Biol Phys*. 2004;59(4):952-959.

doi: 10.1016/j.ijrobp.2003.12.035

12. Ahmed N, Venkataraman S, Johnson K, Sutherland K, Loewen SK. Does motion assessment with 4-dimensional computed tomographic imaging for non-small cell lung cancer radiotherapy improve target volume coverage? *Clin Med Insights Oncol*. 2017;11:1-7.

doi: 10.1177/1179554917698461

13. De Ruysscher D, Faivre-Finn C, Nestle U, *et al*. European organisation for research and treatment of cancer recommendations for planning and delivery of high-dose, high-precision radiotherapy for lung cancer. *J Clin Oncol*. 2010;28(36):5301-5310.

doi: 10.1200/JCO.2010.30.3271

14. Rietzel E, Chen GT, Choi NC, Willet CG. Four-dimensional image-based treatment planning: Target volume segmentation and dose calculation in the presence of respiratory motion. *Int J Radiat Oncol Biol Phys*. 2005;61(5):1535-1550.

doi: 10.1016/j.ijrobp.2004.11.037

15. Steiner E, Shieh CC, Caillet V, *et al*. Both four-dimensional computed tomography and four-dimensional cone beam computed tomography under-predict lung target motion during radiotherapy. *Radiother Oncol*. 2019;135:65-73.

doi: 10.1016/j.radonc.2019.02.019

16. Glide-Hurst CK, Schwenker Smith M, Ajlouni M, Indrin J, Chetty IJ. Evaluation of two synchronized external surrogates for 4D CT sorting. *J Appl Clin Med Phys*. 2013;14(6):4301.

doi: 10.1120/jacmp.v14i6.4301

17. Kong FM, Ritter T, Quint DJ, *et al*. Consideration of dose limits for organs at risk of thoracic radiotherapy: Atlas for lung, proximal bronchial tree, esophagus, spinal cord, ribs, and brachial plexus. *Int J Radiat Oncol Biol Phys*. 2011;81(5):1442-1457.

doi: 10.1016/j.ijrobp.2010.07.1977

18. Grills IS, Fitch DL, Goldstein NS, *et al*. Clinicopathologic analysis of microscopic extension in lung adenocarcinoma: Defining clinical target volume for radiotherapy. *Int J Radiat Oncol Biol Phys*. 2007;69(2):334-341.

doi: 10.1016/j.ijrobp.2007.03.023

19. Yuan S, Meng X, Yu J, *et al*. Determining optimal clinical target volume margins on the basis of microscopic extracapsular extension of metastatic nodes in patients with non-small-cell lung cancer. *Int J Radiat Oncol Biol Phys*. 2007;67(3):727-734.

doi: 10.1016/j.ijrobp.2006.08.057

20. Mori S, Kanematsu N, Mizuno H, Sunaoka M, Endo M. Physical evaluation of CT scan methods for radiation therapy planning: Comparison of fast, slow and gating scan using the 256-detector row CT scanner. *Phys Med Biol*. 2006;51(3):587-600.

doi: 10.1088/0031-9155/51/3/008

21. Pierce G. *Assessing and Improving 4D-CT Imaging for Radiotherapy Applications Western Thesis and Dissertation Repository*; 2011.

22. Alasti H, Cho YB, Vandermeer AD, *et al*. A novel four-dimensional radiotherapy method for lung cancer: Imaging, treatment planning and delivery. *Phys Med Biol*. 2006;51(12):3251-3267.

doi: 10.1088/0031-9155/51/12/017

23. Ju X, Li M, Zhou Z, *et al*. 4D-CT-based plan target volume (PTV) definition compared with conventional PTV definition using general margin in radiotherapy for lung cancer. *Zhonghua Zhong Liu Za Zhi*. 2014;36(1):34-38.

24. Cole AJ, O'Hare JM, McMahon SJ, *et al*. Investigating the potential impact of four-dimensional computed tomography (4DCT) on toxicity, outcomes and dose escalation for radical lung cancer radiotherapy. *Clin Oncol* (*R Coll Radiol*). 2014;26(3):142-150.

doi: 10.1016/j.clon.2013.11.024

25. Kong F, Hu C, Machtay M, *et al*. OA02.04 randomized phase II trial (RTOG1106) on midtreatment PET/CT guided adaptive radiotherapy in locally advanced non-small cell lung cancer. *J Thorac Oncol*. 2021;16(3):S104-S105.

doi: 10.1016/j.jtho.2021.01.277

26. Van Diessen J, De Ruysscher D, Sonke JJ, *et al*. The acute and late toxicity results of a randomized phase II dose-escalation trial in non-small cell lung cancer (PET-boost trial). *Radiother Oncol*. 2019;131:166-173.

doi: 10.1016/j.radonc.2018.09.019

27. Van Herk M, Remeijer P, Rasch C, Lebesque JV. The probability of correct target dosage: Dose-population histograms for deriving treatment margins in radiotherapy. *Int J Radiat Oncol Biol Phys*. 2000;47(4):1121-1135.

doi: 10.1016/s0360-3016(00)00518-6

28. Stroom JC, Heijmen BJ. Geometrical uncertainties, radiotherapy planning margins, and the ICRU-62 report. *Radiother Oncol*. 2002;64(1):75-83.

doi: 10.1016/s0167-8140(02)00140-8

29. Ecclestone G, Heath E, Bissonnette JP. Poster-thur Eve-62: Assessing the clinical application of the van Herk margin formula for lung radiotherapy. *Med Phys*. 2012;39(7Part3):4636.

doi: 10.1118/1.4740170

30. Jasper K, Liu B, Olson R, Matthews Q. Evidence-based planning target volume margin reduction for modern lung stereotactic ablative radiation therapy using deformable registration. *Adv Radiat Oncol*. 2021;6(6):100750.

doi: 10.1016/j.adro.2021.100750

31. Liang Z, Yang J, Liu H, *et al*. Real-time tumor motion monitoring and PTV margin determination in lung SBRT treatment. *Acta Oncol*. 2019;58(12):1786-1789.

doi: 10.1080/0284186X.2019.1648862

32. Murray L, Ramasamy S, Lilley J, *et al*. Stereotactic ablative radiotherapy (SABR) in patients with medically inoperable peripheral early stage lung cancer: Outcomes for the first UK SABR cohort. *Clin Oncol (R Coll Radiol)*. 2016;28(1):4-12.

doi: 10.1016/j.clon.2015.09.007

33. SABR UK Consortium. *Stereotactic Ablative Body Radiation Therapy (SABR): A Resource*. United Kingdom: SABR UK Consortium; 2014.

34. Yamamoto T, Langner U, Loo BW Jr., Shen J, Keall PJ. Retrospective analysis of artifacts in four-dimensional CT images of 50 abdominal and thoracic radiotherapy patients. *Int J Radiat Oncol Biol Phys*. 2008;72(4):1250-1258.

doi: 10.1016/j.ijrobp.2008.06.1937

35. Sentker T, Schmidt V, Ozga AK, *et al*. 4D CT image artifacts affect local control in SBRT of lung and liver metastases. *Radiother Oncol*. 2020;148:229-234.

doi: 10.1016/j.radonc.2020.04.006

36. Jiang SB, Wolfgang J, Mageras GS. Quality assurance challenges for motion-adaptive radiation therapy: Gating, breath holding, and four-dimensional computed tomography. *Int J Radiat Oncol Biol Phys*. 2008;71(1 Suppl):S103-S107.

doi: 10.1016/j.ijrobp.2007.07.2386

ACCSCIENCE PUBLISHING

Advances in Radiotherapy & Nuclear Medicine

ORIGINAL RESEARCH ARTICLE

# Evaluation of multidrug resistance in tumors using $^{99m}$Tc-doxorubicin

**Bianca Gutfilen[1]*, Sergio Augusto Lopes de Souza[1], Thiago Barboza[1], Bruna Fortunato Novis[2], Claudia Lopes Rodrigues Chagas[1], Maria Verônica Fonseca Torres de Oliveira[1], and Vivian M. Rumjanek[2]**

[1]Laboratory of Labeling Cells and Molecules, Department of Radiology, Federal University of Rio de Janeiro, Rio de Janeiro, Brazil

[2]Institute of Medical Biochemistry, Federal University of Rio de Janeiro, Rio de Janeiro, Brazil

## Abstract

Doxorubicin (DOX) is a potent chemotherapeutic agent used as the first-choice drug in treating different types of cancer, such as leukemia, lymphoma, and breast cancer, among others. However, the development of multidrug resistance represents a significant obstacle to the successful treatment of tumors. In this study, we assessed whether labeled DOX could be uptaken by susceptible and multidrug-resistant cell lines and by tumors *in vivo* in animals. The efficiency of DOX labeling was maintained at around 90% in this work. To evaluate the effect of $^{99m}$Tc-DOX on cells expressing active P-glycoprotein (Pgp), we utilized cultured human chronic myeloid leukemia K562 cells and the resistant counterpart Lucena 1 cells. Lucena 1 cell line showed overexpression of Pgp that was not observed in K562. Our results suggested that the resistance to labeled or unlabeled DOX can be reversed by Pgp inhibition and can be easily detected. In conclusion, administering $^{99m}$Tc-DOX into mice enables the differentiation between multidrug-resistant tumors in a non-invasive way and the evaluation of tumor resistance and possible chemosensitizers.

***Keywords:*** Doxorubicin; Multidrug resistance; Tc-99m; $^{99m}$Tc-Doxorubicin

***Corresponding author:**
Bianca Gutfilen
(bgutfilen@hucff.ufrj.br)

**Citation:** Gutfilen B, de Souza SAL, Barboza T, *et al.* Evaluation of multidrug resistance in tumors using $^{99m}$Tc-doxorubicin. *Adv Radiother Nucl Med*. 2024;2(1):2822 https://doi.org/10.36922/arnm.2822

**Received:** January 25, 2024

**Accepted:** March 28, 2024

**Published Online:** April 3, 2024



## 1. Introduction

A biomarker is an indicator of physiologic or pathogenic processes or biological responses to a therapeutic intervention that can be objectively measured and evaluated. Measuring biomarkers can help with disease detection, treatment risk evaluation, or treatment effectiveness determination. In the case of cancer, anthracyclines such as doxorubicin (DOX) are part of the front-line therapy used to treat several malignancies, including leukemia, lymphomas, soft-tissue sarcomas, breast carcinoma, and other solid tumors. DOX was added to the armada of cancer therapy in the late 1960s, and the comprehensive investigations of its pharmacokinetics have enabled a more in-depth understanding of this medication. DOX can be administered as a single agent or in combination with other chemotherapeutic agents. Although DOX is also used for treating other tumors such as ovarian carcinoma, liver cancer, and stomach cancer, it is not the primary choice in the clinical treatment for these cancers due to the emergence of drug resistance.[1-3]

Multidrug resistance (MDR) constitutes the major obstacle to successful cancer treatment. Multidrug-resistant cell lines have been used as models to study MDR *in vitro* and *in vivo*. We selected for this study a cell line derived from K562, a chronic myeloid leukemia cell. The resistant cell line, Lucena 1, has been characterized[4] and features the overexpression of P-glycoprotein (Pgp), an ATP-dependent transporter capable of extruding substrates from the cell, including a range of chemotherapeutic drugs, therefore being less affected by the cytotoxic effects of the drugs.[5-13] Encoded by the *MDR1* gene, Pgp is a 170 kDa protein found in the cytoplasm, serving as a storage pool to maintain a steady-state level of membrane Pgp. Of note, the transport activity of these cells can be inhibited by the chemosensitizers, such as verapamil, trifluoperazine, and cyclosporine.[14-18]

DOX is actively extruded from cancer cells overexpressing Pgp. Thus, high cumulative doses of DOX are required in cancer chemotherapy to achieve a sufficient therapeutic effect. However, higher doses lead to dose-dependent side effects, such as cumulative cardiotoxicity, nephrotoxicity, and extravasation, which compromise its clinical applications. Moreover, intracellular DOX accumulation is a complex process, which includes cellular uptake, retention, relocalization, and efflux from the cell. At any given time, the drug accumulation in cells is the difference between the quantity of drug uptake and efflux. Thus, it is required to design the next generation of DOX derivatives to overcome drug resistance, improve their retention in the cell, and enhance the sustained therapeutic effect.[19]

Many studies have been performed to assess the efficacy of DOX therapies via novel research strategies. Despite the potential benefits of the currently available liposomal DOX delivery systems, relevant problems still persist. For example, cardiotoxicity arising after administration is still evident, although at a reduced frequency. Doxil/Caelyx use is commonly associated with the development of palmar-plantar erythema (PPE), which is believed to reflect the gradual accumulation and nonspecific release of DOX in the extremities. PPE manifests as a painful swelling of the hands and feet that ultimately requires a reduction in the administered dose, therefore resulting in less effective treatment.[20-22]

Based on these aforementioned studies and drawing from our experience in labeling different types of cells and molecules, such as leukocytes, stem cells, thymine, anti-CD3, and anti-TNF-α, for the diagnostic purposes of cancers and other diseases,[23-39] we successfully labeled DOX with $^{99m}$Tc. Previously, we conducted a pilot study in this regard involving women with breast cancer.[40] The current study aims to assess whether $^{99m}$Tc-DOX can be taken up by susceptible and multidrug-resistant cell lines. We used human chronic myeloid leukemia K562 cells and the resistant counterpart Lucena1 cells to evaluate Pgp detection and activity for this purpose. For *in vivo* evaluation, we applied $^{99m}$Tc-DOX in mice with Lewis lung carcinoma (3LL lineage).

## 2. Materials and methods

### 2.1. Radiolabeling of DOX

DOX (Eurofarma, Brazil) was labeled based on the direct reduction of 1 mCi (37 mBq) of $^{99m}TcO_4^-$ freshly eluted from a $^{99}$Mo/$^{99m}$Tc generator (IPEN/CNEN) with stannous chloride ($SnCl_2$; Sigma-Aldrich, USA). This labeling process is under patent registration. In the preparation of the radiopharmaceutical, all reagents were used under sterile conditions.

### 2.2. Chromatography

Chromatography was performed using methanol, isopropyl alcohol, and distilled water (3:2:5) as the mobile phase. Thin-layer chromatography (TLC) was used to characterize the labeled DOX using Whatman grade 4 paper. The TLC was performed using 2 μL of $^{99m}$Tc-DOX. The radioactivity of the strips was counted in Gamma Counter (Wizard 2, PerkinElmer), as presented in Table 1.

### 2.3. Stability evaluation

The stability of $^{99m}$Tc-DOX was evaluated in saline solution. The percentage of free $^{99m}TcO_4^-$ and the radioactivity of 99mTc-DOX were measured at different periods (immediately, 1, 3, 5, and 24 h).

### 2.4. Cell line culture

The human chronic myeloid leukemia K562 cells and the resistant counterpart Lucena1 cells (4) were cultured in 25 $cm^3$ cell culture flasks, at the final concentration of $2 \times 10^4$ cells/mL, in 5 mL of RPMI-1640 medium (Sigma-Aldrich, USA) supplemented with 10% fetal calf serum

**Table 1. Efficiency of DOX labeling compared with control carried out with sodium pertechnetate ($Na^{99m}TcO4$-)**

| Whatman paper number 4 | Bottom (%) | Top (%) | Total (%) |
|---|---|---|---|
| $^{99m}$Tc-DOX | 90.9 | 63.0 | 100 |
| $Na^{99m}TcO_4$- | 0.7 | 99.3 | 100 |

Note: Bottom (%) and top (%) referring to the Whatman paper strips.

(FCS; Cultilab, Brazil) and antibiotics at 37°C in 5% $CO_2$ atmosphere. Cells were passaged twice a week.

### 2.5. Detection of Pgp expression

For Pgp detection, cells were washed using phosphate-buffered saline (PBS) containing 5% FCS and incubated at 4°C for 30 min with mouse anti-human P-glycoprotein – FITC antibody (BD Pharmigen, USA) at a dilution of 1:4 (v/v). Negative control cells were incubated at 4°C for 30 min, without the antibody, in PBS containing 5% FCS. Following this, cells were washed and resuspended in PBS containing 5% FCS. At least 10,000 events were recorded within the gated region of the flow cytometer FACSCan (Beckton & Dickinson, USA).

### 2.6. Assessment of Pgp activity

For the assessment of Pgp activity, cells were washed using a medium containing 10% FCS and incubated at 37°C for 30 min with Rhodamine 123 (Rho; Sigma-Aldrich, USA), a Pgp's fluorescent substrate, at a concentration of 200 ng/mL, in the presence or absence of 5 μM verapamil (Sigma-Aldrich, USA), a Pgp inhibitor. After incubation, cells were washed and further incubated at 37°C for 30 min with a medium containing 10% FCS in the presence or absence of verapamil to allow cells to extrude or not the fluorescent substrate. After incubation, the cells were washed once more and resuspended in PBS containing 5% FCS. At least 10,000 events were recorded within the gated region of the flow cytometer FACSCan (Beckton & Dickinson, USA).

### 2.7. Determination of cell viability

K562 or Lucena I cells were seeded onto a 96-well plate at $2 \times 10^4$ cells/mL in RPMI 1640 (Sigma-Aldrich, USA) medium containing 10% FCS. Cells were kept for 3 days at 37°C in a 5% $CO_2$ atmosphere in the presence of 300 ng/mL of the chemotherapic DOX or its radiolabeled form $^{99m}$Tc-DOX and/or the Pgp inhibitor verapamil (5 μM). Controls were cells maintained in the absence of these substances. Each sample had three replicates. After a 72-h culture, cells were incubated with 20 μL of 3-(4,5-dimethylthiazol-2-yl)-2,5-diphenyltetrazolium bromide (MTT; Sigma-Aldrich, USA), at a concentration of 5 mg/mL, for 3 h at 37°C in a 5% $CO_2$ atmosphere. Following MTT incubation, a 200 μL aliquot of 100% DMSO (Vetec Química Fina, Brazil) was added to each culture to dissolve the crystals. The absorbance was measured at 490 nm using Sunrise™ microplate absorbance reader (Tecan, Switzerland).

### 2.8. *In vivo* development of Lewis lung carcinoma from 3LL cells

3LL cells were grown in high-glucose DMEM culture medium (Vitrocell, Brazil) supplemented with 10% FBS (Invitrogen, Brazil USA), 2 mM l-glutamine, 100 U/mL penicillin, and 100 μg/mL, 1% sodium pyruvate, and 1% nonessential amino acids (Sigma-Aldrich, US) for 48 h. After reaching confluency, the cells were collected with trypsin-EDTA (Invitrogen) and centrifuged at 1200 rpm for 10 min. Cells ($10^6$ cells/mL) were suspended in DMEM without serum. This cell suspension (100 μL, $10^5$ cells per animal) was injected subcutaneously in C57/Bl6 mice's left paws, and tumor growth was monitored for 15 days.

### 2.9. Statistical analysis

Student's *t*-test was employed to analyze the significance of the difference in Pgp expression and cell viability. Differences were considered statistically significant when $P < 0.05$.

## 3. Results

### 3.1. Radiolabeling and stability

The labeling efficiency was maintained at around 90% (Table 1). Moreover, the DOX was found to be stably labeled by $^{99m}$TC, especially in the first 5 h following labeling (Table 2).

### 3.2. Determination of Pgp expression and activity in K562 and Lucena 1 cell lines

Pgp expression in both K562 and Lucena 1 lines is graphically depicted in Figure 1A. Lucena 1 cell line exhibited overexpression of Pgp that is not observed in K562. The transporter activity of the protein (Figure 1B) was evaluated using a fluorescent substrate, Rho. When incubated with Rho, the K562 cells demonstrated a significant increase in intracellular fluorescence, surpassing the fluorescence intensity showcased by Lucena 1. However, in the presence of verapamil, a Pgp inhibitor, Lucena 1 cells showed a significant increase in intracellular fluorescence, a magnitude similar to that seen in K562 cells, suggesting that Pgp activity accounts for the Rho extrusion observed in Lucena 1 cells.

**Table 2. Labeling efficiency using Whatman grade 4 paper in different periods**

| Time (h) | Origin (%) | Top (%) |
|---|---|---|
| 0 | 90.9 | 9.1 |
| 1 | 86.3 | 13.7 |
| 3 | 83.6 | 16.1 |
| 5 | 82.4 | 17.6 |
| 24 | 74.3 | 25.7 |

Note: Origin (%) and top (%) referring to the Whatman paper number 4 strips.

### 3.3. Effect of $^{99m}$Tc-DOX on cell viability

To determine if the labeling process affected the cytotoxicity of $^{99m}$Tc-DOX, the two cell lines, K562 and Lucena 1 cells, were exposed to radiolabeled and unlabeled DOX (Figure 2). Both unlabeled DOX and $^{99m}$Tc-DOX equally affected K562 cells, decreasing their viability to 19 ± 15% and 11 ± 16%, respectively. The effects of the radiolabeled and unlabeled drugs on Lucena 1 cells (Figure 2A), however, were not statistically significant. Thus, it is evident that K562 cells (Figure 2B) displayed sensitivity to both drugs, but Lucena 1 cells were resistant to either substance. This finding aligns with our postulation that the drug remained intact after labeling, retaining the structure that contributes to its cytotoxicity. The cells were also exposed to DOX or $^{99m}$Tc-DOX combined with verapamil to evaluate if the resistance seen in Lucena cells was attributed to Pgp activity. As shown in Figure 2, the exposure to verapamil alone did not change the viability of either cell line. However, in the presence of DOX or $^{99m}$Tc-DOX combined with verapamil, Lucena 1 cells showed a statistically significant decrease in viability, suggesting that the resistance to labeled or unlabeled DOX can be reversed by Pgp inhibition. In addition, DOX structural characteristics that confer its capacity as a substrate to Pgp remained unaffected by the labeling process.

### 3.4. Biodistribution of $^{99]m}$Tc-DOX in mice with Lewis lung carcinoma

The biodistribution of the $^{99]m}$Tc-DOX was evaluated in normal mice and mice with Lewis lung carcinoma. The biodistribution results in normal mice, as shown in Figure 3A, indicate uptake of $^{99m}$Tc in the stomach and thyroid. Figure 3B shows the biodistribution in normal

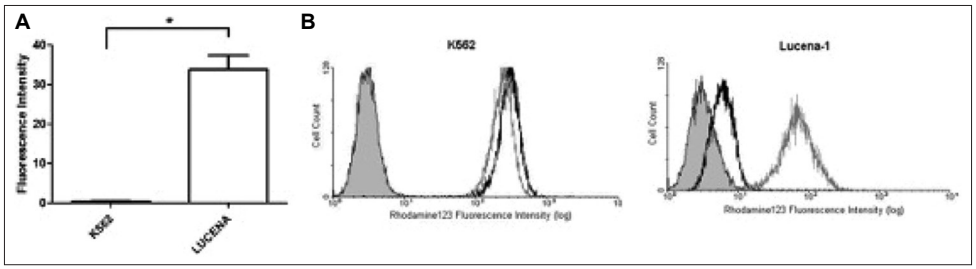


**Figure 1.** Pgp expression and activity in K562 and Lucena 1 cells. (A) Pgp expression in K562 and Lucena 1 cells. Cells were cultured for 72 h and then incubated with verapamil. Fluorescence intensity was measured by means of flow cytometry. The bar chart represents mean fluorescence intensity per cell line. The values are expressed as mean ± standard deviation from three separate experiments. *$P < 0.05$. (B) Pgp activity in K562 and Lucena 1 cells. Pgp activity was measured based on Rho accumulation; verapamil was used as a positive control modulator. Fluorescence intensity was measured by means of flow cytometry. The representative histograms shown are outputs of three independent experiments, where filled gray histogram denotes negative control, open black histogram denotes cells incubated with Rho, and open gray histogram denotes cells incubated with Rho and verapamil.

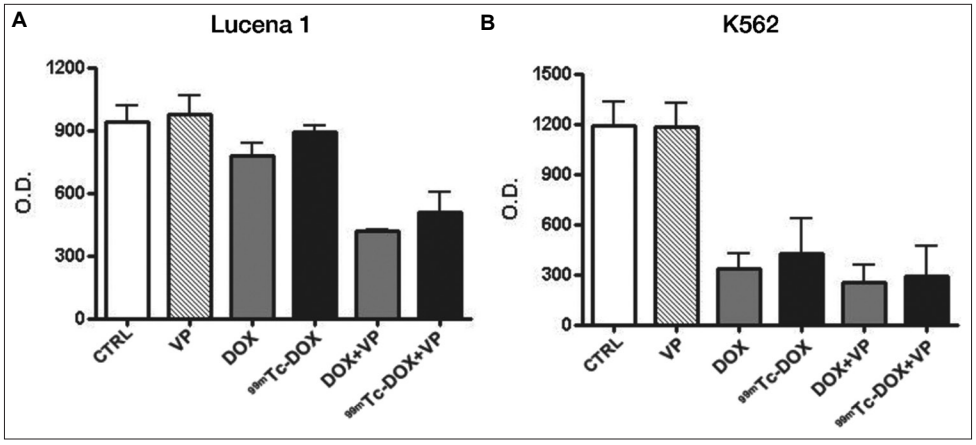


**Figure 2.** Cell viability in the presence of verapamil and DOX. (A) K562 cell viability in the presence of verapamil and DOX. Cells were cultured under the stated conditions for 3 days prior to cell viability measurement using MTT assay. (B) Lucena-1 cell viability in the presence of verapamil and DOX. Cells were cultured under the stated conditions for 3 days prior to cell viability measurement using MTT assay.

Notes: CTRL: Absence of DOX and verapamil; VP: In the presence of verapamil (5 μM); DOX: In the presence of DOX (300 ng/mL); $^{99m}$Tc-DOX: In the presence of $^{99m}$Tc-DOX (300 ng/mL); DOX + VP: In the presence of DOX (300 ng/mL) and verapamil (5 μM); $^{99m}$Tc-DOX+VP: In the presence of $^{99m}$Tc-DOX (300 ng/mL) and verapamil (5 μM). The values represent mean ± standard deviation of data from three independent experiments.

Abbreviation: O.D.: Optical density.

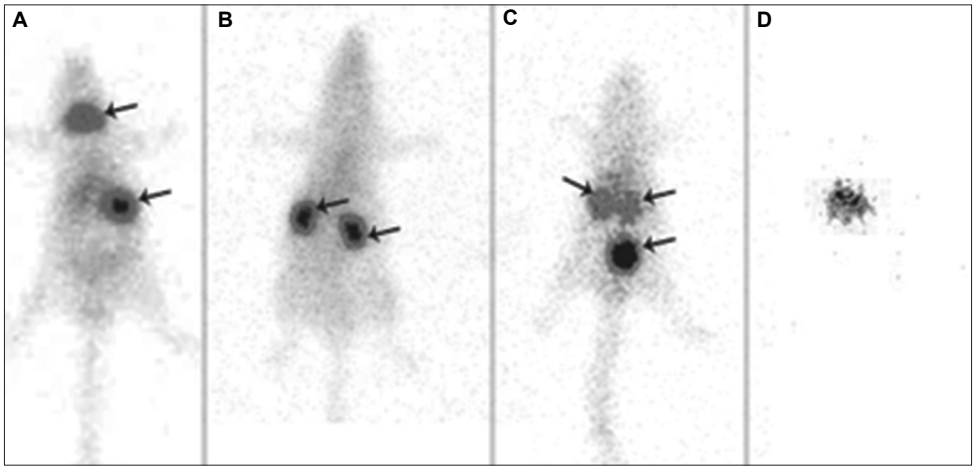


**Figure 3.** Biodistribution studies in mice. (A) $^{99m}$Tc-DOX was administered in normal mice. Images were acquired after 1 h of intravenous administration. There is an uptake in the thyroid and stomach. (B) Normal mice show uptake of $^{99m}$Tc-DOX by the kidneys 1 h after administration. (C) Mice with Lewis lung carcinoma show $^{99m}$Tc-DOX uptake in the liver and kidneys. There is no uptake in the thyroid and stomach. (D) *Ex vivo* examination of $^{99m}$Tc-DOX uptake by Lewis lung carcinoma.

mice, with $^{99m}$Tc-DOX uptake by the kidneys. Figure 3C shows $^{99m}$Tc-DOX biodistribution in mice with inoculated tumors, with a clear indication of $^{99m}$Tc-DOX uptake in the liver and kidneys, suggesting showing the strong and stable labeling of DOX with $^{99m}$Tc. There is no uptake of $^{99m}$Tc-DOX by the thyroid or stomach. When scanned *ex vivo*, the Lewis lung carcinoma manifested a targeted uptake of $^{99m}$Tc-DOX (Figure 3D).

## 4. Discussion

The medical specialty of nuclear medicine serves a very important purpose of enabling noninvasive detection of biochemical, molecular, and histological markers of tumor to facilitate the evaluation of tumor aggressiveness, invasiveness, and resistance to therapy. These findings from these applications may provide rational criteria for fine-tuning therapeutic strategies for each patient.[41]

Ohtani *et al.*[42] have investigated the uptake of $^{3}$H-vincristine by K562 cells to study MDR associated with Pgp. It is of precautionary importance to have a profound understanding of such drug resistance so as to decrease morbidity owing to unsuccessful therapy and to allow the selection of individuals who may benefit from the co-administration of MDR-inhibiting drugs.[43] The major shortcoming of using $^{3}$H for *in vivo* behavior studies is that it is a pure β emitter and thus cannot be used to noninvasively detect the distribution in different tissues or organs in live animals using imaging. $^{3}$H also has a long half-life (12.33 years), which limits its utility in patients.

Kostakoglul.[44] evaluated Pgp-mediated transport functions through PET technology, using $^{11}$C-labeled colchicine, verapamil, and daunorubicin in cell lines and animal studies. Similarly, Solbach *et al.*[45] labeled a chemotherapeutic agent, vinblastine, with $^{11}$C to image cancer patients. As a β emitter radionuclide with a half-life of 20 min, $^{11}$C can only be used in PET scanners and is not widely available. Although the labeling method applied could only yield a radiochemical purity of only 53%, the application of $^{11}$C allowed for the successful diagnosis of metastatic renal cell carcinomas. Since the radiosynthesis method applied by Solbach *et al.*[45] was very laborious, we resorted to using the direct labeling method, which is simpler to conduct and has a constant labeling efficiency of 90%.

Kurdziel and Kiesewetter[46] have attempted to label a chemotherapeutic agent, paclitaxel, for imaging multidrug-resistant tumors with a PET tracer, $^{18}$F. Adopting the same study design, they carried out *in vitro* radiotracer uptake studies using $^{18}$F-FPAC, $^{99m}$Tc-sestamibi, and $^{99m}$Tc-tetrofosmin (a known MDR substrate), as well as $^{18}$F-FDG (as a negative control). A similar differential uptake between the sensitive and resistant cell lines was seen in all radiolabeled MDR substrates but not for $^{18}$F-FDG (the uptake was not associated with MDR). The limitation of using this radiopharmaceutical is the limited availability of PET tracers in many countries.

The interaction of DOX prevents DNA replication and transcription by inhibiting topoisomerase II. However, DOX is actively extruded from cancer cells overexpressing Pgp. High cumulative doses of DOX are required in cancer chemotherapy to achieve a sufficient therapeutic effect.[47,48] In light of this, we developed a new radiopharmaceutical ($^{99}$mTc-DOX) to evaluate the mechanism of DOX behavior that could be used further in animals and patients. $^{99m}$Tc is

a suitable radionuclide for *in vivo* imaging, as it is a gamma emitter with a short half-life of 6 h. We used a culture of K562 and Lucena 1 (a multidrug-resistant cell line) to investigate whether $^{99m}$Tc-DOX retains its cytotoxicity and structural characteristics. $^{99}$]Tc-DOX, similar to unlabeled DOX, was shown to be cytotoxic to chronic myeloid leukemia cell lines (K562) and maintain its capacity as a Pgp substrate *in vitro*. Furthermore, the cells were not radiosensitive to the amount of radionuclide present in the molecule. This could be observed by incubating multidrug-resistant cells with $^{99m}$Tc-DOX and verifying that cytotoxicity was only observed when the drug was internalized and retained inside the cell.

DOX labeled with radionuclides have previously been tested to study the characteristics of DOX in tumors. Polyak *et al.*[49] and Bao *et al.*,[50] using different DOX liposomal delivery systems, performed a direct radiolabeling of DOX, achieving an efficiency of approximately 70%. In contrast, we used a non-liposomal DOX, obtaining a 90% efficiency by direct labeling.

Another approach to evaluating tumor growth is using radiopharmaceuticals against DNA bases. Sun *et al.*[51] imaged DNA synthesis with PET using $^{18}$F-1-(2'-deoxy-2'-fluoro-beta-D-arabinofuranosyl)thymine ($^{18}$F-FMAU), a pyrimidine analog, which is phosphorylated by thymidine kinase and incorporated into DNA. Their results demonstrated that $^{18}$F-FMAU was selectively retained in the DNA of proliferating cells and was resistant to degradation.[51]

Koukourakis *et al.*[52] labeled liposomal DOX with $^{99m}$Tc and evaluated its uptake in patients with brain tumors. The radiolabeled DOX accumulation was 13- to 19-fold higher in glioblastomas and 7- to 13-fold higher in metastatic lesions than in the normal brain. Kumar *et al.*[53] studied the DOX labeled with $^{99m}$Tc *in vitro* and in Ehrlich ascites tumor-bearing mice, and demonstrated the physiological distribution of 99mTc-DOX in kidneys and liver. The tumor had a focused uptake of the radiopharmaceutical at 1.5 h up to 4 h. Bao *et al.*[50] demonstrated that the labeled pegylated DOX in normal rats had a slow blood clearance and a high uptake in the bowel and surrounding tissues. In another study, Yang *et al.*[54] investigated the behavior of DOX liposomes labeled with $^{111}$]In after their intravenous administration to intracranial human glioblastoma tumor-bearing mice suffering blood–brain barrier disruption induced by focused ultrasound.

In this study, DOX was labeled using a direct method, an approach that allows for high labeling efficiencies. It is important to point out that there is a difference in the biodistribution of $^{99m}$Tc and $^{99m}$Tc-DOX. $^{99m}$Tc-DOX is uptaken by the kidneys in normal mice, while mice with Lewis lung carcinoma show uptake in the liver and kidneys, the organs responsible for excretion. *Ex vivo* studies, on the other hand, provided an avenue for visualizing the $^{99m}$Tc-DOX uptake in the tumor. In a separate study, we found that breast carcinoma lesions exhibited increased uptake of $^{99m}$Tc-DOX, which was eliminated through renal and hepatic routes.[40]

## 5. Conclusion

The present study illustrates the potential of labeling DOX with $^{99m}$Tc, an approach that may prove to be conducive to the design of the next-generation DOX derivatives used in overcoming drug resistance, improving intracellular DOX retention, and enhancing sustained therapeutic effect. Follow-up studies are warranted to confirm whether $^{99m}$Tc-DOX can serve as a drug resistance marker.

## Acknowledgments

We appreciate the contribution of Dra. Eliene Oliveira Kozlowski kindly prepared the culture of 3LL cells and conducted the tumor induction experiment.

## Funding

This study was supported by grants from Fundação Carlos Chagas Filho de Amparo à Pesquisa do Estado do Rio de Janeiro (FAPERJ) and Conselho Nacional de Desenvolvimento Científico e Tecnológico (CNPq).

## Conflict of interest

The authors declare they have no competing interests.

## Author contributions

*Conceptualization:* Vivian M. Rumjanek, Bianca Gutfilen
*Investigation:* All authors
*Methodology:* All authors
*Writing – original draft:* All authors
*Writing – review & editing:* Bianca Gutfilen, Sergio Augusto Lopes de Souza, Vivian M. Rumjanek

## Ethics approval and consent to participate

National Cancer Institute, Ministry of Health, Brazil.

## Consent for publication

Not applicable.

## Availability of data

Data are available from the corresponding author on reasonable request.

## References

1. Dickey JS, Rao VA. Current and proposed biomarkers of anthracycline cardiotoxicity in cancer: Emerging opportunities in oxidative damage and autophagy. *Curr Mol Med*. 2012;12(6):763-771.

   doi: 10.2174/156652412800792561

2. Speth PA, van Hoesel QG, Haanen C. Clinical pharmacokinetics of doxorubicin. *Clin Pharmacokinet*. 1988;15(1):15-31.

   doi: 10.2165/00003088-198815010-00002

3. Alkreathy HM, Damanhouri ZA, Ahmed N, Slevin M, Osman AMM. Mechanisms of cardioprotective effect of aged garlic extract against doxorubicin-induced cardiotoxicity. *Integr Cancer Ther*. 2012;11(4):364-370.

   doi: 10.1177/1534735411426726

4. Rumjanek VM, Trindade GS, Wagner-Souza K, *et al*. Multidrug resistance in tumour cells: Characterisation of the multidrug resistant cell line K562-Lucena 1. *An Acad Bras Ciênc*. 2001;73(1):57-69.

   doi: 10.1590/s0001-37652001000100007

5. Bernardo AA, Pinto-Silva FE, Persechini PM, *et al*. Effect of extracellular ATP on the human leukaemic cell line K562 and its multidrug counterpart. *Mol Cell Biochem*. 2006;289(1-2):111-124.

   doi: 10.1007/s11010-006-9154-2

6. de Souza Votto AP, Renon VP, Yunes JS, *et al*. Sensitivity to microcystins: A comparative study in human cell lines with and without multidrug resistance phenotype. *Cell Biol Int*. 2007;31(11):1359-1366.

   doi: 10.1016/j.cellbi.2007.05.010

7. Leite D, Kassuya C, Mazzuco T, *et al*. The cytotoxic effect and the multidrug resistance reversing action of lignans from *Phyllanthus amarus*. *Planta Med*. 2006;72(15): 1353-1358.

   doi: 10.1055/s-2006-951708

8. Maia RC, Silva EA, Harab RC, Lucena M, Pires V, Rumjanek VM. Sensitivity of vincristine-sensitive K562 and vincristine-resistant K562-Lucena 1 cells to anthracyclines and reversal of multidrug resistance. *Braz J Med Biol Res*. 1996;29(4):467-472.

9. Maia RC, Vasconcelos FC, de Sá Bacelar T, *et al*. LQB-118, a pterocarpanquinone structurally related to lapachol [2-hydroxy-3-(3-methyl-2-butenyl)-1,4-naphthoquinone]: A novel class of agent with high apoptotic effect in chronic myeloid leukemia cells. *Invest New Drugs*. 2011;29(6): 1143-1155.

   doi: 10.1007/s10637-010-9453-z

10. Netto CD, Santos ESJ, Castro CP, da Silva AJM, Rumjanek VM, Costa PRR. (±)-3,4-Dihydroxy-8,9-methylenedioxypterocarpan and derivatives: Cytotoxic effect on human leukemia cell lines. *Eur J Med Chem*. 2009;44(2):920-925.

    doi: 10.1016/j.ejmech.2008.01.027

11. Salustiano EJS, Netto CD, Fernandes RF, *et al*. Comparison of the cytotoxic effect of lapachol, α-lapachone and pentacyclic 1,4-naphthoquinones on human leukemic cells. *Invest New Drugs*. 2010;28(2):139-144.

    doi: 10.1007/s10637-009-9231-y

12. Votto APS, Domingues BS, Souza MMD, *et al*. Toxicity mechanisms of onion (*Allium cepa*) extracts and compounds in multidrug resistant erythroleukemic cell line. *Water*. 2010;43:429-437.

13. Wagner-Souza K, Echevarria-Lima J, Rodrigues LAP, Reis M, Rumjanek VM. Resistance to thapsigargin-induced intracellular calcium mobilization in a multidrug resistant tumour cell line. *Mol Cell Biochem*. 2003;252(1-2):109-116.

    doi: 10.1023/a:1025586225941

14. Brock I, Hipfner DR, Nielsen BS, *et al*. Sequential coexpression of the multidrug resistance genes MRP and mdr1 and their products in VP-16 (etoposide)-selected H69 small cell lung cancer cells. *Cancer Res*. 1995;55(3):459-462.

15. Liu Z, Stevenson GD, Barrett HH, *et al*. Imaging recognition of inhibition of multidrug resistance in human breast cancer xenografts using 99mTc-labeled sestamibi and tetrofosmin. *Nucl Med Biol*. 2005;32(6):573-583.

    doi: 10.1016/j.nucmedbio.2005.04.014

16. Tanaka PY, Calore EE. P-glycoprotein expression in non-Hodgkin's lymphomas of human immunodeficiency virus infected patients. *Pathol Res Pract*. 2007;203(1):1-7.

    doi: 10.1016/j.prp.2006.09.004

17. Crow MJ, Grant G, Provenzale JM, Wax A. Molecular imaging and quantitative measurement of epidermal growth factor receptor expression in live cancer cells using immunolabeled gold nanoparticles. *Am J Roentgenol*. 2009;192(4):1021-1028.

    doi: 10.2214/AJR.07.3535

18. Dizdarevic S, Peters AM. Imaging of multidrug resistance in cancer. *Cancer Imaging*. 2011;11(1):1-8.

    doi: 10.1102/1470-7330.2011.0001

19. Chhikara BS, Mandal D, Parang K. Synthesis. Anticancer activities, and cellular uptake studies of lipophilic derivatives of doxorubicin succinate. *J Med Chem*. 2012;55(4): 1500-1510.

    doi: 10.1021/jm201653u

20. Lammers T, Storm G, Kiessling F. Nanomedicine formulations for combination therapies. *Nano Rev*. 2010; 1:1-3.

doi: 10.3402/nano.v1i0.5705

21. Lammers T, Hennink WE, Storm G. Tumour-targeted nanomedicines: Principles and practice. *Br J Cancer*. 2008;99(3):392-397.

doi: 10.1038/sj.bjc.6604483

22. Kaminskas LM, McLeod VM, Kelly BD, *et al*. Doxorubicin-conjugated PEGylated dendrimers show similar tumoricidal activity but lower systemic toxicity when compared to PEGylated liposome and solution formulations in mouse and rat tumor models. *Mol Pharm*. 2012;9(3):422-432.

doi: 10.1021/mp200522d

23. Gutfilen B, Rossini A, Martins FP, da Fonseca LM. Tc-99m-leukocytes--is it an intracellular labelling? *J Clin Lab Immunol*. 1999;51(1):1-7.

24. Gutfilen B, Lopes de Souza SA, Martins FPP, Cardoso LR, Pinheiro Pessoa MC, Fonseca LMB. Use of 99mTc-mononuclear leukocyte scintigraphy in nosocomial fever. *Acta Radiol*. 2006;47(7):699-704.

doi: 10.1080/02841850600791526

25. Gutfilen B, Rodrigues E, Soraggi R, Barbosa Da Fonseca LH. Preliminary observation of 99mTc-thymine imaging in breast neoplasms. *Nucl Med Commun*. 2001;22(10): 1133-1137.

doi: 10.1097/00006231-200110000-00013

26. Lopes FPPL, de Azevedo MNL, Marchiori E, da Fonseca LMB, de Souza SAL, Gutfilen B. Use of 99mTc-anti-CD3 scintigraphy in the differential diagnosis of rheumatic diseases. *Rheumatology*. 2010;49(5):933-939.

doi: 10.1093/rheumatology/kep471

27. Roimicher L, Lopes FPPL, de Souza SL, *et al*. (99m)Tc-anti-TNF-α scintigraphy in RA: A comparison pilot study with MRI and clinical examination. *Rheumatology* (*Oxford*). 2011;50(11):2044-2050.

doi: 10.1093/rheumatology/ker234

28. Lopes FPPL, de Souza SAL, dos Santos Teixeira PF, *et al*. 99mTc-Anti-TNF-α scintigraphy: A new perspective within different methods in the diagnostic approach of active graves ophthalmopathy. *Clin Nucl Med*. 2012;37(11):1097-1101.

doi: 10.1097/RLU.0b013e31826c0c16

29. Rebelo Pinto ES, Lopes F, de Souza S, *et al*. A pilot study evaluating 99mTc-anti-TNF-alpha scintigraphy in Graves' ophtalmopathy patients with different clinical activity score. *Horm Metab Res*. 2013;45(10):765-768.

doi: 10.1055/s-0033-1349891

30. Ribeiro MP, Souza SAL, Lopes FPPL, Rosado-de-Castro PH, Fonseca LMB, Gutfilen B. 99mTc-thymine scintigraphy may be a promising method in the diagnosis of breast cancer. *Clinics* (*Sao Paulo*). 2013;68(3):283-289.

doi: 10.6061/clinics/2013(03)oa01

31. de Souza S, Nentzinsky V, do Carmo C, Roimicher L, da Fonseca L, Gutfilen B. Scintigraphy for detecting tumour necrosis factor-α on the skin of patients with psoriatic arthritis. *Scand J Rheumatol*. 2017;46(5):377-380.

doi: 10.1080/03009742.2016.1264627

32. Silva JD, Lopes-Pacheco M, de Castro LL, *et al*. Eicosapentaenoic acid potentiates the therapeutic effects of adipose tissue-derived mesenchymal stromal cells on lung and distal organ injury in experimental sepsis. *Stem Cell Res Ther*. 2019;10(1):264.

doi: 10.1186/s13287-019-1365-z

33. Aguiar FS, Melo AS, Araújo AMS, *et al*. Autologous bone marrow-derived mononuclear cell therapy in three patients with severe asthma. *Stem Cell Res Ther*. 2020;11(1):167.

doi: 10.1186/s13287-020-01675-x

34. Gutfilen B, Pellini MP, de Roure e Neder J, *et al*. 99mTc labeling white blood cells with a simple technique: Clinical application. *Ann Nucl Med*. 1994;8(1):85-89.

doi: 10.1007/BF03164991

35. Lopes de Souza SA, Barbosa da Fonseca LM, Torres Gonçalves R, *et al*. Diagnosis of renal allograft rejection and acute tubular necrosis by 99mTc-mononuclear leukocyte imaging. *Transplant Proc*. 2004;36(10):2997-3001.

doi: 10.1016/j.transproceed.2004.11.100

36. Couto BG, Goldenberg RCS, da Fonseca LMB, *et al*. Bone marrow mononuclear cell therapy for patients with cirrhosis: A Phase 1 study. *Liver Int*. 2011;31(3):391-400.

doi: 10.1111/j.1478-3231.2010.02424.x

37. Carvalho AB, Quintanilha LF, Dias JV, *et al*. Bone marrow multipotent mesenchymal stromal cells do not reduce fibrosis or improve function in a rat model of severe chronic liver injury. *Stem Cells*. 2008;26(5):1307-1314.

doi: 10.1634/stemcells.2007-0941

38. Battistella V, de Freitas GR, da Fonseca LMB, *et al*. Safety of autologous bone marrow mononuclear cell transplantation in patients with nonacute ischemic stroke. *Regen Med*. 2011;6(1):45-52.

doi: 10.2217/rme.10.97

39. Barbosa da Fonseca LM, Gutfilen B, Rosado de Castro PH, *et al*. Migration and homing of bone-marrow mononuclear cells in chronic ischemic stroke after intra-arterial injection. *Exp Neurol*. 2010;221(1):122-128.

doi: 10.1016/j.expneurol.2009.10.010

40. Araujo FI, Proença FPP, Ferreira CG, *et al*. Use of $^{99]m}$ Tc-doxorubicin scintigraphy in females with breast cancer: A pilot study. *Br J Radiol*. 2015;88(1052):20150268.

doi: 10.1259/bjr.20150268

41. Muzzammil T, Moore MJ, Hedley D, Ballinger JR. Comparison of (99m)Tc-sestamibi and doxorubicin to monitor inhibition of P-glycoprotein function. *Br J Cancer*. 2001;84(3):367-373.

doi: 10.1054/bjoc.2000.1621

42. Ohtani H, Ikegawa T, Honda Y, *et al*. Effects of various methoxyflavones on vincristine uptake and multidrug resistance to vincristine in P-gp-overexpressing K562/ADM cells. *Pharm Res*. 2007;24(10):1936-1943.

doi: 10.1007/s11095-007-9320-6

43. Mezi S, Primi F, Capoccetti F, Scopinaro F, Modesti M, Schillaci O. *In vivo* detection of resistance to anthracycline based neoadjuvant chemotherapy in locally advanced and inflammatory breast cancer with technetium-99m sestamibi scintimammography. *Int J Oncol*. 2003;22(6):1233-1240.

44. Kostakoglu L. Noninvasive detection of multidrug resistance in patients with hematological malignancies: Are we there yet? *Clin Lymphoma*. 2002;2(4):242-248.

doi: 10.3816/clm.2002.n.006

45. Solbach C, Patt M, Reimold M, *et al*. [$^{11}$C]Vinblastine syntheses and preliminary imaging in cancer patients. *J Pharm Pharm Sci*. 2007;10(2):266s-76s.

46. Kurdziel KA, Kiesewetter DO. PET imaging of multidrug resistance in tumors using 18F-fluoropaclitaxel. *Curr Top Med Chem*. 2010;10(17):1792-1798.

doi: 10.2174/156802610792928077

47. Fornari FA, Randolph JK, Yalowich JC, Ritke MK, Gewirtz DA. Interference by doxorubicin with DNA unwinding in MCF-7 breast tumor cells. *Mol Pharmacol*. 1994;45(4): 649-656.

48. Momparler RL, Karon M, Siegel SE, Avila F. Effect of adriamycin on DNA, RNA, and protein synthesis in cell-free systems and intact cells. *Cancer Res*. 1976;36(8):2891-2895.

49. Polyak A, Palade EA, Balogh L, *et al*. *In vitro* and biodistribution examinations of Tc-99m-labelled doxorubicin-loaded nanoparticles. *Nucl Med Rev Cent East Eur*. 2011;14(2):55-62.

doi: 10.5603/nmr.2011.00016

50. Bao A, Goins B, Klipper R, Negrete G, Phillips WT. Direct 99m Tc labeling of pegylated liposomal doxorubicin (Doxil) for pharmacokinetic and non-invasive imaging studies. *Pharmacology*. 2004;308(2):419-425.

doi: 10.1124/jpet.103.059535

51. Sun H, Sloan A, Mangner TJ, *et al*. Imaging DNA synthesis with [18F]FMAU and positron emission tomography in patients with cancer. *Eur J Nucl Med Mol Imaging*. 2005;32(1):15-22.

doi: 10.1007/s00259-004-1713-8

52. Koukourakis MI, Koukouraki S, Fezoulidis I, *et al*. High intratumoural accumulation of stealth® liposomal doxorubicin (Caelyx®) in glioblastomas and in metastatic brain tumours. *Br J Cancer*. 2000;83(10):1281-1286.

doi: 10.1054/bjoc.2000.1459

53. Kumar P, Singh B, Sharma S, *et al*. Preclinical evaluation of [99m]Tc-Labeled doxorubicin as a potential scintigraphic probe for tumor imaging. *Cancer Biother Radiopharm*. 2012;27(3):221-225.

doi: 10.1089/cbr.2011.1086

54. Yang FY, Wang HE, Liu RS, *et al*. Pharmacokinetic analysis of 111In-labeled liposomal doxorubicin in murine glioblastoma after blood-brain barrier disruption by focused ultrasound. *PLoS One*. 2012;7(9):e45468.

doi: 10.1371/journal.pone.0045468

ACCSCIENCE PUBLISHING

Advances in Radiotherapy & Nuclear Medicine

SHORT COMMUNICATION

# $^{18}$F-FDG positron emission tomography-computed tomography and Richter transformation: A retrospective study with a cohort of 12 consecutive patients

**Salah Oueriagli Nabih*, Chaymae Bensaid, Meryem Aboussabr, Omar Ait Sahel, Yassir Benameur, and Abderrahim Doudouh**

Department of Nuclear Medicine, Mohammed V Military Teaching Hospital, Mohamed V University, Rabat, Morocco

## Abstract

Richter transformation (RT) refers to a transformational process of chronic lymphocytic leukemia (CLL) into a more aggressive form. CLL is considered an indolent lymphoma with no avidity to $^{18}$F-fluorodeoxyglucose positron emission tomography/computed tomography ($^{18}$F-FDG PET/CT). RT transforms CLL into a diffuse large B-cell lymphoma, Hodgkin's lymphoma, or prolymphocytic leukemia, and the lymphoid tissue becomes highly FDG avid. The main value of $^{18}$F-FDG PET/CT in CLL patients lies in its ability to exclude RT with high negative predictive value and identify sites of increased $^{18}$F-FDG uptake that is suitable for biopsy. In our retrospective analysis, we examined 12 patients suspected of RT, who were included in our study between November 2018 and December 2022. $^{18}$F-FDG PET/CT was considered for patients with enlarged lymph node, fever, and elevated lactate dehydrogenase levels. A cutoff standardized uptake value (SUVmax) = 5 was chosen empirically based on our institutional practice. Extranodal disease was suspected if abnormal $^{18}$F-FDG uptake was observed in the liver, spleen, bone marrow, or another organ. In this study, the specificity of $^{18}$F-FDG PET/CT was 44.5%, with positive and negative predictive values of 37.5% and 100%, respectively. Frequencies of cases with increased uptake of $^{18}$F-FDG in the "only nodal sites" and "nodal and extranodal sites," relative to positive biopsies, were 20% and 66%, respectively.

***Keywords:*** $^{18}$F-FDG PET/CT; Predictive value; Chronic lymphocytic leukemia; Richter syndrome transformation

***Corresponding author:**
Salah Oueriagli Nabih
(salah.nabihoueriagli@gmail.com)

**Citation:** Nabih SO, Bensaid C, Aboussabr M, Sahel OA, Benameur Y, Doudouh A. $^{18}$F-FDG positron emission tomography-computed tomography and Richter transformation: A retrospective study with a cohort of 12 consecutive patients. *Adv Radiother Nucl Med*. 2024;2(1):2431. https://doi.org/10.36922/arnm.2431

**Received:** December 14, 2023

**Accepted:** March 15, 2024

**Published Online:** March 27, 2024



## 1. Introduction

Chronic lymphocytic leukemia (CLL) is an indolent disease characterized by the proliferation of B-cell lymphocytes. CLL may be converted into a more aggressive type, usually a diffuse large B-cell lymphoma (DLBCL) and less frequently a Hodgkin's lymphoma or prolymphocytic leukemia, through a process called Richter transformation (RT).[1,2] The early detection of RT and identification of high-risk CLL patients are performed with hybrid metabolic imaging using 18-flu=orine fluorodeoxyglucose positron emission tomography-computed tomography ($^{18}$F-FDG PET/CT) owing to

its ability to distinguish RT with high negative predictive value and identify sites of increased $^{18}$F-FDG uptake that is suitable for biopsy. This study aimed to precisely evaluate the positive and negative predictive values and predict the most affected lymph node sites, which can be validated with histopathological confirmation.

## 2. Methods

### 2.1. Patient recruitment

A retrospective analysis of consecutive CLL patients who underwent $^{18}$F-FDG PET/CT at our institution between November 2018 and December 2022 was performed. The indication for PET/CT was suspicion of RST. $^{18}$F-FDG PET/CT was considered for patients with CLL presented with elevated lactate dehydrogenase (LDH) levels, enlarged lymph node, and fever in the absence of infection. Patients were excluded from the study if they had not undergone bone marrow or lymph node biopsy after a positive PET/CT (e.g., patients with high suspicion of RT requiring urgent treatment).

### 2.2. $^{18}$F-fluorodeoxyglucose positron emission tomography-computed tomography imaging

All $^{18}$F-FDG PET/CT scans were performed on an integrated PET/CT scanner (GE Discovery STE8, GE Healthcare, USA). The patients fasted for at least 8 h before undergoing scanning with any premedication. Blood glucose levels and body weight were measured shortly before the injection. All patients had blood glucose levels below 6.27 mmol/L. Image acquisition was conducted 45 – 60 min after intravenous injection with a net dose of 3 MBq/kg of $^{18}$F-FDG and an average uptake time of 50 min. The mean net injected $^{18}$F-FDG dose, calculated based on body weights ranging from 50 to 80 kg and excluding residual activity in the syringe, was 193 MBq.

PET/CT images were acquired from the head to the upper thighs for 3 min per bed position. PET images were reconstructed using standard vendor-provided reconstruction algorithms, which incorporated ordered-subset expectation maximization, including the two iterations, 28 subsets, and a 128 × 128 reconstruction matrix. PET images were subjected to attenuation correction using data from the CT component of the examination. CT examination covering the area from the skull base to the upper thighs was performed using the following parameters: 120 mA for current intensity and 140 kVp for voltage, with a table speed of 13.5 mm/rotation. Axial CT images were reconstructed with a section thickness of 3.75 mm.

All PET/CT studies were reviewed by two nuclear physicians. Both physicians examined the PET, CT, and fused PET/CT images at a combined reading session. The fused PET/CT images were used primarily for localizing lesions and differentiating abnormal metabolic activity from physiological $^{18}$F-FDG uptake within adjacent organs. Metabolic activity within sites of abnormal $^{18}$F-FDG uptake was analyzed qualitatively and semi-quantitatively on the PET images. The determination of the standardized uptake value (SUVmax) within the volume of interest followed the formula:

$$\text{SUVmax} = (\text{Measured activity within the volume of interest in MBq/mL})/(\text{Injected dose of } ^{18}\text{F-FDG in MBq})/(\text{Patient's body weight in g}) \quad (I)$$

The accuracy and consistency of SUV measurements with $^{18}$F-FDG PET/CT were maintained by our in-house quality control program. The program is performed by our service team weekly and relies on the use of radioactive $^{18}$F-containing sources and calibration phantoms (i.e., for replicating human tissues), adherence to standardized protocols, in-depth result analysis, and ongoing training of personnel to maintain optimal performance. These practices allow for meticulous monitoring of equipment performance, ensuring measurement fidelity and obtaining reliable results during medical imaging examinations.

On the PET/CT images, sites of abnormal $^{18}$F-FDG uptake were documented with respect to the intensity of the uptake and its anatomic location, and these parameters were then compared to the $^{18}$F-FDG intensity in the liver, with values ranging from 2.4 to 4.5 and a mean value of 3.2. In our study, an SUVmax >5 within a lymph node or extranodal site was considered suggestive of RT, whereas SUVmax <5 indicated a more indolent phase of CLL. A cutoff SUVmax = 5 was chosen empirically based on our institutional practice and other similar studies.[3,4] Extranodal disease was suspected if abnormal $^{18}$F-FDG uptake was observed within an extranodal soft-tissue mass or in the liver, spleen, bone marrow, or another organ. The $^{18}$F-FDG PET/CT findings were then correlated with histological findings from the bone marrow or lymph node biopsies performed on patients with positive PET/CT.

### 2.3. Histopathological and descriptive analyses

Histopathological examination is the gold standard for the diagnosis of RT and was used in this study for patients with positive PET/CT. Biopsy was performed either on the lymph nodes, extranodal site, or the bone marrow. Descriptive analyses of the patient's age, sex, and the nodal and extranodal sites of increased uptake were performed accordingly.

## 3. Results

A total of 12 patients suspected of RT were included in our study. Their mean age at the time of their $^{18}$F-FDG PET/CT scan was 66 years (range: 53 – 76 years). There was a

male predominance (i.e., eight male [66%] and four female [34%] patients) among the patients. From the $^{18}$F-FDG PET/CT scans, eight (66%) scans were positive, and four (34%) scans were negative. Patients with a positive PET/CT result subsequently underwent histopathological examination. Among them, three individuals had evidence of RT, particularly in the form of DLBCL.

The patients started treatment for CLL before confirming RT, and the treatment included active monitoring, chemotherapy, and immunotherapy. Furthermore, the three RT-positive patients adopted the R-CHOP chemotherapy regimen. In general, most CLL patients can lead a prolonged life with the disease, while some CLL patients may have quicker CLL progression. Unfortunately, three patients with untransformed CLL were deceased during the study.

The specificity of $^{18}$F-FDG PET/CT for detecting RT was 44.5%, with positive and negative predictive values of 37.5% and 100%, respectively. Frequencies of cases with increased uptake in the "only nodal sites" and "nodal and extranodal sites," relative to positive biopsies, were 20% and 66%, respectively. Cervical (28.5%) and inguinal (28.5%) lymph nodes were the most affected in the supradiaphragmatic and infradiaphragmatic areas, respectively. The complete $^{18}$F-FDG PET/CT results are displayed in Tables 1-3.

## 4. Discussion

CLL is defined by the proliferation of phenotypically monoclonal B-cell lymphocytes derived from blood, marrow, or lymph nodes.[5] CLL is considered an indolent or low-grade lymphoma, and the CLLs of 5%–10% of patients reportedly develop into an aggressive form through RT.[6-10]

The use of $^{18}$F-FDG PET/CT can effectively identify biopsy sites in tumors (i.e., intense metabolically active nodes), and in combination with other biological markers, physicians can accurately assess the CLL stage and prognosis of patients to make better, more informed treatment decisions.[7,8]

CLL is characterized by low $^{18}$F-FDG avidity in PET/CT imaging, corresponding to the low mitotic activity of the lymphocytes.[3-9] However, RT would increase the avidity of lymphoid tissues to $^{18}$F-FDG (Figure 1). The increased SUVmax in lymph nodes correlated with high suspicion for RT and should be further evaluated. Furthermore, $^{18}$F-FDG PET/CT may be used to identify intensely metabolically active nodes for biopsy.[10]

The main value of $^{18}$F-FDG PET/CT in CLL patients is its ability to detect RT with a negative predictive value of 97% and identify sites of increased $^{18}$F-FDG uptake that is suitable for biopsy or surveillance.[3] In our study, cervical and inguinal lymph nodes were, respectively, the most affected in the supradiaphragmatic and infradiaphragmatic areas, respectively (Figures 1 and 2). The SUVmax in the cervical nodes had a range of 6.1–7.7, but the SUVmax was more intense in the inguinal lymph nodes with a range of 6.8–26.1. Our findings also displayed that increased uptake in the nodal and the extranodal sites were predictive of

**Table 1. PET/CT findings of the study population**

| Patient | Sex/age | Supradiaphragmatic nodal sites of increased $^{18}$F-FDG uptake (SUVmax) | Infradiaphragmatic nodal sites of increased $^{18}$F-FDG uptake (SUVmax) | Extranodal sites of increased $^{18}$F-FDG uptake (SUVmax) | Range of SUVmax | PET value | Biopsy |
|---|---|---|---|---|---|---|---|
| 1 | M/63 | Left axillary (3.1) | Left external iliac (2.9) | No uptake | 2.1 – 3.1 | (-) | N/A |
| 2 | M/62 | Left lung hilar (8.8) | Right inguinal (2.0) | Lung (8.2); liver (6.5); L3 (7.8) | 2.0 – 8.8 | (+) | (+) |
| 3 | M/68 | Right sub maxillary (7.7) | Left inguinal (6.8) | Right femur (4.1) | 2.8 – 7.7 | (+) | (-) |
| 4 | F/74 | Left axillary (7.0) | Right inguinal (26.1) | Spleen (10.3); right ischion (6.4) | 1.8 – 26.1 | (+) | (+) |
| 5 | F/53 | Left cervical (6.6) | Right inguinal (7.5) | No uptake | 3.5 – 7.5 | (+) | (-) |
| 6 | F/71 | Right axillary (2.3) | Mesenteric nodes (3.2) | No uptake | 1.8 – 3.2 | (-) | N/A |
| 7 | F/76 | Left axillary (2.7) | Left crural (3.8) | No uptake | 2.0 – 3.8 | (-) | N/A |
| 8 | M/71 | Right cervical (6.1) | Lombo-aortic (3.8) | No uptake | 2.7 – 6.1 | (+) | (-) |
| 9 | M/73 | No uptake | No uptake | No uptake | N/A | (-) | N/A |
| 10 | M/70 | Right lung hilar (5.8) | Right inguinal (4.1) | No uptake | 2.1 – 5.8 | (+) | (-) |
| 11 | M/65 | Left axillary (8.0) | Right inguinal (8.1) | No uptake | 2.1 – 8.1 | (+) | (+) |
| 12 | M/53 | Right sus clavicular (6.3) | Left external iliac (5.4) | No uptake | 3.0 – 6.3 | (+) | (-) |

Abbreviations: (+): Positive; (-): Negative; F: Female; FDG: Fluorodeoxyglucose; L3: 3$^{rd}$ vertebra of the lumbar spine; M: Male; N/A: Not available; PET: Positron emission tomography; PET/CT: Positron emission tomography-computed tomography; SUVmax: Standardized uptake value.

**Table 2. Percentage of increased $^{18}$F-FDG uptake in lymph node areas**

| Lymph nodes | Percentage of increased $^{18}$F-FDG uptake (%) |
|---|---|
| Cervical | 28.5 |
| Inguinal | 28.5 |
| Axillary | 14 |
| Lung hilar | 14 |
| Lombo-aortic | 14 |
| Other | 1 |

Abbreviation: FDG: Fluorodeoxyglucose.

**Table 3. Predictive value of PET/CT for detecting RT in 12 patients**

| Parameters | Value |
|---|---|
| PET value (number of patients) | |
| Positive | 4 |
| Negative | 8 |
| Predictive values (%) | |
| Positive | 37.5 |
| Negative | 100 |
| Specificity (%) | 44.5 |
| False positive (%) | 62.5 |
| Nodal sites (%) | |
| Nodal and extranodal sites | 37.5 |
| Only nodal sites | 62.5 |
| Positive biopsy at nodal sites (%) | |
| Nodal and extranodal sites | 66 |
| Only nodal sites | 20 |

Abbreviations: PET/CT: Positron emission tomography-computed tomography; RT: Richter transformation.

RT (Figures 2 and 3) (nodal and extranodal sites/positive biopsy = 66%; nodal sites/positive biopsy = 20%).

Nonetheless, the study had several limitations, including a small sample size of 12 patients. The cohort lacked diversity in demographic characteristics and disease stage, affecting its representation of the broader RT population. The retrospective design of this study relied on past medical records, which could contain incomplete information and introduce selection bias and confounding variables. The exclusion criteria of the study could also introduce bias, limiting the applicability and reliability of the present findings to a diverse patient population.

Bruzzi *et al.*, Falchi *et al.*, and Mauro *et al.* reported high negative (97%, 92%, and 94%, respectively) and low positive (53%, 38%, and 51%, respectively) predictive values of $^{18}$F-FDG PET/CT for detecting RST, and this could be attributed to the limitation of PET/CT to differentiate between RT and other $^{18}$F-FDG-avid tumors.[3,4,12] Papajik *et al.* suggested that there is no significant advantage in performing $^{18}$F-FDG-PET/CT over CT as a surveillance tool in CLL patients with CLL, but $^{18}$F-FDG-PET/CT may be beneficial in confirming RT diagnosis in RT-suspected CLL patients.[11] Collectively, the positive and negative predictive values reported in our study were consistent with those of other studies (i.e., above 37% and 100%, respectively), but specificity reported in our study (i.e., 44.5%) was comparable to that as reported by Falchi *et al.* (i.e., 47%) (Table 4).[12] Our findings also revealed a high incidence of false positive cases (62.5%), and this could be attributed to an accelerated phase of CLL instead of frank lymphomatous transformation.[4]

**Table 4. Summary of PET/CT predictive values for detecting RT nodes % of increased uptake**

| Study | RT cases | SUVmax | Specificity (%) | Predictive value (%) | |
|---|---|---|---|---|---|
| | | | | Positive | Negative |
| Bruzzi *et al.*[3] | 10 | 5 | 80 | 53 | 97 |
| Mauro *et al.*[4] | 17 | 5 | 71.2 | 51.3 | 94 |
| Falchi *et al.*[12] | 95 | 5 | 47 | 38 | 92 |

Abbreviations: PET/CT: Positron emission tomography-computed tomography; RT: Richter transformation; SUVmax: Standardized uptake value.

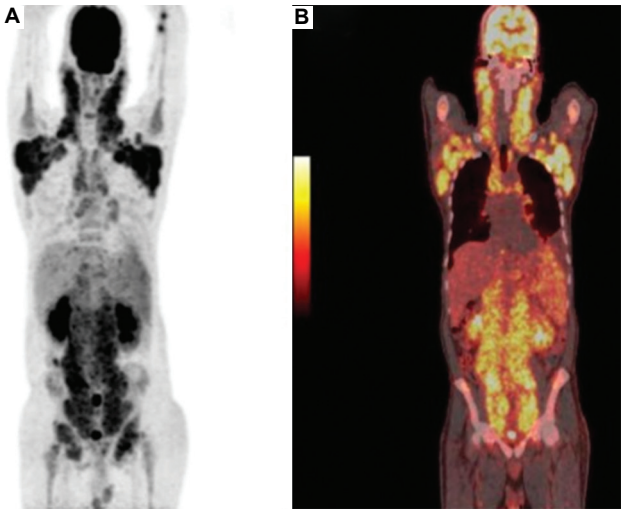


**Figure 1.** Images of a 53-year-old female CLL patient. (A) MIP and (B) fusion images of the patient's coronal section. The images displayed intense $^{18}$F-FDG uptake in the cervical (SUVmax = 6.5) and axillary (SUVmax = 6.3) lymph nodes and low $^{18}$F-FDG uptake in the lombo-aortic lymph nodes (SUVmax = 4.3). A biopsy of the left axillary nodes performed after PET/CT was positive.
Abbreviations: CLL: Chronic lymphocytic leukemia; FDG: Fluoro-deoxy-glucose; MIP: Maximum intensity projection; PET/CT: Positron emission tomography-computed tomography; SUVmax: Standardized uptake value.

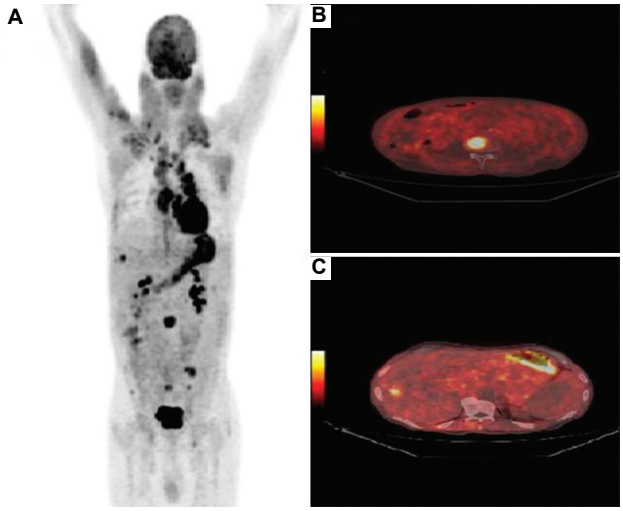


**Figure 2.** Images of a 62-year-old male CLL patient. (A) MIP image of the patient's coronal section and (B and C) fusion images of the patient's axial section. The MIP image (A) displayed intense $^{18}$F-FDG uptake in the mediastinal lymph nodes (pre-vascular, para-aortic, and hilar pulmonary lymph nodes; SUVmax = 8.8). The fusion image (B) demonstrated multiple skeletal hypermetabolisms (L3 with SUVmax = 7.8). The fusion image (C) demonstrated suspected hypermetabolic liver foci (SUVmax = 6.5). A biopsy of the pre-vascular nodes performed after PET/CT was positive. Abbreviations: CLL: Chronic lymphocytic leukemia; FDG: Fluoro-deoxy-glucose; L3: 3$^{rd}$ vertebra of the lumbar spine; MIP: Maximum intensity projection; PET/CT: Positron emission tomography-computed tomography; SUVmax: Standardized uptake value.

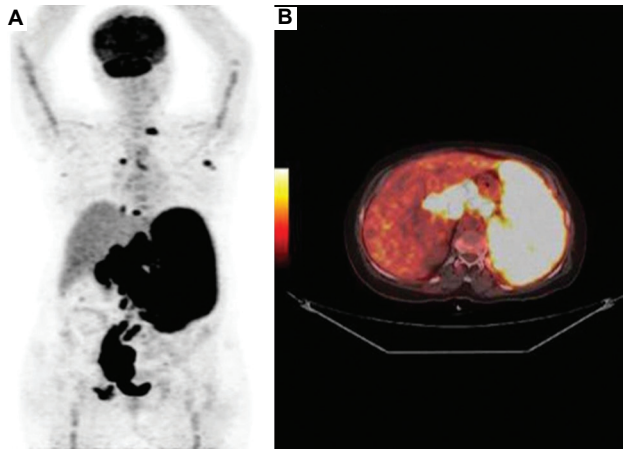


**Figure 3.** Images of a 74-year-old female CLL patient (followed since 2018). (A) MIP image of the patient's coronal section and (B) fusion image of the patient's axial section. The MIP image (A) displayed intense $^{18}$F-FDG uptake in the lombo-aortic lymph nodes (SUVmax = 26.3). The fusion image (B) demonstrated hypermetabolism in the abdominal lymph nodes and an intense $^{18}$F-FDG uptake in the spleen (SUVmax = 10.3).
Abbreviations: CLL: Chronic lymphocytic leukemia; FDG: Fluoro-deoxy-glucose; MIP: Maximum intensity projection; SUVmax: Standardized uptake value.

## 5. Conclusion

While the $^{18}$F-FDG PET/CT scan has proven valuable in assessing patients suspected of RT, it is essential to acknowledge the limitations identified in the study. The retrospective nature, small sample size, and potential bias in patient selection challenged the reliability and practicality of the findings. Despite these constraints, the study highlighted the significance of PET/CT imaging in confirming clinical suspicions and guiding biopsy site selection. Moving forward, larger prospective studies with diverse cohorts are warranted to enhance the robustness of evidence and provide a more comprehensive understanding of the role of PET/CT scans in RT evaluation.

## Acknowledgments

None.

## Funding

None.

## Conflict of interest

The authors declare no conflicts of interest.

## Author contributions

*Conceptualization:* Salah Oueriagli Nabih
*Investigation:* Chaymae Bensaid
*Methodology:* Salah Oueriagli Nabih
*Writing – original draft:* Salah Oueriagli Nabih, Chaymae Bensaid
*Writing – review & editing:* All authors

## Ethics approval and consent to participate

All procedures involving human participants performed in studies were in accordance with the ethical standards of the Institutional and/or National Research Committee and the 1964 Helsinki Declaration and its later amendments or comparable ethical standards. Written informed consent was obtained from patients for participating in this study.

## Consent for publication

Written informed consent was obtained from patients for publication of this original research article and any accompanying images. The institutional review board of Mohammed V Military Teaching Hospital approved this publication, and the requirement to obtain informed consent was waived.

## Availability of data

The documents described in the manuscript, including new software, databases, and all relevant raw data, are available upon reasonable request by the authors.

## References

1. Albano D, Camoni L, Rodella C, Giubbini R, Bertagna F. 2-[$^{18}$F]-FDG PET/CT role in detecting richter transformation

of chronic lymphocytic leukemia and predicting overall survival. *Clin Lymphoma Myeloma Leuk*. 2021;21:e277-e283.

doi: 10.1016/j.clml.2020.12.003

2. Wąsik-Szczepanek E, Szymczyk A, Szczepanek D, *et al*. Richter syndrome: A rare complication of chronic lymphocytic leukemia or small lymphocytic lymphoma. *Adv Clin Exp Med*. 2018;27(12):1683-1689.

   doi: 10.17219/acem/75903

3. Bruzzi JF, Macapinlac H, Tsimberidou AM, *et al*. Detection of Richter's transformation of chronic lymphocytic leukemia by PET/CT. *J Nucl Med*. 2006l;47:1267-1273.

4. Mauro FR, Chauvie S, Paoloni F, *et al*. Diagnostic and prognostic role of PET/CT in patients with chronic lymphocytic leukemia and progressive disease. *Leukemia*. 2015;29(6):1360-1365.

   doi: 10.1038/leu.2015.21

5. Shaikh F, Janjua A, Van Gestel F, Ahmad A. Richter transformation of chronic lymphocytic leukemia: A review of fluorodeoxyglucose positron emission tomography-computed tomography and molecular diagnostics. *Cureus*. 2017;9(1):e968.

   doi: 10.7759/cureus.968

6. Tsimberidou AM, O'Brien S, Khouri I, *et al*. Clinical outcomes and prognostic factors in patients with Richter's syndrome treated with chemotherapy or chemoimmunotherapy with or without stem-cell transplantation. *J Clin Oncol*. 2006;24(15):2343-2351.

   doi: 10.1200/JCO.2005.05.0187

7. Gonzalez D, Martinez P, Wade R, *et al*. Mutational status of the TP53 gene as a predictor of response and survival in patients with chronic lymphocytic leukemia: Results from the LRF CLL4 trial. *J Clin Oncol*. 2011;29(16):2223-2229.

   doi: 10.1200/JCO.2010.32.0838

8. Tam CS, Shanafelt TD, Wierda WG, *et al*. *De novo* deletion 17p13.1 chronic lymphocytic leukemia shows significant clinical heterogeneity: The M. D. Anderson and Mayo Clinic experience. *Blood*. 2009;114(5):957-964.

   doi: 10.1182/blood-2009-03-210591

9. Mayr C, Speicher MR, Kofler DM, *et al*. Chromosomal translocations are associated with poor prognosis in chronic lymphocytic leukemia. *Blood*. 2006;107(2):742-751.

   doi: 10.1182/blood-2005-05-2093

10. Rhodes JM, Mato AR. PET/Computed tomography in chronic lymphocytic leukemia and richter transformation. *PET Clin*. 2019;14:405-410.

    doi: 10.1016/j.cpet.2019.03.007

11. Papajík T, Mysliveček M, Urbanová R, *et al*. 2-[$^{18}$F]fluoro-2-deoxy-D-glucose positron emission tomography/computed tomography examination in patients with chronic lymphocytic leukemia may reveal Richter transformation. *Leuk Lymphoma*. 2014;55:314-319.

    doi: 10.3109/10428194.2013.802313

12. Falchi L, Keating MJ, Marom EM, *et al*. Correlation between FDG/PET, histology, characteristics, and survival in 332 patients with chronic lymphoid leukemia. *Blood*. 2014;123(18):2783-2790.

    doi: 10.1182/blood-2013-11-536169

ACCSCIENCE PUBLISHING

Advances in Radiotherapy & Nuclear Medicine

SHORT COMMUNICATION

# Gamma knife radiosurgery following whole-brain radiation

**Natasha Mathur[1], Badal Juneja[2], Alan Turtz[3], Howard Warren Goldman[3], Qianyi Xu[2], Dave Mulvihill[2], and Gregory J. Kubicek[2]***

[1]Cooper Medical School of Rowan University, Camden, New Jersey, United States of America

[2]Department of Radiation Oncology, MD Anderson-Cooper Cancer Center, Camden, New Jersey, United States of America

[3]Department of Neurological Surgery, Cooper University Hospital, One Cooper Plaza, Camden, New Jersey, United States of America

## Abstract

In this study, we aimed to determine outcomes for patients requiring salvage stereotactic radiosurgery (SRS) who have progression of brain metastatic disease after initial treatment with whole-brain radiation (WBRT). This is a retrospective analysis of a prospective database of 112 patients who were treated with salvage SRS after experiencing failure following WBRT treatment with salvage SRS. Collectively, the patients had a median overall survival of 7 months after salvage SRS. Patients who had more than two brain metastases had a significantly shorter median survival but were not subjected to increased risk for distant brain failure. We also found that a short intervening time between WBRT and central nervous system (CNS) failure did not seem to worsen the nervous system control or reduce patient survival. Small cell lung cancer (SCLC) was associated with decreased overall survival and CNS control. In conclusion, SRS use following WBRT is safe and effective in the majority of patients. Patients with rapid failure after WBRT can be successfully salvaged with SRS. The findings also shed light on the overall poor outcomes, coupled with low median survival and high rates of CNS failure, in patients suffering multiple metastases stemming from SCLC.

***Keywords:*** Stereotactic radiosurgery; Radiation therapy; Salvage; Central nervous system

***Corresponding author:**
Gregory J. Kubicek
(Greg.kubicek @gjk55@miami.edu)

**Citation:** Mathur N, Juneja B, Turtz A, *et al.* Gamma knife radiosurgery following whole-brain radiation. *Adv Radiother Nucl Med*. 2024;2(1):2231.
https://doi.org/10.36922/arnm.2231

**Received:** November 11, 2023

**Accepted:** March 11, 2024

**Published Online:** March 28, 2024



## 1. Introduction

Cancer metastasis to the brain is a common pathological event. It has been estimated that there are 98,000 to 170,000 cases of cancer metastasis to the brain per year in the United States alone. Therapies for this clinical challenge include whole-brain radiation therapy (WBRT) and stereotactic radiosurgery (SRS).[1] Declining cognition, decreased quality of life, and reduced blood counts are some of the notable negative impacts of employing WBRT, which is, however, superior to SRS in terms of reduced likelihood of inducing subsequent CNS failure.[2-5]

Although WBRT can reduce subsequent brain failure as compared to SRS, CNS failure would still develop in patients after undergoing WBRT.[4-6] Several studies have shown that the rate of distant brain metastases after WBRT is around 25% to 50%,[7,8] which can

be potentially brought down through improved systemic control using new agents such as immunotherapy.[2,4,6,9,10]

Patients with intracranial progression after WBRT present a therapeutic dilemma. The radiation options include repeat WBRT or salvage SRS. Several studies reported that repeat WBRT led to a survival time of around 4 months.[2,10] A limited number of studies focusing on salvage SRS after WBRT failure found SRS a safe and effective treatment contributing to a survival time of between 8 and 9 months.[11,12]

While SRS for limited brain metastases after WBRT appears to be a good treatment option, several questions in this aspect remain unanswered. It is unknown if a short time interval to failure after WBRT would make further radiation futile and if there is a cut-off in the number of CNS metastases that can be salvaged with SRS after WBRT failure.

## 2. Methods

This is an IRB approved by Cooper Medical School of Rowan University (EX1092) for retrospective review of prospective SRS database at a single institution from 2007 to 2019. We prospectively collected all treatment information for our SRS cases; additional information required for this study was retrospectively collected. Patient charts were reviewed, and multiple variables were recorded.

Kaplan–Meier with log-rank test was used to compare survival outcomes between variables. Independent *t*-test was used to distinguish differences between means of continuous variables, such as number of central nervous system (CNS) metastases and Karnofsky performance scale (KPS) score. Chi-squared test was utilized to test the significance for categorical variables, such as primary cancer. In addition, recursive partitioning analysis (RPA) was used as a stratification tool. Survival was calculated from the time SRS was performed.

Radiosurgery was performed with Gamma Knife® Icon™ (Elekta, Stockholm Sweden). The majority of patients underwent thin-slice magnetic resonance imaging (MRI) scanning on the day of SRS for SRS planning although patients with high-quality MRI <2 weeks old could use the diagnostic MRI for SRS planning. SRS was usually prescribed to the 50% isodose line although small metastases could be treated with a higher isodose line to reduce normal brain dose. Radiation dose for brain metastases was based on the size of brain metastases: 0–2 cm treated to 20 Gy, 2–3 cm treated to 18 Gy, and 3–4 cm treated to 15 Gy.

Standard follow-up at our institution for patients with brain metastases is an MRI scan with contrast every 3 months for the first 2 years and then every 4 months at a multi-disciplinary neuro-oncology clinic until the 3rd year, under the assumption that scans are normal.[12] If suspected of having recurrence versus radiation necrosis, asymptomatic patients are started on pentoxifylline (Trental) and vitamin E with repeat scans performed in 8 weeks. If the abnormality persists, patients are indicated for dynamic MRI imaging consisting of MRI spectroscopy and MRI perfusion to determine whether radiation necrosis or disease progression is the cause, and biopsy will be performed if feasible. Cases are often presented in multi-disciplinary tumor board. Table 1 illustrates patient characteristics of interest.

## 3. Results

A total of 112 patients and 699 treated brain metastases were evaluated. There were 18 patients who underwent SRS multiple times, ranging from two to five times (a total of 134 SRS sessions). The median time from WBRT to SRS was 266 days (range: 23–1722 days). The majority of previous WBRT was 30 Gy in 10 fractions. The median number of CNS metastases treated with salvage SRS was 4 (range: 1–29) (Table 1).

The median follow-up durations for all patients and surviving patients were 116 days and 168 days, respectively, and the median overall survival was 210 days (7 months). The median survival by RPA status was 279, 176, and 95 days for RPA 1, 2, and 3, respectively ($P < 0.007$). Small cell lung cancer (SCLC) and breast cancer were statistically

**Table 1. Patient characteristics**

| Characteristics | Statistics (*n*=112) |
|---|---|
| Primary cancer (*n*, %) | |
| Small cell lung cancer | 34 (30.3%) |
| Non-small cell lung cancer | 34 (30.3%) |
| Breast cancer | 29 (25.9%) |
| Melanoma | 6 (5.4%) |
| KPS | |
| Median | 80 |
| Range | 50–100 |
| KPS≥70 | 94 |
| Brain metastases treated | |
| Median | 4 |
| Range | 1–29 |
| Percent >5 | 30.3% |
| Interval from previous whole-brain radiation days | |
| Median | 266 |
| Range | 23–1722 |

Abbreviation: KPS: Karnofsky performance scale.

significant predictors of survival ($P < 0.0007$ and $P < 0.011$, respectively). Patients with breast cancer had increased median survival time of 289 days (9.6 months) compared to patients with SCLC with a median survival of 127 days (4.2 months). We found that patients who had more than 2 metastases had a decreased survival time compared to patients who had 1 to 2 metastases ($P < 0.001$). Patients with 0 – 2 metastases had a median survival time of 11.3 months (340 days) while those with 3 or more metastases had 5.0 months (149 days) (Figure 1). Time from CNS failure after WBRT was not associated with a decrease in survival.

Forty-seven patients succumbed to subsequent CNS failure after both WBRT and salvage SRS, with a median time to distant CNS failure of 226 days (range: 22–864 days). Whether treated as a discrete variable (under 60 days, under 90 days, *etc.*) or as a continuous variable, time interval from WBRT to SRS did not seem to be able to predict worse CNS control. The results also showed that the number of brain metastases treated did not have an influence on subsequent brain failure when examined as either continuous or discrete (as a cut-off) variable. Our analysis also unveiled that SCLC is statistically significant predictor for worse distant brain failure ($P < 0.007$), with a median of 88 days to distant failure.

As mentioned above, SCLC could predict both worse overall survival as well as increased rate of distant failure. Of the 34 SCLC patients analyzed, nine (26%) had survival longer than 6 months, but there were only two patients who had survival longer than 6 months and did not experience subsequent CNS failure; both of these patients suffered from solitary brain metastasis. Of the SCLC patients with at least 3 months of follow-up (18 patients), 12 patients developed distant brain failure, while the rest (six patients) with 3 months of follow-up and no distant brain relapse developed brain metastases (9 metastases in one patient, 5 in one, 2 in one, and 1 in three).

Local failure was a rare event. Five local failure cases were reported, with a median time to local failure of 766 days. Patients with local failure had a median interval from WBRT to SRS of 1198 days.

The presence of radiation necrosis was determined through dynamic MRI imaging and discussion in multi-disciplinary tumor board. Rate of radiation toxicity was low, with only four patients developing presumed radiation necrosis. Prior treatment for two of these patients consisted of radiation, chemotherapy, and surgery, while the other two patients received only radiation.

## 4. Discussion

We found that salvage SRS following WBRT is a safe and effective approach for most patient subsets, as very few cases of radiation necrosis or local failure were detected. All patients had a median survival of 7 months, which is consistent with other reports. In other studies, Chao *et al.* reported a median survival of 9.9 months following salvage SRS while Caballero *et al.* revealed that the patients had a median survival of 8.1 months after the same treatment.[11,13] The slight difference in the median survival reported in this study from these studies is very likely attributed to a higher composition of lung cancer and especially SCLC cases in this study; both of these studies[11,13] consisted of approximately 47% of patients with primary lung cancer while our study had approximately 60% of patients with the same kind of cancer. In similar to this study, there

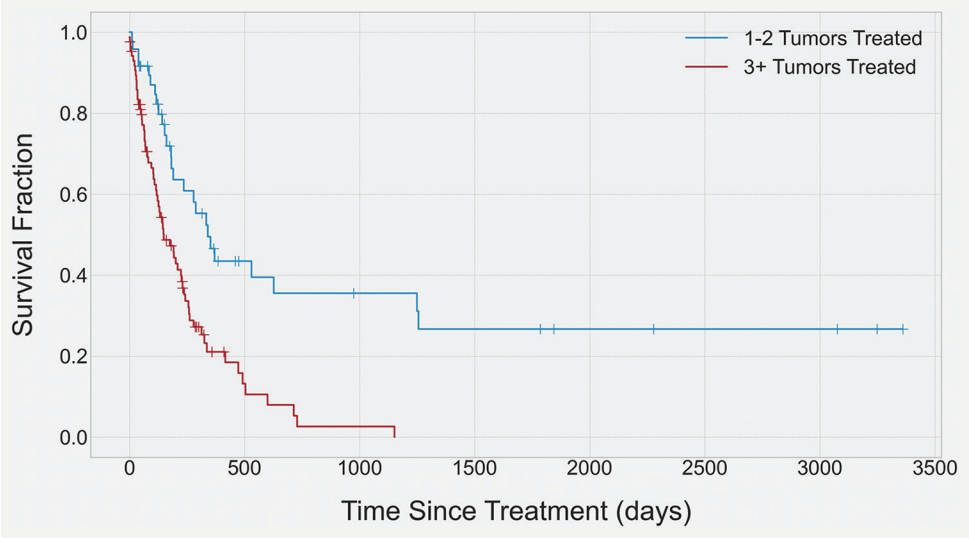


**Figure 1.** Median survival time (in days) for patients based on number of metastases present at initial visit.

were differences in survival based on primary tumor, and Caballero *et al.* reported that breast cancer patients had a survival of 11.2 months versus 5.5 months of survival in SCLC patients.[11]

The other radiation option for failure after WBRT is to repeat WBRT. Sadikov *et al.* reported that 72 patients having undergone repeat radiation treatment had a median survival of 4.1 months.[10] In the same vein, Wong *et al.* reported a nearly identical median survival, *i.e.*, 4 months, from an analysis involving 86 patients.[2] While survival for patients who had undergone repeat WBRT was shorter than those treated with SRS, this difference may be secondary to bias in patient selection.

There are several other limitations in this study, as well as other relevant studies. While data for some variables were prospectively collected, data for certain variables were retrospectively collected. Furthermore, given the nature of the illness, many patients were lost to follow-up. In addition, some essential information, such as information on chemotherapy, immunotherapy and targeted therapy, reasons for WBRT, and degree of extra-cranial disease, that are very instrumental to this analysis were not recorded. Determining local failure versus radiation necrosis is a very challenging endeavor, and although some patients had been biopsied, such determination was often made based on dynamic MRI imaging and tumor board discussion.

The findings from this study contribute significantly to our understanding about the efficacy of this treatment approach. First, the lack of correlation of the time from WBRT failure with poor SRS outcome, even when the patients had CNS failure within 60 days of WBRT, underscores the potential of salvage SRS treatment regardless of time of failure after WBRT. Second, we also detected a difference in survival after SRS based on the number of treated brain metastases. As expected, patients with fewer brain metastases had better survival compared to patients with multiple brain metastases treated with salvage SRS (Figure 1). Importantly, we did not observe an increase in distant brain failure related to the number of treated brain metastases; this finding is expected since patients with multiple treated brain metastases typically have reduced survival and thus shortened time for distant brain failure to develop and manifest. We found that patients with multiple metastases had survival outcomes comparable to those treated with repeat WBRT. In this study, the median survival for patients with multiple metastases was 5 months, slightly higher than the median survival of 4 months in patients undergoing repeat WBRT reported in other studies.[2,10] Despite the overall poor survival outcomes for multiple brain metastases after WBRT failure, salvage SRS stands as a better and preferred choice compared to repeat WBRT, since it is logistically easier to implement salvage SRS, which also less likely to induce toxicity as compared to repeat WBRT.

Another important finding that we should highlight from this study is the poor outcome for SCLC patients with multiple metastases. Overall, patients with SCLC had poor treatment outcome. SCLC is a potential predicator for both worse CNS control and worse overall survival. In this study, none of the recruited SCLC patients having three or more metastases did not have subsequent CNS failure. Our data also underline the need to exercise caution in treating relapsed SCLC with multiple brain metastases and to evaluate alternative treatment options such as systemic therapy, observation, and best supportive care.[14,15]

## 5. Conclusion

Salvage SRS after WBRT is a safe and effective treatment approach for the majority of patients, irrespective of the time interval from WBRT. A subset of SCLC patients with multiple brain metastases had an overall bad treatment outcome, and thus, alternative treatment options for this subset should be explored.

## Acknowledgments

None.

## Funding

None.

## Conflict of interest

The authors declare that they have no competing interests.

## Author contributions

*Conceptualization:* Gregory J. Kubicek, Howard Warren Goldman
*Formal analysis:* Badal Juneja
*Investigation:* Natasha Mathur
*Methodology:* Gregory J. Kubicek
*Writing – original draft:* Natasha Mathur
*Writing – review & editing:* Badal Juneja, Alan Turtz, Howard Warren Goldman, Qianyi Xu, Dave Mulvihill, Gregory J. Kubicek

## Ethics approval and consent to participate

This study is approved by IRB, Cooper Medical School of Rowan University (Approval no. EX1092). Per IRB individual patient consent was waived.

## Consent for publication

Informed consent was waived by the IRB.

## Availability of data

Data are available from the corresponding author upon reasonable request.

## References

1. Amsbaugh MJ, Kim CS. Brain metastasis. In: *StatPearls*. Treasure Island (FL): StatPearls Publishing; 2021.

2. Wong WW, Schild SE, Sawyer TE, Shaw EG. Analysis of outcome in patients reirradiated for brain metastases. *Int J Radiat Oncol Biol Phys.* 1996;34(3):585-590.

   doi: 10.1016/0360-3016(95)02156-6

3. Yomo S, Hayashi M. The efficacy and limitations of stereotactic radiosurgery as a salvage treatment after failed whole brain radiotherapy for brain metastases. *J Neurooncol.* 2013;113(3):459-465.

   doi: 10.1007/s11060-013-1138-y

4. Son CH, Jimenez R, Niemierko A, Loeffler JS, Oh KS, Shih HA. Outcomes after whole brain reirradiation in patients with brain metastases. *Int J Radiat Oncol Biol Phys.* 2012;82(2):e167-e172.

   doi: 10.1016/j.ijrobp.2011.03.020

5. McTyre E, Scott J, Chinnaiyan P. Whole brain radiotherapy for brain metastasis. *Surg Neurol Int.* 2013;4(5):S236-S244.

   doi: 10.4103/2152-7806.111301

6. Suzuki R, Wei X, Allen PK, *et al*. Outcomes of re-irradiation for brain recurrence after prophylactic or therapeutic whole-brain irradiation for small cell lung Cancer: A retrospective analysis. *Radiat Oncol.* 2018;13(1):258.

   doi: 10.1186/s13014-018-1205-9

7. Andrews DW, Scott CB, Sperduto PW, *et al*. Whole brain radiation therapy with or without stereotactic radiosurgery boost for patients with one to three brain metastases: Phase III results of the RTOG 9508 randomised trial. *Lancet.* 2004;363(9422):1665-1672.

   doi: 10.1016/S0140-6736(04)16250-8

8. Aoyama H, Shirato H, Tago M, *et al*. Stereotactic radiosurgery plus whole-brain radiation therapy vs stereotactic radiosurgery alone for treatment of brain metastases. *JAMA.* 2006;295(21):2483-2491.

   doi: 10.1001/jama.295.21.2483

9. Foo K, Patel A, Richards G, *et al*. Effects of whole brain radiation on blood counts. *J Solid Tumors.* 2016;7(1):23.

   doi: 10.5430/jst.V7n1P23

10. Sadikov E, Bezjak A, Yi QL, *et al*. Value of whole brain re-irradiation for brain metastases--single centre experience. *Clin Oncol (R Coll Radiol).* 2007;19(7):532-538.

    doi: 10.1016/j.clon.2007.06.001

11. Caballero JA, Sneed PK, Lamborn KR, *et al*. Prognostic factors for survival in patients treated with stereotactic radiosurgery for recurrent brain metastases after prior whole brain radiotherapy. *Int J Radiat Oncol Biol Phys.* 2012;83(1):303-309.

    doi: 10.1016/j.ijrobp.2011.06.1987

12. Kubicek GJ, Yocum N, Thomas C, Goldman HW. Neuro-oncology multidisciplinary clinic and improvements in patient outcome. *Am J Clin Oncol.* 2020;43(11):798-801.

    doi: 10.1097/COC.0000000000000751

13. Chao ST, Barnett GH, Vogelbaum MA, *et al*. Salvage stereotactic radiosurgery effectively treats recurrences from whole-brain radiation therapy. *Cancer.* 2008;113(8):2198-2204.

    doi: 10.1002/cncr.23821

14. Giorgio CG, Giuffrida D, Pappalardo A, *et al*. Oral temozolomide in heavily pre-treated brain metastases from non-small cell lung cancer: Phase II study. *Lung Cancer.* 2005;50(2):247-254.

    doi: 10.1016/j.lungcan.2005.05.026

15. Langley RE, Stephens RJ, Nankivell M, *et al*. Interim data from the Medical Research Council QUARTZ Trial: Does whole brain radiotherapy affect the survival and quality of life of patients with brain metastases from non-small cell lung cancer? *Clin Oncol (R Coll Radiol).* 2013;25(3):e23-e30.

    doi: 10.1016/j.clon.2012.11.002

ACCSCIENCE PUBLISHING

Advances in Radiotherapy & Nuclear Medicine

CASE REPORT

# Secondary syphilis: An unusual cause of osteolytic lesion diagnosed by $^{99m}$Tc-MDP SPECT and presenting features

**Xia Lu[1]*, Chifeng Xu[1], Haizhong Zhou[1], Qin Xiao[2], and Huiying He[3]***

[1]Department of Nuclear Medicine, Northern Jiangsu People's Hospital, Yangzhou, China

[2]Department of Pathology, Northern Jiangsu People's Hospital, Yangzhou, China

[3]Department of Pathology, School of Basic Medical Sciences, Peking University Third Hospital, Peking University Health Science Center, Beijing, China

## Abstract

Herein, we present the case of a 68-year-old woman complaining of pain of the right knee, which was initially misdiagnosed by plain radiography as fracture on inner right tibia plateau but was finally clarified as osteolytic lesion secondary to syphilis affecting the whole right knee. The final diagnosis was made based on the valuable findings from bone scanning, which allows for imaging of abnormalities with much larger extent, a scale that is out of the examination capacity of plain radiography. Bone scanning was employed in this case, coupled with the use of $^{99m}$Tc-MDP, to assess abnormal bone metabolism at the whole right knee next to the tibia plateau. The imaging results illustrated the diverse features of bone involvement of secondary syphilis, including periostitis, osteolysis as well as osteomyelitis, occurring together or in isolation.

***Keywords:*** Secondary syphilis; Osteomyelitis; $^{99m}$Tc-MDP SPECT; Right knee

***Corresponding authors:**
Xia Lu
(lxgf2222@163.com)
Huiying He
(huiyinghe@bjmu.edu.cn))

**Citation:** Lu X, Xu C, Zhou H, Xiao Q, He H. Secondary syphilis: An unusual cause of osteolytic lesion diagnosed by $^{99m}$Tc-MDP SPECT and presenting features. *Adv Radiother Nucl Med*. 2024;2(1):2204. https://doi.org/10.36922/arnm.2204

**Received:** November 8, 2023

**Accepted:** January 26, 2024

**Published Online:** March 26, 2024



## 1. Background

Syphilis remains a major public health concern worldwide. It has been estimated that the global incidence of syphilis stands as 10.6 million/year and has been showing increasing trend over past two decades in China, making it the most common sexually transmitted disease in the country.[1-3] Unfortunately, the epidemiologic studies on syphilis conducted thus far have largely neglected an in-depth analysis on the transmission of syphilis from husbands who have multiple sex partners to their wives, an area in this subject that deserves more attention.[4]

Bone and joint involvement in secondary syphilis rarely occurs but is more commonly seen in congenital and tertiary syphilis. In a retrospective study of 854 patients diagnosed with secondary syphilis, only 2 (0.2%) patients were found to have bone lesions.[5] Early diagnosis and effective treatment are crucial for improving the outcomes of syphilis and preventing further spread of the disease.[6] Improvement of a wide array of imaging modalities, along with a deepening understanding of the imaging features of osseous syphilis, could lead to easier diagnosis of the disease. However, there has been a lack of reports on functional nuclear medicine imaging

features of osteolytic lesions caused by secondary syphilis in the past decades.

We herein present the case of a 68-year-old woman complaining of pain of the right knee, which was initially misdiagnosed by plain radiography as fracture on inner right tibia plateau but was finally clarified as osteolytic lesion due to secondary syphilis affecting the whole right knee.

## 2. Case presentation

A 68-year-old housewife without any significant medical history was admitted to the hospital for the pain afflicted to her right knee, a condition that lasted for 10 days before admission and exhibited poor response to painkiller. A radiological examination initially indicated to the patient revealed a serious osteolytic lesion on inner right tibia plateau (Figure 1B and D), which was suggestive of obsolete fracture, but the patient denied having suffered from knee injury. Hematoxylin and eosin staining, on the other hand, showcased significant lymphocyte infiltration in the center of the lesion but histopathologic features that could reveal the cause of osteolytic lesion were not observed (Figure 1E). Without knowing the exact cause of the fracture rendered the administration of appropriate clinical treatment for the patient impossible.

Therefore, a bone scanning examination was performed. The imaging results showed intense uptake of $^{99m}$Tc-methylene diphosphonate ($^{99m}$Tc-MDP) in the whole right knee joint and proximal tibia, indicating a rare inflammatory bone lesion beyond the facture (Figure 1A and C). The inflammatory nature of the lesion prompted us to query the patient again. Further disclosure from her revealed certain vital diagnostic clues: She had been diagnosed with syphilis, acquired from her husband through an intimate infection, and had been cured after undergoing a penicillin treatment for a month 8 years ago. Based on the positive results from non-treponemal test (TRUST 1:4) and *Treponema pallidum* antibody test (403.54 s/co), with the latter registering an increased antibody titer in serum, we ruled that the patient was diagnosed with osteolytic lesion caused by secondary syphilis, which was validated by Warthin–Starry silver staining test (Figure 1F). Accordingly, the patient was prescribed a course of antibiotics treatment and also surgically treated with total knee arthroplasty (Figure 1G).

## 3. Discussion

Single-photon emission computed tomography (SPECT) scans using radiotracers for bone such as $^{99m}$Tc-methylene diphosphonate ($^{99m}$Tc-MDP) could provide detailed information about the physiological and anatomical state of bone, which could help with the detection of early bony lesions of secondary syphilis. Imaging bone with $^{99m}$Tc-MDP SPECT remains the mainstay of bone lesion diagnosis, despite the rapid advances in other technologies, such as positron emission tomography (PET/CT) and magnetic resonance imaging (MRI).

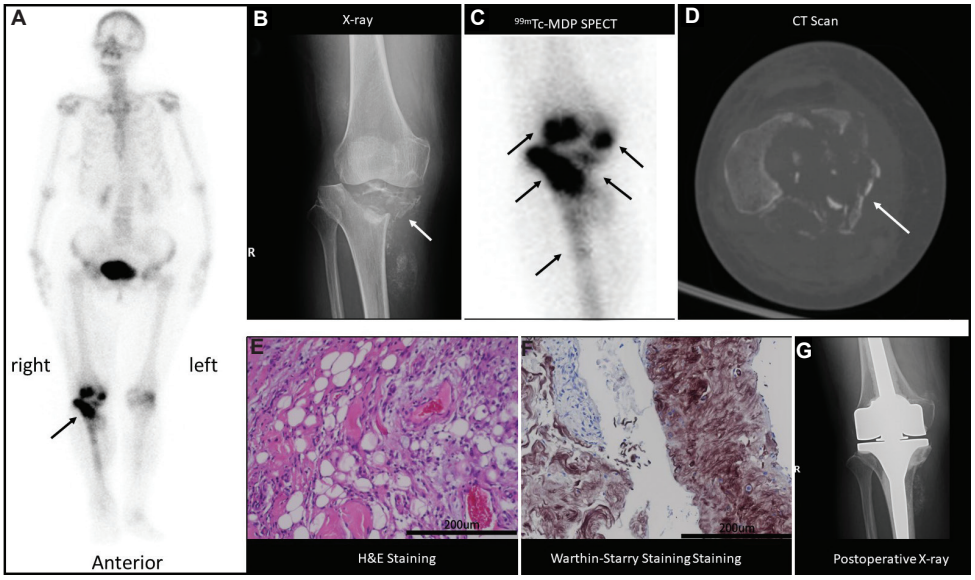


**Figure 1.** A rare case of bone lesion due to secondary syphilis. (A) Anterior whole-body bone scanning showed markedly increased activity in the right knee joint and proximal tibia. (C) Regional image of right knee from whole-body bone scanning. (B and D) Radiographical findings showed severe injury of inner right tibial plateau. (E) Hematoxylin and eosin staining revealed hyperplastic synovial tissues with marked lymphocytic infiltration (×100 magnification). Scale bar: 200 um. (F) Warthin–Starry staining revealed the presence of *Treponema pallidum* stained in brown color (×100 magnification). Scale bar: 200 um. (G) Treatment of total knee arthroplasty.

This case highlights the importance of bone scanning in the diagnosis of secondary syphilis and presents a case of single predominant damage of the right knee joint, which is distinct from other reported cases. It has been reported that only 24% of the cases of secondary syphilis with bone involvement showed high-titer results in nontreponemal serologic tests.[7] Many of these cases demonstrated multifocal bone involvement but reports on secondary syphilis affecting the sternum, skull, and fibula remain scarce.[7-10] Bony lesions due to secondary syphilis are pathologically complex and may exhibit in the form of periostitis, osteolysis, and osteomyelitis, which may occur together or in isolation. It is widely recognized that the accumulation of technetium-labeled radiopharmaceuticals in bony lesions is a primary indication of increased osteoid formation, increased blood flow, increased mineralization of osteoid, and interrupted sympathetic nerve supply.[11] However, none of above mechanisms seem to explain the increased radionuclide activity in bony lesion occurring on the right knee. Instead, infiltration of inflammatory cells, such as lymphocyte and macrophage, resulting in the increased uptake of bone-seeking radiopharmaceuticals seems to offer a plausible explanation for the current case of bone lesions due to secondary syphilis. Nevertheless, this postulated mechanism warrants validation in further experiments.

## 4. Conclusion

The current report showcases the insidious nature of bone lesions secondary to syphilis, evidenced by the manifestations of apparent symptoms years after acquiring the sexually transmitted disease. The bone lesion may have a poor prognosis if an early diagnosis and effective treatment is not possible. A crossover of multiple disciplines through physiologic studies and imaging should be considered in diagnosing sexually transmitted infections with bone lesions involvement.

## Acknowledgments

The authors would like to thank the participating patient, as well as the colleagues and nurses who made this work possible.

## Funding

This work was supported by the foundation of "Lvyang Jinfeng" talents attracting plan (LYJF00040) and Jiangsu Provincial Health Commission General Project (H2023055).

## Conflict of interest

The authors declare that they have no competing interests.

## Author contributions

*Conceptualization:* Xia Lu
*Formal analysis:* Haizhong Zhou
*Investigation:* Qin Xiao
*Methodology:* Chifeng Xu
*Writing – original draft:* Xia Lu
*Writing – review & editing:* Huiying He

## Ethics approval and consent to participate

Verbal consent was obtained from the patient before participation.

## Consent for publication

The patient gave consent verbally for releasing their data in this paper.

## Availability of data

Data are available from the corresponding author upon reasonable request.

## Referencess

1. Pham MD, Ong JJ, Anderson DA, Stoové M. Point-of-care diagnostics for diagnosis of active syphilis infection: Needs, challenges and the way forward. *Int J Environ Res Public Health*. 2022;19(13):8172.

   doi: 10.3390/ijerph19138172

2. Wan Z, Zhang H, Xu H, *et al*. Maternal syphilis treatment and pregnancy outcomes: A retrospective study in Jiangxi Province, China. *BMC Pregnancy Childbirth.* 2020;20(1):648-654.

   doi: 10.1186/s12884-020-03314-y

3. Tuddenham S, Ghanem KG. Emerging trends and persistent challenges in the management of adult syphilis. *BMC Infect Dis*. 2015;15:351-359.

   doi: 10.1186/s12879-015-1028-3.

4. Han L, Xiong WX, Li MZ, *et al.* Couple-level determinants of syphilis infection among heterosexual married couples of reproductive age in Guangdong Province, China: A population-based cross-sectional study. *Front Public Health*. 2022;10:1004246.

   doi: 10.3389/fpubh.2022.1004246

5. Mindel A, Tovey SJ, Timmins DJ, Williams P. Primary and secondary syphilis, 20 years' experience. 2. Clinical features. *Genitourin Med*. 1989;65(1):1-3.

   doi: 10.1136/sti.65.1.1

6. Chen JH, Zheng X, Liu XQ. Usefulness of positron emission tomography in patients with syphilis: A systematic review of observational studies. *Chin Med J* (*Engl*). 2017;130(9):1100-1112.

doi: 10.4103/0366-6999.204940

7. Park KH, Lee MS, Hong K, *et al*. Bone involvement in secondary syphilis: A case report and systematic review of the literature. *Sex Transm Dis*. 2014;41(9):532-537.

   doi: 10.1097/OLQ.0000000000000164

8. Colquhoun M, Kirresh O, Keikha M, Haddow L. Osteolytic lesions as the sole presenting feature of secondary syphilis. *BMJ Case Rep*. 2021;14(6):e242814.

   doi: 10.1136/bcr-2021-242814

9. Taihi L, Paycha F, Mamou Y, *et al*. The great imitator secondary syphilis of bone unveiled through combination of MRI and (99mTc)-bisphosphonates SPECT/CT. *Eur J Nucl Med Mol Imaging*. 2021;48(3):933-934.

   doi: 10.1007/s00259-020-04985-7

10. Kusler J, Arthurs S. Rare case of four osseous lesions of the skull in a patient with secondary syphilis. *Case Rep Infect Dis*. 2018;2018:3148758.

    doi: 10.1155/2018/3148758

11. Thakore K, Viroslav A, Vansant J. Role of bone scintigraphy in the detection of periostitis in secondary syphilis. *Clin Nucl Med*. 1994;19(6):536-541.

    doi: 10.1097/00003072-199406000-00016

ACCSCIENCE PUBLISHING

Advances in Radiotherapy & Nuclear Medicine

CASE REPORT

# Cross-sectional imaging in symmetrical bilateral extranodal recurrence of follicular lymphoma: A case report

**Cesare Oliveti[1]*, Barbara Catalfamo[2], Annachiara Mollace[1], Claudia Italia Maria De Santis[1], Roberta Mancini[1], Giuseppe Lucio Cascini[2], and Francesco Manti[1]**

[1]Department of Experimental and Clinical Medicine, Division of Radiology, Magna Graecia University of Catanzaro Azienda Ospedaliero-Universitaria Renato Dulbecco, Catanzaro, Calabria, Italy

[2]Department of Diagnostic Imaging Nuclear Medicine Unit, Magna Graecia University of Catanzaro, Azienda Ospedaliero Universitaria Renato Dulbecco, Catanzaro, Calabria, Italy

## Abstract

Follicular lymphoma (FL) constitutes nearly 30% of all lymphomas, making it the second most prevalent B-cell lymphoma. It exhibits an indolent course within the spectrum of non-Hodgkin lymphoma, with variable 5-year progression-free survival rates. Histologically graded 1–3, FL primarily affects bone marrow and lymphoid organs but may also involve extranodal tissues, such as bilateral muscle tissue. This report outlines the diagnostic challenges associated with disease recurrence in such unusual locations, emphasizing the need for vigilance among clinicians and radiologists. Through imaging and biopsy, we confirmed recurrence in the patient. The study highlights the role of $^{18}$F-FDG PET/CT in detecting uncommon FL sites and guiding treatment decisions while emphasizing the importance of multidisciplinary care for optimal patient management.

***Keywords:*** Ultrasound; Follicular lymphoma; Computed tomography; $^{18}$F-FDG PET/CT; Extranodal

***Corresponding author:**
Cesare Oliveti
(cesare.oliveti.1990@gmail.com)

**Citation:** Oliveti C, Catalfamo B, Mollace A, *et al*. Cross-sectional imaging in symmetrical bilateral extranodal recurrence of follicular lymphoma: A case report. *Adv Radiother Nucl Med*. 2024;2(1):2828. https://doi.org/10.36922/arnm.2828

**Received:** January 26, 2024

**Accepted:** March 19, 2024

**Published Online:** March 27, 2024



## 1. Background

Follicular lymphoma (FL) accounts for nearly 30% of all lymphomas, making it the second most prevalent B-cell lymphoma.[1] FL typically exhibits a clinically indolent course within the spectrum of non-Hodgkin lymphoma (NHL) owing to its slow-growing nature, derived from B cells. The 5-year progression-free survival rates, categorized by risk factors, are as follows: low risk (0 risk factors): 80%; intermediate risk (1–2 risk factors): 51%; high risk (3–5 risk factors): 19%. Histologically, FL is stratified into grades 1–3, signifying an increasing abundance of lymphoma cells or blasts.[2] While FL predominantly affects bone marrow and lymphoid organs,[1] occasional involvement of extranodal tissues and organs occurs, as observed in our clinical case involving bilateral muscle tissue. This case report aims to elucidate the challenging diagnostic process of disease recurrence in this atypical location and to alert clinicians and radiologists to the potential rare extranodal manifestations of FL.

## 2. Case presentation

A 55-year-old woman was admitted to our university hospital in August 2020 for evaluation of cervical and axillary lymphadenopathies. Abdominal ultrasound revealed multiple enlarged lymph nodes, alongside an unexpected retroperitoneal mass encircling the left kidney, accompanied by hydronephrosis and left pleural effusion. Subsequent computed tomography (CT) scan of the abdomen and pelvis validated ultrasound findings, revealing a 15 × 21 cm abdominal mass and multiple enlarged lymph nodes spanning from the abdominal aorta to the origin of the internal iliac arteries. In addition, an excisional axillary lymph node biopsy unveiled a localization of grade 2 FL. The flow cytometry demonstrated a substantial population of CD20-CD19-positive cells coexpressing CD10. Fluorescence *in situ* hybridization exhibited positivity for BCL2 translocation, coupled with a Ki-67 proliferation index of 35%. Staging positron emission tomography (PET) with 2-deoxy-2-[fluorine-18] fluoro-D-glucose ($^{18}$F-FDG) manifested intense and pathological glucose metabolism in multiple supra- and subdiaphragmatic lymph nodes and left pleural effusion, devoid of extranodal disease evidence. Subsequently, based on the stage and FL International Prognostic Index 2 (FLIPI 2) score, the patient underwent first-line treatment with seven cycles of R-CHOP (cyclophosphamide, doxorubicin, vincristine, prednisone, and rituximab) from September 2020 to February 2021, resulting in a metabolic complete response according to $^{18}$F-FDG-PET. Subsequently, the patient underwent clinical and radiological surveillance during the rituximab maintenance therapy, exhibiting minimal clinical symptoms except for asthenia and mild weight loss. After 2 years, a follow-up total-body CT scan revealed bilateral enlargement of the lumbar region contiguous to the external oblique muscles, displaying no notable disparities in density or contrast enhancement compared to surrounding muscular tissues (Figure 1) and absence of pathological lymph nodes or signs of disease recurrence.

Further diagnostic evaluation encompassed an $^{18}$F-FDG-PET examination, demonstrating intense FDG uptake bilaterally in the lumbar regions adjoining the external oblique muscles, consistent with CT findings (Figure 2).

The metabolic data aligned with suspected disease recurrences predicated on the focal pattern and intensity of $^{18}$F-FDG uptake. Consequently, an ultrasound scan was conducted to characterize the tissue and anatomical location and guide a biopsy. Soft tissue ultrasound unveiled hypoechoic polylobulate lesions conspicuously demarcated with vascularization signals on color Doppler imaging within the muscle (Figure 3).

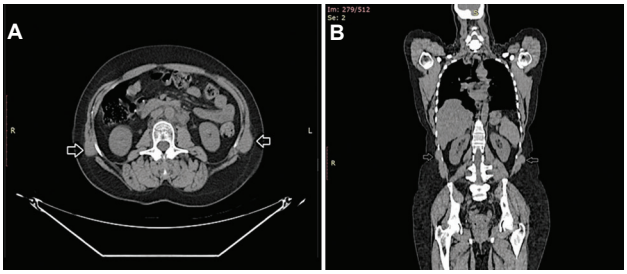


**Figure 1.** Axial plane (A) and coronal plane (B) reconstruction computed tomography scan. The scan illustrates focal and bilateral enlargement of external oblique muscles without distinct margins (white arrow).

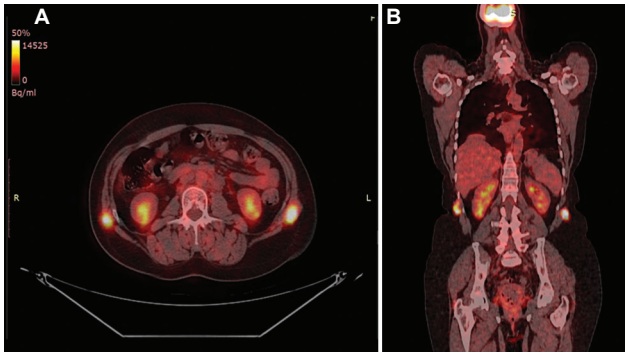


**Figure 2.** Axial plain (A) and coronal plain (B) reconstruction fused $^{18}$F-FDG PET/CT scan. The scan illustrates intense $^{18}$F-FDG uptake in the pathological tissue superimposed on the focal and bilateral enlargement of the external oblique muscles (white arrow).

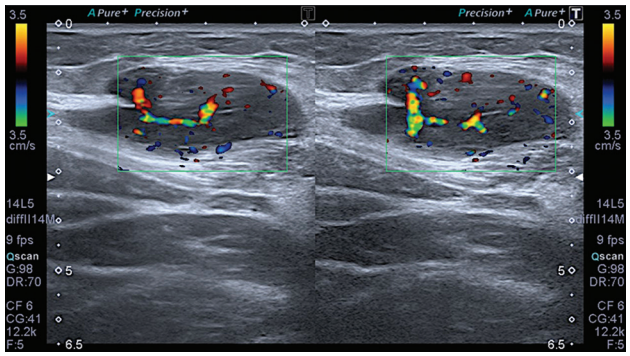

**Figure 3.** Ultrasound revealing hypoechoic polylobulate lesions distinctly delineated in a "nodular focal" pattern with vascularization signal on the color-Doppler module.

Subsequently, a percutaneous ultrasound-guided biopsy was performed under local anesthesia (2% lidocaine) to procure samples from the hypoechoic areas of both regions within the external oblique muscle. The biopsy confirmed the suspected diagnosis of FL, grade 3B (CD20+, CD10+, PAX5+, BCL2+, and Ki-67 20%), in both muscle samples. Following the confirmation of the diagnosis with symptoms including night sweats and unintentional weight loss, the patient underwent autotransplantation.

## 3. Discussion

FL represents the most common form of indolent lymphoma, characterized by potential extranodal involvement affecting various organs.[1,3,4] Extranodal sites, with or without nodal involvement, typically encompass the head and neck, gastrointestinal tract, central nervous system, lungs, bones, muscles, and skin. While muscle infiltration by lymphoma is rare, it primarily manifests in the gluteal and pelvic muscles and is often attributable to hematogenous or lymphatic dissemination. Two discernible patterns of muscle involvement are discernible through imaging: diffuse infiltration with muscle enlargement and focal intramuscular masses.[5]

### 3.1. Advantages and limitations of imaging modalities for diagnosis and staging

Accurate diagnosis, localization, and staging are paramount for determining the optimal treatment strategy.[6] CT with contrast enhancement typically serves as the frontline imaging modality for lesion identification and extent determination, according to Lugano classification.[7]

Surov *et al*. elucidated various presentations of muscle lymphoma on CT, with contrast-free studies revealing focal or diffuse muscle swelling with irregular hypodense regions and/or indistinct margins. Post-contrast administration enables differentiation of contrasting enhancement grades, with descriptions including small rim-enhancing lesions with central hypoattenuation.[8]

Magnetic resonance imaging (MRI) serves as an alternative imaging modality; however, its costliness and nonspecific characteristics in musculoskeletal lymphoma may limit its utility.[9] In recent years, $^{18}$F-FDG PET has emerged as a pivotal tool in lymphoma staging and therapy response assessment, attributable to its capacity to identify metabolically active lesions.[7,10]

The effectiveness of $^{18}$F-FDG PET/CT in staging and restaging B and T-cell lymphomas and Hodgkin's lymphoma primarily stems from its ability to detect FDG-avid lymph nodes of normal size (<1 cm) and extranodal sites that are potentially undetectable on CT scans. In our case, CT follow-up depicted solely symmetrical muscle enlargement at the thoracic-abdominal site without focal contrast enhancement discernible to an inexperienced radiologist. Nonetheless, radiologists may encounter difficulty diagnosing disease recurrence solely based on these CT imaging characteristics.

The contrast-enhanced CT exhibits limited sensitivity in detecting lymphomatous involvement of normal-sized lymph nodes, bone marrow, spleen, and extranodal tissues. The intensity of FDG uptake in lymphoma is influenced by several factors, including histological characteristics, grade, viability, tumor cell fraction, proliferation, and modulation of glucose metabolism or local perfusion. For instance, grade 3 FL manifests heightened FDG metabolism compared to other histologic subtypes.[11]

### 3.2. Clinical implications and multidisciplinary approach

Recent studies underscore $^{18}$F-FDG PET/CT as the gold standard for detecting extranodal involvement, monitoring post-therapeutic disease activity, and recommending it for staging patients with potentially curative-intent FDG-avid lymphomas.[12] Although recognized for its utility in avid FDG lymphoma, this technique finds critical application in indolent lymphomas like FL. In this case, the focal and intense $^{18}$F-FDG uptake in the PET scan, although symmetric, suggested extranodal disease relapse.[13]

Given the findings, ultrasound was pursued to obtain a clearer delineation of the lesions. Ultrasound revealed hypoechoic polylobulate lesions distinctly demarcated in a "nodular focal" pattern with a vascularization signal on the color-Doppler module.[14] Ultrasound facilitated targeted biopsy collection, as these superficial lesions are challenging to define on CT examination.

Ultrasound examination enabled the definition of a predominant deep muscle lesion with upper dermis sparing, and US-guided biopsy confirmed disease recurrence within less than 2 years of follicular B-cell lymphoma, warranting patient referral for bone marrow transplantation.

The peculiarity of our case is underscored not only by the rare involvement of deep muscle but also by lesions that are indistinguishable from adjacent tissues on CT examination, even after post-contrast agent administration, potentially misleading even experienced radiologists. However, CT remains the primary modality for staging and follow-up, enabling the identification of lymphoadenomegaly and lesions, although with limitations due to lesion characteristics. The $^{18}$F-FDG PET/CT scan proves invaluable for detecting and localizing rare instances of lymphoma in muscles, providing a comprehensive examination of all body segments.

This case report underscores the pivotal role of $^{18}$F-FDG PET in specific scenarios where CT fails to provide adequate information.[15] Furthermore, it emphasizes the significance of accurate staging and restaging through diverse imaging modalities, necessitating a multidisciplinary approach to ensure patients receive the most appropriate treatment. Clinical management is contingent upon disease stage, symptoms, extent, and burden, with treatment modalities including observation, anti-CD20 antibody therapy with or without chemotherapy, radiotherapy, or stem cell transplantation.[16]

## 4. Conclusion

This paper aims to elucidate an unusual instance of skeletal muscle recurrence in a patient with a history of FL. It underscores the importance of radiologist vigilance in identifying unexpected, inconspicuous lesions, emphasizing that some uncommon lesions may lack contrast enhancement. A precise clinical classification and comprehensive medical history are imperative for discerning the necessity of additional scans.

The combination of PET with $^{18}$F-FDG and CT has become a crucial imaging modality for identifying or predicting high-grade transformation and/or selecting optimal biopsy sites. In this patient, $^{18}$F-FDG PET/CT successfully detected and localized a rare FL site, underscoring the utility of hybrid machines like PET/CT in providing both metabolic and morphological information using a singular method.

The staging and prognosis of newly diagnosed patients are influenced by PET. Quantitative measurements based on the maximum standard uptake value ($SUV_{max}$) provide information on FDG metabolism, although the correlation between high $SUV_{max}$ and histological transformation remains unclear. Positron emission tomography surpasses CT in response assessment. Recent research suggests that PET holds promise as the gold standard imaging modality for FL staging, response assessment, and restaging,[17,18] necessitating a multidisciplinary approach for optimal patient care.

## Acknowledgments

None.

## Funding

None.

## Conflict of interest

The authors declare that they have no competing interests.

## Author contributions

*Conceptualization:* Cesare Oliveti, Giuseppe Lucio Cascini
*Formal analysis:* Cesare Oliveti, Roberta Mancini
*Investigation:* Cesare Oliveti, Claudia Italia Maria De Santis
*Methodology:* Cesare Oliveti, Barbara Catalfamo
*Writing – original draft:* Cesare Oliveti, Annachiara Mollace, Francesco Manti
*Writing – review & editing:* Cesare Oliveti, Giuseppe Lucio Cascini

## Ethics approval and consent to participate

Not applicable.

## Consent for publication

The patient included in this research gave written and informed consent to publish the data contained within this study.

## Availability of data

Not applicable.

## References

1. Freedman A. Follicular lymphoma: 2018 update on diagnosis and management. *Am. J. Hematol.* 2018;93(2):296-305.
doi: 10.1002/ajh.24937
2. Swerdlow SH, Campo E, Pileri SA, *et al*. The 2016 revision of the world health organization classification of lymphoid neoplasms. *Blood*. 2016;127(20):2375-2390.
doi: 10.1182/blood-2016-01-643569
3. Sutamtewagul G, Link BK. Novel treatment approaches and future perspectives in follicular lymphoma. *Ther Adv Hematol.* 2019;10:204062071882051.
doi: 10.1177/2040620718820510
4. Kaseb H, Ali MA, Koshy NV. Follicular lymphoma. In: *StatPearls*. Treasure Island, FL: StatPearls Publishing; 2024.
5. Alamdari A, Naderi N, Peiman S, Shahi F. Non-Hodgkin lymphoma with primary involvement of skeletal muscle. *Int J Hematol Oncol Stem Cell Res*. 2014;8:55-57.
6. Glass AG, Karnell LH, Menck HR. The national cancer data base report on non-Hodgkin's lymphoma. *Cancer*. 1997;80(12):2311-2320.
7. Cheson BD, Fisher RI, Barrington SF, *et al*. Recommendations for initial evaluation, staging, and response assessment of hodgkin and non-hodgkin lymphoma: The lugano classification. *J Clin Oncol.* 2014;32(27):3059-3068.
doi: 10.1200/JCO.2013.54.8800
8. Surov A. Imaging findings of skeletal muscle lymphoma. *Clin Imaging*. 2014;38(5):594-598.
doi: 10.1016/j.clinimag.2014.03.006
9. Gao S, Shu H, Yang H. Imaging features of skeletal muscle lymphoma: A case report and literature review. *BMC Med Imaging*. 2021;21(1):136.
doi: 10.1186/s12880-021-00667-4
10. Kostakoglu L, Goldsmith SJ. Fluorine-18 fluorodeoxyglucose positron emission tomography in the staging and follow-up of lymphoma: Is it time to shift gears? *Eur J Nucl Med.* 2000;27(10):1564-1578.
doi: 10.1007/s002590000340
11. Paes FM, Kalkanis DG, Sideras PA, Serafini AN. FDG PET/CT of extranodal involvement in non-hodgkin lymphoma and hodgkin disease. *Radiographics* 2010;30(1):269-291.

doi: 10.1148/rg.301095088

12. Fardin S, Gholami S, Werner TJ, Rook AH, Alavi A. Imaging evaluation of cutaneous lymphoma using functional and structural imaging. In: *Imaging in Dermatology*. Netherlands: Elsevier, 2016. p. 485-490.

    doi: 10.1016/B978-0-12-802838-4.00035-2

13. Fueger BJ, Yeom K, Czernin J, Sayre JW, Phelps ME, Allen-Auerbach MS. Comparison of CT, PET, and PET/CT for staging of patients with indolent non-hodgkin's lymphoma. *Mol Imaging Biol.* 2009;11(4):269-274.

    doi: 10.1007/s11307-009-0200-9

14. Mandava A, Koppula V, Wortsman X, Catalano O, Alfageme F. The clinical value of imaging in primary cutaneous lymphomas: Role of high resolution ultrasound and PET-CT. *Br J Radiol.* 2019;92(1095):20180904.

    doi: 10.1259/bjr.20180904

15. Alnouby A, Ibraheem Nasr IM, Ali I, Rezk M. F-18 FDG PET-CT versus contrast enhanced CT in detection of extra nodal involvement in patients with lymphoma. *Indian J Nucl Med.* 2018;33(3):183-189.

    doi: 10.4103/ijnm.IJNM_47_18

16. Ferrer A, López-Guillermo A, Montoto S, Estrach T, Colomo L, Montserrat E. Successful treatment of isolated cutaneous relapse of follicular lymphoma with rituximab. *Ann Hematol.* 2001;80(8):479-481.

    doi: 10.1007/s002770100314

17. Trotman J, Pettitt AR. Is it time for pet-guided therapy in follicular lymphoma? *Blood* 2022;139(11):1631-1641.

    doi: 10.1182/blood.2020008243

18. Gallamini A, Zwarthoed C. Interim FDG-PET imaging in lymphoma. *Semin Nucl Med.* 2018;48(1):17-27.

    doi: 10.1053/j.semnuclmed.2017.09.002

# Our Journals

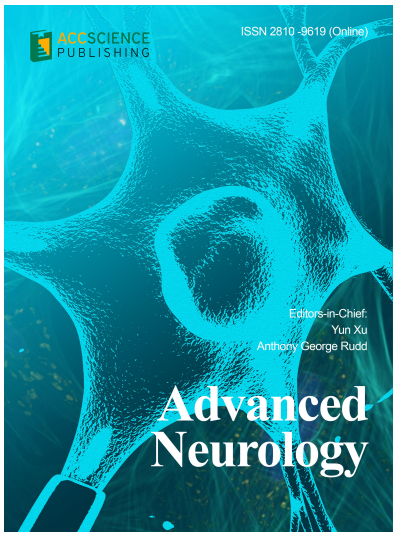


*Advanced Neurology* is a peer-reviewed and open-access journal that aims to publish and disseminate novel research in the breadth of neurology and neuroscience. The journal aims to advance our understanding in the nervous system and provide a platform to neuroscientists and physicians to showcase their findings in original fundamental and clinical research as well as to present new ideas that highlight the changes in the neurological clinical practice.

*Advanced Neurology* covers subject areas, including but not limited to the following:

- Neurological disorders
- Neurodegenerative disease
- Cerebrovascular disease
- Epilepsy and movement disorders
- Neuroimmune disease
- Neurological infections
- Muscle disease
- Molecular and cellular neuroscience
- Systems neuroscience
- Cognitive neuroscience
- Computational modeling of nervous system

*Global Translational Medicine* is a quarterly journal that focuses on medicine, biological sciences, and biomaterials engineering. The goal of *Global Translational Medicine* is to provide a platform to researchers for showcasing their latest research works in translational medicine so as to advance the field towards the betterment of human health. Despite the advancement of omics and new technologies, the process of transforming these technologies and scientific research results into effective therapies and putting them into clinical use still has a long way to go. *Global Translational Medicine* provides a platform to fill the gaps in preclinical and inter-disciplinary research, to promote clinical translation of scientific research results, and to contribute to the conception of new and improved preventive measures as well as diagnostic and therapeutic techniques of diseases.


*Global Translational Medicine* covers the following themes: cardiovascular disease, metabolism/diabetes/obesity, neuroscience/neurology, cancer, biomaterials and their applications in medicine, proteomics/metabolomics, pharmacogenomics, biomarkers, bioinformatics and data mining, animal and clinical research, and medical methods arising from interdisciplinary crossover.

## Start a new journal

Write to us via email if you are interested to start a new journal with AccScience Publishing. Please attach your CV, professional profile page and a brief pitch proposal in your email. We shall inform you of our decision whether we are interested to collaborate in starting a new journal.

**Contact:** info@accscience.com

https://accscience.com/journal/ARNM

Contact
www.accscience.com
8 Burn Road, #15-03 Trivex, Singapore 369977
Email: editorial@accscience.com
Phone: +65 8182 1586